OPTIMAL TANK GEOMETRY AND BRAKING AND STEERING RESPONSE ANALYSIS OF A TANK VEHICLE

Bingxiong Lin

A Thesis
in
The Department
of
Mechanical and Industrial Engineering

Presented in Partial Fulfillment of the Requirements
for the Degree of Master of Applied Science at
Concordia University
Montreal, Quebec
Canada

May 2005

Your file Votre référence
ISBN: 978-0-494-16252-1
Our file Notre référence
ISBN: 978-0-494-16252-1

ABSTRACT

Optimal Tank Geometry and Braking and Steering Response Analysis of a Tank Vehicle

Bingxiong Lin

Heavy vehicles exhibit limited directional performance and stability limits due to their large dimensions and weights. The liquid tankers are among the freight vehicles with relatively lower stability limits due to the special condition of their cargo that tends to shift in the longitudinal and lateral planes under braking/acceleration and turning maneuvers, when partly-filled. The objective of the present work is to derive an optimal geometry of the cargo tank to enhance the direction performance of the partly-filled vehicle combination during braking/acceleration and turning maneuvers. An optimal longitudinal section of the tank is identified to reduce the fore-aft load shift encountered during braking maneuvers. The identified geometry is coupled with an optimal lateral section, reported in the literature, to synthesize the tank that would yield reduced load shifts in the lateral as well as longitudinal planes. The potential performance benefits of the resulting design are assessed in relation to conventional and many other possible designs in terms of magnitudes of load transfer and variations in the mass moments of inertia under varying levels of longitudinal and lateral acceleration fields, and fill levels. The results demonstrated superior performance potentials of the optimal design in view of lower magnitudes of load shifts, and thereby lower destabilizing forces and moments. A direction dynamic model of an articulated vehicle comprising the optimal tank design is formulated to study the directional performance limits under braking and turning maneuvers. The analyses are performed under different braking and steering inputs, and

the response characteristics are evaluated as a function of the fill level. The directional performance characteristics of the optimal tank vehicle are compared with those of a conventional circular cross-section tank vehicle for various maneuvers and fill conditions. The results show that an articulated vehicle with the proposed optimal cross-section tank exhibits improved dynamic performances under braking/acceleration and turning maneuvers for a range of fill conditions.

Acknowledgements

The author wishes to thank to the thesis supervisors Dr. Subhash Rakheja and Dr. Ion Stiharu for their invaluable guidance and sustained encouragement through out the course of this research and for their offer for this study opportunity.

The author would like to express his appreciation to Dr. Wang, Cuiling and Ms. Ma, Xiaoqing for their professional guidance while approaching this thesis. And thanks to his colleague Mr. Shen, Zhaohui.

The author deeply thanks his entire family for their understanding throughout these years; especially for his wife Liu, Pingsi, his children Lin, Hongsheng and Lin, Qifeng, they gave him the motivation to complete this work.

The financial support provided by NATEQ is acknowledged.

Table of Contents

LIST OF FIGURES

LIST OF TABLES

NOMENCLATURE

Symbol	Description
a_f	acceleration vector of sprung mass f (f=1, 2)
a_{l2}	acceleration vector of liquid cargo cg
a_{lx}, a_{ly}, a_{lz}	longitudinal, lateral and vertical components of acceleration vector of liquid cargo cg
a_{uzi}	vertical acceleration of unsprung mass i
a_{x1}, a_{y1}, a_{z1}	longitudinal, lateral and vertical components of acceleration vector of tractor sprung mass
a_{x2}, a_{y2}, a_{z2}	longitudinal, lateral and vertical components of acceleration vector of trailer sprung mass
A_0	wetted tank cross-section area under static condition
A_c	tank cross-section area
A_l	total area of liquid in a partly filled
AT_{ij}	aligning moment due to tire j on axle i
b_i	half-track width of inner tires on axle i
C_c	dissipation of fifth wheel
c_0	constant in three-dimensional liquid free surface equation
C_{ij}	viscous damping coefficient
C_l	instantaneous cgposition of liquid cargo within a partly-filled tank
C_{l0}	static cgposition of liquid cargo within a partly-filled tank
CF_{ij}	suspension Coulomb friction
D_{rollf}, D_{pitchf}, D_{yawf}	roll, pitch, and yaw rotation matrices

d_i	dual tire spacing of tires on axle i
D_{fi}	matrix for coordinate transformation from ith unsprung mass system to fth sprung mass system
D_{sf}	matrix for coordinate transformation from fth sprung mass system to the inertial system
D_f, D_r, D_t	parameters for dampers
DLF	wheel dynamic load factor
DLF_l	left wheel dynamic load factor
DLF_r	right wheel dynamic load factor
e_i	deflection of the i-th spring from it's equilibrium position.
f_i	right-hand-side equation of arc i (i=1, 2, ..., 5) of a generic tank cross-section
f_s	liquid free surface equation
F_{gx}, F_{gy}, F_{gz}	forces due to gravity of trailer sprung mass and liquid cargo
F_{lx}, F_{ly}, F_{lz}	body forces per unit mass of liquid along tank body-fixed OX, OY and OZ directions
F_{ri}	lateral force acting through the ith roll center
F_x^M, F_y^M	maximu values of longitudinal and lateral force components
X_k	longitudinal force developed at the kth tire-road interface
FY_i	lateral force developed by tires on axle i
F_{zr}, F_{zl}	instantaneous vertical loads on right- and left-wheels of an axle
F_{zri}, F_{zli}	instantaneous vertical loads on right- and left-wheels of axle i
FS_{i1}, FS_{i2}	forces developed by left and right suspension springs on axle i
FT_{ij}	vertical force due to tire j on axle i

FY_{ij}	lateral force developed at the jth tire road interface on axle i
g	acceleration of gravity
h	fill height of liquid cargo in a tank
h_0	intercept of liquid free surface with Z-axis
H_1, H_2	overall width and height of a tank cross-section
H_{ri}	height of the ith roll center from the ground plane
H_{ui}	height of the ith unsprung weight center from the ground plane
$i_n,\ j_n,\ k_n$	a right-hand orthogonal coordinate system fixed in space
$i_{sf},\ j_{sf},\ k_{sf}$	body-fixed axis system on sprung mass f
i_{ui}, j_{ui}, k_{ui}	body axis system fixed on unsprung mass i
$\vec{i}_{sf}\ ,\ \vec{j}_{sf}\ ,\ \vec{k}_{sf}$	unit vectors describing body coordinate system fixed on sprung mass unit f
$I_{xf},\ I_{yf},\ I_{zf}$	roll, pitch and yaw mass moments of inertia of sprung unit f
$I_{xl},\ I_{yl},\ I_{zl}$	roll, pitch and yaw mass moments of inertia of liquid cargo about tank body-fixed axis system
$I_{xl2}, I_{yl2}, I_{zl2}$	roll, pitch and yaw mass moments of inertia of liquid cargo with respect to tank trailer sprung mass system
I_{xui}	roll mass moment of inertia of unsprung mass i
I_{zui}	yaw mass moment of inertia of unsprung mass i
J_k	effective mass moment of inertia of the kth wheel about its spin axis
$K_{f1}\ ,\ K_{f2}$	parameters of the tractor front spring
K_{r1}, K_{r2}	parameters of the tractor rear spring
K_{t1}, K_{f2}	parameters of the trailer spring

K_c	The spring rate of fitth wheel
KT_{ij}	vertical stiffness of tire j on axle i
KY_{ij}	lateral stiffness of tire j on axle i
L	tank length
L_1 , L_2	longitudinal distance from front / middle wheel set center to origin of c. g of tractor sprung mass
L_k , L_3	longitudinal distance from fifth wheel and real wheel set center to origin of c. g of trailer sprung mass
L_p	perimeter of a tank cross-section
LTR	lateral load transfer ratio
m_f	mass of sprung unit f
m_l, m_{l2}	mass of liquid cargo
m_{ui}	unsprung mass i
M_{lx}, M_{ly}, M_{lz}	roll, pitch and yaw moments due to liquid cargo
M_o	overturning moment due to liquid cargo
N_1, N_2	axle numbers on a sprung mass unit
p_f, q_f, r_f	rotational velocities (roll, pitch and yaw rates) of sprung mass f
p_{ui}	roll rate of unsprung mass i
$\dot{p}_f$, $\dot{q}_f$, $\dot{r}_f$	angular accelerations of sprung mass f
P	liquid pressure
P_b	treadle pressure
P_{bk}	effective line pressure in brake system k

Q	domain of area integral
R	radius of a circular arc
RC_i	radius of circular arc i of a tank cross-section (i=1, 2, …, 5)
R_{ti}	effective radius of tires on axle i
R_{tk}	effective rolling radius of kth wheel
RWA	rearward amplification ratio
S, s	time in second
s_i	half the suspension lateral spread of axle i
s_x, s_y	longitudinal slip s_x and lateral slip s_y
t	time
T_{bk}	braking torque about spin axis of the kth wheel
T_{bs}	total brake torque due to all four brakes on a tandem set
T_d	tandem axle spread
u_f, v_f, w_f	translational (longitudinal, lateral and vertical) velocities of sprung mass f
$\dot{u}_f$, $\dot{v}_f$, $\dot{w}_f$	translational accelerations of sprung mass f
U	vehicle forward speed
U_i	Forward speed of wheel set (i=1, 2, …, 5)
U_{Mo}	minimization function based upon overturning moment due to liquid cargo
U_Y	minimization function based upon liquid lateral load shift
U_{XZ}	minimization function based upon weighted sum of liquid load shift and cg height

$U_{\Sigma Y}$	minimization function based upon liquid lateral load shift for a range of fill volumes
$U_{\Sigma YZ}$	minimization function based upon weighted sum of liquid load shift and cg height for a range of fill volumes
V	domain of volume integration
V_0	initial fill volume of liquid within a tank
V_f	estimated volume of liquid within a tank
m_1	weight of tractor sprung mass
m_2	weight of tank trailer structure
m_f	sprung weight supported by front axle due to tractor alone
m_{fr}	vertical shear force acting through tractor frame
m_l	weight of liquid cargo in a tank
m_{ui}	unsprung weight i
X_l, Y_l, Z_l	instantaneous longitudinal, lateral and vertical cg coordinates of liquid cargo in terms of tank body-fixed system
X_{l2}, Y_{l2}, Z_{l2}	instantaneous cg coordinates of liquid cargo in terms of tank trailer sprung mass system
X_{ui}	longitudinal location of axle i from c. g of the sprung mass to which the axle is attached
x, y, z	Longitudinal, lateral, and vertical coordinates of a point on periphery of a tank cross-section
XC_i, YC_i, ZC_i	coordinates of center of arc i of a tank cross-section
X_i, Y_i, Z_i	coordinates of arc intersection points of a tank cross-section
X_{l0}, Y_{l0}, Z_{l0}	static cg coordinates of liquid cargo in terms of tank body-fixed system

Y_{z1}, Z_{z2}	coordinates of left hand side and right hand side intersection points of liquid free surface with the tank cross-section
Y_B, Z_B	coordinates of right-hand-side intersection point (B) of liquid free surface with the tank cross-section
Z_{5i}	vertical distance between fifth wheel and c. g of the ith sprung weight
Z_b, Z_{b2}	vertical distance between tank base and c. g of tank trailer sprung mass
Z_{cg}	tank cross-section cg height
Z_{cgo}	upper limit of tank cross-section cgheight
Z_{fi}	vertical height of tractor frame with respect to c. g of the ith sprung weight
Z_{ri}	vertical distance between the ith roll center and c. g of the sprung mass
Z_{ui}	vertical distance between c. g of unsprung mass and roll center on axle i
Z_{AC}, Z_{BD}	equations of lines AC and BD in terms of X-coordinate
Z_{AF}, Z_{BH}	equations of curves AF and BH in terms of X-coordinate
Z_{x1}, Z_{x2}	lower and higher intersection points of the liquid free surface with longitudinal section x
Δ	symbol put in front of a variable to represent variation of the variable
ΔX	variation in vehicle response vector
ΔX_l, ΔY_l, ΔZ_l	variations in cg coordinates of liquid cargo
$\Delta Y_{l\beta}$	lateral deviation of cargo cg under a steady lateral acceleration and specified fill ratio β
α_l	gradient of liquid free surface in the pitch plane
α_i	angle of circular arc i of a generic tank cross-section (i=1, 2, …, 5)
α_{ui}	pitch angle of unsprung mass i

β	liquid fill volume ratio
β_l, β_u	lower and upper limits of fill volume ratio
χ	vector of design variables
δ_f	front wheel steer angle
δ_{ij}	suspension spring deflection
ε	liquid volume error per unit tank length
ε_f	articulation angle
$\gamma_1, \gamma_2, \gamma_3$	weighting factors for liquid load shift and cg height (ΔY_l, ΔZ_l, and Z_{cg}) in tank optimization solution
φ_l	gradient of liquid free surface in the roll plane
μ	road adhesion coefficient
$\theta_{sf}, \alpha_{sf}, \varphi_{sf}$	roll, pitch and yaw angles of sprung mass f
θ_{si}	roll angle of sprung weight supported by axle i
θ_{ui}	roll angle of unsprung weight i
ρ	mass specific weight of liquid cargo
ω_k	angular velocity of k^{th} wheel about its spin axis

CHAPTER 1 INTRODUCTION AND LITERATURE REVIEW

1.1 General

Heavy-duty trucks are generally known to exhibit lower directional stability and maneuverability limits due to their high center of gravity (cg) location and large payload. In the case of liquid cargo trucks, the movement of the fluid payload under partial fill conditions could lead to even lower stability limits [1]. The combination of these two conditions (high cg and moving payload) coupled with potentially hazardous cargo, make the partially filled tank trucks high-risk vehicles on the public roads. Tank vehicles thus exhibit rollover threshold values that are lower than other freight vehicles, and are more frequently involved in single vehicle accidents [2]. The roll and yaw stability limits of tank trucks are dependent upon many vehicle and cargo related factors, such as effective roll stiffness, weights and dimensions, fill volume and operating speed. Apart from these, the tank design factors, namely, the cross-section, and number and locations of baffles, affect the yaw and roll stability of such vehicles.

The stability performance of a tank vehicle could be enhanced through reduction in weights and dimensions, and by increasing the effective track and roll stiffness of the vehicle. The variations in the weights and dimensions, and the vehicle track, however, are governed by the current road laws and transportation economy. The enhancement of the stability limits through modifications in the tank geometry thus appears to be meritorious. It has been established that a circular cross-section tank yields higher cg height, while the modified oval cross-section tank yields higher lateral slosh due to its larger width [3, 4]. Both the designs thus yield lower roll stability. A recent study has suggested a conical

cross-section with wider bottom to ensure lower cg height and narrow upper section to limit the magnitude of slosh [5]. Such a tank design thus yields improved roll stability limits. Similar geometric considerations in the pitch plane of the tank could help achieve improved yaw stability and braking performance, which has not yet been explored.

This dissertation research aims at deriving alternate tank geometry in the roll and pitch plans to realize enhanced stability limits of a partly-filled vehicle under braking as well as turning.

1.2 Review of Literature

The development of near optimal tank geometry for realizing enhanced stability limits involves considerations of the vehicle system dynamics, load shifts in the lateral and longitudinal planes, and tank geometry and design factors. The reported relevant studies are thus reviewed to formulate the scope and objectives of the dissertation research.

1.2.1 Directional Dynamics of Tank Vehicles

In order to comprehend the dynamic conditions induced by the sloshing liquid, a model of a tanker truck that effectively characterizes the behavior of the vehicle is needed. The vehicle dynamics and the fluid sloshing, however, must be investigated in a coupled manner, to capture the overall behavior of the tank truck system. Such a model would not only serve as a virtual proving ground for the partially filled tank trucks but will also permit assessments of various design parameters in view of overall vehicle stability. Moreover, the model could be used to simulate driving through a prescribed course in an effort to predict the stability of the liquid tanker vehicle under specific fill levels, while performing specific maneuvers.

The analytical methods for analyses of directional dynamics of vehicles have been mostly derived from studies on conventional freight vehicles. Ervin [6] studied the influence of size and weight variables on the threshold of rollover stability using plane models, involving axle loading, gross vehicle weight, track width, payload, and cg location. The center of gravity height of the vehicle and its track width were the two most important factors affecting the rollover of articulated vehicles. The study further concluded that vehicles with softer suspensions will roll more easily than those with firmer suspensions. The study also included the tank vehicles and implied that tanker trucks could be more stable than the rigid cargo trucks, provided the cg height was closer to the ground.

Laird [7] performed a study on the measurement of roll properties on heavy vehicles and proposed a method for evaluating the overall stability performance. The study identified important variables judged to be critical for heavy vehicle dynamics and used the plane model, developed by Ervin [6], to evaluate the stability limits. A total of four critical parameters were identified, namely, the roll stiffness, the roll-center height, lateral compliance and cg height. The study, however, did not consider tanker trucks and fluid slosh.

The design of tank trucks has been addressed in a few studies only. Gupta [8] carried out parametric variations to investigate the integrity of the liquid tanker body. The study utilized the concept of sub-structuring and enabled a component reanalysis using matrix partitioning for effective analyses of the tank shape and stresses. The contributions due to the liquid motion within the tank, however, were ignored. It was not until 1989, when a sustained effort was made to understand the behavior of the liquid tank trucks

with an active vehicle/payload interaction. Ranganathan [9-11] studied the influence of fluid slosh on the static roll stability of a tank truck by coupling the roll plane model of an articulated vehicle with a kineto-static fluid slosh model. The study established that the fluid slosh affects the overall static rollover threshold of an articulated vehicle. The conclusion of this work was that the effects of fluid slosh could not be overlooked due to their significance in reducing the rollover limit of the vehicle. This model assumed negligible contributions due to fluid viscosity and slosh dynamic force, while the fundamental slosh frequency was assumed to be considerably higher than the highest steering frequency. Although the quasi-static models do not predict the slosh forces, the computed mean values of the vehicle motion revealed reasonably good agreement with the experimental results [12]. It was further concluded that liquid load shift within a partly filled tank affects the directional or steering response characteristics of a tank vehicle in an adverse manner [11].

Popov et al. [13-16] developed a comprehensive nonlinear liquid slosh model represented by a two-dimensional, Navier-Stokes and continuity equation, together with appropriate boundary conditions along the rigid walls and the free surface, while considering incompressible fluid. Analytical formulations were presented for steady-state and transient analysis of the liquid motion within rectangular and circular cross-section containers subject to a uniform acceleration. The differential equations were solved numerically in an Eulerian mesh, using the finite difference methodology [17]. The validity of the dynamic slosh model was also presented through laboratory tests performed on a scaled model tank. The study investigated the influence of various input parameters on the main loading factors, such as the liquid forces, overturning moments,

heights of the free surface, and the damped frequencies of liquid sloshing. The authors recommended further studies on different tank shapes and three-dimensional analyses of the coupled liquid motions in the lateral and longitudinal directions, under vehicle motions caused by simultaneous braking and steering.

Rakheja et al. [18] proposed the concept of an early warning safety monitoring system for articulated freight vehicles. While the study focused on rigid cargo vehicles, it provided useful information for validating the model assumptions for the tank truck in either empty or full conditions. The study employed a wide range of truck combinations, cg height, track width, and suspension spring rates. The results attained from field tests for a two-axle truck, with scaled down version of a tank were later reported by Rakheja et al. [19]. The results were compared with the results obtained from a three dimensional tank truck model incorporating a quasi-static roll plane fluid slosh model. The comparisons revealed reasonably good agreement between the analytical model and the experimental results in terms of load transfer, roll rates, and lateral acceleration. The rollover threshold of a partly-filled tank truck has also been evaluated through roll moment equilibrium on the basis of the model proposed by Ervin [6] and an offset payload moment due to fluid slosh [20]. In this work, the entire fluid mass was assumed to be placed at the end of the pendulum, and positioned as a function of the cg of the fluid. The results of this method were compared with those derived from the kineto-static rollover model [9]. The simplified approach performed reasonably well for the cylindrical, elliptical and modified oval shaped tanks.

Ranganathan [19] formulated an equivalent mechanical system to model the complex fluid slosh in a circular tank. This mechanical system consisted of a simple

pendulum with a mass attached to the end and an additional fixed mass, assuming that only a portion of the fluid undergoes slosh. The mechanical model was validated in terms of fundamental slosh frequency of the fluid. The model was applied to estimate the rollover threshold of the vehicle. The model was further extended to the pitch plane to study the stability of the vehicle during braking maneuvers with longitudinal sloshing [22].

The majority of the studies on directional dynamics of partly-filled tank trucks have employed the well-known yaw/roll model developed by the University of Michigan Transportation Research Institute (UMTRI) [23]. Sayers and Riley [24] have described the modeling assumptions that are used in formulating the yaw and roll model for the heavy trucks. Although the model originally did not address the moving fluid cargo, the studies conducted at Concave Research Center integrated a kineto-static fluid slosh model to the original model to investigate the yaw and roll behavior of tank trucks. Kang [5, 25-29] applied this model to investigate the dynamic response and stability characteristics of partially-filled tank vehicles through systematic development and integration of various tank models, including a generic tank shape. The studies proposed a set of tank cross-sections to reduce the overturning moment caused by the load shift in the roll plane. The generic tank configuration, realized upon integration of 8 circular arcs, was used to identify an optimal cross-section. The potential performance benefits of the optimal geometry were illustrated through development and analysis of static roll plane and constant-speed three-dimensional directional dynamic models. The study also utilized the phase –IV model [29] to study the vehicle dynamic behavior under combined braking and steering maneuvers.

A generic tank geometry was formulated to describe various commonly used tanks in transportation of fuel oils and other liquids in the roll plane, and to achieve both low cg height and minimal lateral load transfer for varying fill volumes [5]. Three multivariable and constrained minimization functions were formulated on the basis of the overturning moment caused by the moving cargo under partial fill conditions, lateral load shift with prescribed cross-section cg height, and weighted sum of cg height and shifts in the cg coordinates of the liquid cargo, respectively. The optimization problems were solved subject to the constraints imposed on the total cross-section area, overall width and height, and perimeter to derive optimal cross-section parameters corresponding to typical ranges of fill volumes. The optimal solutions in all the cases invariably converged towards a nearly conical cross section, whose geometric parameters were found to be dependent upon the fill volume.

The directional response and dynamic roll stability characteristics of partly-filled tank vehicles are strongly dependent upon dynamic interactions between the moving liquid cargo and the vehicle. The movement of liquid load within the tank affects the directional response and control characteristics of partly-filled tank vehicles in a considerable manner. Dynamic roll stability characteristics of partly-filled tank vehicles may be enhanced by reducing the magnitude of overturning moments caused by liquid cargo load under a constant-speed directional maneuver. Although the directional dynamics and roll stability characteristics of partly-filled tank vehicles have been investigated in a few studies, all the analyses have been performed for conventional tank geometry, including circular and modified-oval cross-section tanks. The roll dynamics of a five-axle tractor-semitrailer combination equipped with partly-filled tanks of various

cross-sections, including conventional and optimal, have been investigated under various steady and transient directional maneuvers, and fill conditions[30]. The performance measures derived for an optimal cross-section were compared with those of conventional tanks to demonstrate the superior performance potential of the proposed optimal tanks.

1.2.2 Development of a Comprehensive Dynamic Model of Partly-Filled Tank Vehicles for Braking-in-a-Turn Analysis

The combined braking and steering is one of the most commonly encountered highway maneuvers, which have been associated with many vehicle accidents. During variable speed directional maneuvers, the load transfer in the longitudinal direction due to acceleration or deceleration, coupled with the lateral load transfer due to steering, can lead to wheel lock-up, resulting in possible yaw instability and/or loss of directional control of the vehicle. The load transfers in the longitudinal and lateral directions are further amplified in the case of partially-filled tank vehicles due to the unrestricted liquid cargo movement in the roll and pitch planes [30-32]. Although a number of comprehensive variable speed directional dynamic models of heavy vehicles have been reported in the literature, they cannot be directly employed for dynamic analysis of the partly-filled tank vehicles under combined braking and steering maneuvers, due to lack of consideration of the cargo-vehicle interactions[4, 33].

A three-dimensional quasi-static model of a partly-filled tank of a generic cross-section was proposed and integrated into a comprehensive variable-speed dynamic model of an articulated vehicle for investigating the cargo load shift and its influence on the directional response, stability and braking performance of the vehicle under combined steering and braking maneuvers [30]. The three-dimensional model of the liquid cargo

within a partly-filled generic tank was developed assuming inviscid fluid and negligible contribution due to the fundamental slosh frequency. The liquid load movement encountered under combined steering and braking was characterized in terms of variations in instantaneous cg coordinates in the roll and pitch planes, and the mass moments of inertia of the liquid bulk. The longitudinal, lateral and vertical translations of the cg coordinates of the cargo load and its mass moments of inertia were further derived as functions of the longitudinal and lateral body forces imposed on the liquid bulk, fill volume and tank geometry.

The model was used to compute the liquid cargo shifts in the roll and pitch planes, and the mass moments of inertia of the liquid bulk, as functions of the lateral and longitudinal acceleration, fill volume and the tank cross-section. The directional performance characteristics of the tank vehicle were further evaluated in terms of the dynamic load transfer, yaw rate, the sprung masses roll angles and the braking deceleration response of the combination. The performance characteristics of the partly-filled tank vehicle were compared with those of an equivalent rigid cargo vehicle to demonstrate the destabilizing effects of the liquid load shift under combined steering and braking maneuvers. Parametric sensitivity analysis were further carried out to examine the influence of steering and braking inputs, cargo fill volume, tire-road friction property, and tank cross-section on the dynamic response and stability characteristics of the tank vehicle.

1.3 Highlights of the Vehicle Dynamic Simulation

With the increasing population of the heavy articulated vehicles or the road trains, which consist of a tractor unit and one or more semi-trailers or full trailers, safety

concerns for their operation have been rising. This has stimulated intensive theoretical and experimental studies of the directional control and stability of this type of vehicle. A number of computer simulation models have been developed [34]. A brief description of the basic assumptions and limitations of some of the better known models is given below [23, 35-38].

The Linear Yaw Plane Model

This is a linear mathematical model for studying the directional behavior of the multiple articulated vehicles with yaw and lateral degrees–of–freedom (DOF). The linear Yaw Plan model was developed at the University of Michigan Transportation Research Institute (UMTRI), and it involves following major assumptions and simplifications:

a. The roll dynamics of the vehicle is neglected.
b. The vehicle is assumed to travel at a constant forward velocity.
c. The degrees of freedom considered in the model are limited to the lateral and yaw motions of the tractor and articulation in the horizontal plane of the other sprung masses of a multiple articulated vehicle.
d. The cornering force and the aligning moment generated at the tire-road interface are assumed to be linear functions of the slip angle of the tire.
e. The articulation angles made by the various units of the vehicle train are small.
f. There are no significant tires forces present in the longitudinal direction.
g. Pitch and roll moments of the sprung masses are small, and hence neglected.
h. Each unit of the articulated vehicle is assumed to be a rigid body.

Three-Dimensional Total Braking and Steering (TBS) Model

TBS (total braking and steering) model is a simplified nonlinear mathematical model developed for simulating the vehicle response to steering and braking inputs. It was developed by Leucht and Moncarz et al. [38, 39], where, the basic assumptions are similar to those outlined for the linear yaw plane model. The model, however, incorporates a nonlinear tire model to represent the cornering force-slip angle relationship, while the dynamic load transfer is taken into account in determining the normal load on each tire.

Three-Dimensional Yaw/Roll Model

The Yaw/Roll model was developed at UMTRI for the purpose of predicting the directional and roll responses of the articulated vehicles in steering maneuvers. In the model, the forward velocity of the lead unit is assumed to remain constant during the maneuver. Each sprung mass is treated as a rigid body with up to five degrees of freedom (dependent upon the constraints at the hitch): lateral, vertical, yaw, roll, and pitch. The axles are treated as beam axles, which are free to roll and bounce with respect to the sprung mass to which they are attached. The major assumptions associated with the Yaw/Roll Model are summarized below:

a. The relative roll motion between the unsprung and the sprung masses occurs about the roll center, which is located at fixed distances beneath the sprung masses.
b. The nonlinear force-displacement behavior of the suspension is linearized about the operating point.
c. The cornering force and the aligning moment produced by a given tire are a

nonlinear function of the slip angle and the vertical load. The influence of the wheel camber on the lateral force generation is neglected.

d. The model permits the analysis of articulated vehicles, which are equipped with any of the four coupling mechanisms, namely; conventional fifth wheel, inverted fifth wheel, pintlehook, and kingpin.

Comprehensive Braking and Steering Model (Phase IV)[40]

The Phase IV model was developed with the objective of helping engineers and safety researchers to evaluate new vehicle designs and meet tougher regulations imposed on the trucking industry by the U. S. federal government. A series of models were developed to simulate for the braking and steering responses of heavy vehicles. The first of these models, named Phase, was a 15 degree of freedom pitch plane simulation of a vehicle towing a single trailer [41]. The subsequent model was Phase II, a 3-dimensional model that included the roll and yaw degrees of freedom. Thus, the Phase II was able to simulate the directional response due to steering, as well as braking inputs. The Phase III model extended the earlier work with better tire models, a path-follower model of the driver, for double and triple trailer, and an improved braking model that included anti-lock braking system [42, 43]. The final Phase 4 model, which extended the earlier works with improved suspension, brake torque and steering dynamics, and the frame compliance models.

Although the Phase 4 model is quite powerful, its use has been limited by several factors. Most of these factors fall into one of two categories. First, due to its complexity, the program execution requires substantial time and effort to develop a valid input data set representing the subject vehicle. Second, the program was designed (in the 1970's) for use in batch mode, and had no user interface. The numeric output from Phase 4 was

voluminous, and thus, was difficult and time-consuming to interpret [44].

TruckSim Simulation Software

TruckSim is the first software package that detailed heavy-truck vehicle dynamics models with a modern graphical user interface[24, 45]. TruckSim is much easier to use than the older vehicle simulation programs due to its enhanced graphical user interface that permits for the use of the built-in database of component properties and for specifying alternate component characteristics. The software is designed to work with MATLAB / SIMULINK software to define the relations for different vehicle components. TruckSim further links the simulation results to a user-friendly post-processing tool consisting of animations and plotting programs. The vehicle and its properties are defined by relationships, constant parameters or look-up tables. The above vehicle dynamics simulation programs are designed for analyses rigid cargo vehicles and can not simulate for the directional dynamics of partly-filled tank trucks.

1.4 Highlights of the Engineering Design Optimization

Shape optimization is a fundamental objective of designers of components, and devices of systems. It pursues the determination of the dimensional variables, which maximize the ability of the part to perform the intended function, under the prescribed operating conditions [46, 47]. The optimal design of the liquid tank of a truck, in the classical sense, is the minimization of the goal parameters by varying or determining dimensional variables. The shape parameters are considered as unknowns during the optimizations process, and the results may not be unique. As the structure and the boundary conditions become complex, it is not easy to develop a general algorithm, which provides an optimum configuration. Thus the formulation of the problem becomes

case dependent and the computation time needed in the search for the optimal solution can be extensive, if the search strategy is not carefully matched to the situation.

In general, approaches for shape optimization problems are a mixture of engineering concepts and mathematical principles subjected to rigorous constraints. Typically the shape optimization or shape synthesis problem has the following characteristics in the formulation of an objective function [48]:

1. The designer has to deal with a large number of design variables;
2. The design variables are difficult to constrain in a finite way;
3. The design variables are functions of the geometry itself.

The first known attempt in developing a mathematical formulation for shape optimization has been attributed back to Galieo (1638) who found that the minimum weight cantilever is a parabolic beam [49]. Afterwards, the development of the differential calculus provided an elegant mathematical tool for the evaluation of the maximum and the minimum of the differentiable relationships or functions. Consequently, mathematical optimization procedures continued to be developed with the contribution of the classical works of Bernoulli, Euler and Lagrange. It was at the beginning of the nineteenth century when the shape optimization field was presented as a branch of the optimal control theory [50]. Since the early 1960's when it was first suggested that numerical approximation techniques could be combined with mathematical programming methods to develop structural optimization algorithms, computers have been extensively utilized in advancing the synthesis of structures and mechanical elements [51].

The extension of the shape optimal design concept to structural and mechanical

problems from the classical theoretical problems (e.g. flow and profiles) was fully developed around 1970 [52-55]. The application of programming and variation techniques in mechanical systems has been applied mainly in the area of structural design, synthesis of control systems optimization of space vehicle's performance and machine design [56, 57]. The aerospace and automotive industries are the primary supporters and users of the shape optimization research. When reviewing the vast literature published in the area of shape optimization, more than two different approaches to a problem could be identified. In the first approach, approximation techniques are combined with mathematical programming optimization in a classical fashion. The approximation methods are featured only as another tool or as another step in the procedure. The second approach is one where the approximation techniques have a more significant role in the procedure.

Since computer-aided geometric design became more popular and accepted in engineering applications, a natural process was to couple the CAD tools with the structural optimization. Esping [58] used a CAD approach to the minimum weight design problem. Braibant and Fleury [59] used CAD philosophy of geometric description to formulate a shape optimal design of an elastic structure. Wang et al. [60] also used similar geometric description in the sensitivity analysis for shape optimization of continuum structure. Ding and Gallagher [61] presented a rotational reduced-basis reanalysis and an approximation reanalysis method, which are based on the size of the equilibrium equation. These techniques can be advantageously used in the shape and structural optimization process.

The design of the liquid tank truck is a special case in shape optimization. The

optimization relates to the variations in the liquid dynamic characteristic in the partly filled tank to the operation of vehicle dynamic control. It is common in many practical engineering design applications, to have the formulation, such that the objective functions are not given explicitly in terms of the design variables. Under such circumstances, given the values of the design variables, the value of the objective function is obtained by some intermediate calculations and analyses [62].

For relative analyses of different cases aiming at the same objective, it is necessary to construct the same optimal functions through similar steps. In this thesis, there are two kinds of optimization methods that will be considered for the problem formulations: the first is Univariate Method of Grid and Random methods; the second is Sequential Quadratic Programming (SQP), which was programmed in MATLAB codes. The random search of Univariate Method of Grid and Random methods is nearly as simple as the grid. Every point in the space is equally likely to be tested, and the point of this method is somewhat more sophisticated than the random walk, which is based on a sequence of improved approximations to the minimum, each derived from the preceding approximation. The sequence is determined from the prescription [63]:

$$X_{q+1} = X_q + a_q S_q \qquad (1\text{-}1)$$

where S_q are a cyclic ordering of the unit vectors $S_1=(1,0,0,\ldots,0)$, $S_2=(0,1,0,\ldots,0),\ldots.$, $S_n=(0,0,0,\ldots 1)$, $S_{n+1}=(1,0,0\ldots,0)$, etc., and the a_q are positive or negative step lengths chosen so that $F(X_{q+1}) < F(X_q)$. With this choice for the S_q, the Equation (1-1) follows the statement: "change one variable at a time."

The accelerated incremental scheme operates according to the following steps.

a. Determine whether a_q should be positive or negative. In other words, for

the particular S_q in question, does the function decrease in the plus or minus direction?

b. Take a step of $\pm t$, where t is some pre-selected step length, and calculate $F_t \equiv F(X_q \pm tS_q)$.

c. If F_t is less than $F_q \equiv F(X_q)$ then replaces F_q by F_t, increase t to t_p, and repeat steps b and c. Otherwise set $X_{q+1} = X_q \pm t_p S_q$, where t_p is the last "successful" value. Choose the next S_q and repeat steps a, b, and c for the new direction (variable).

d. Stop when no direction S_q produces an improvement in the value of the function.

Methods represent the state of the art in nonlinear programming methods. Schittkowski [64] has implemented and tested a version of SQP that outperforms every other tested method in terms of efficiency, accuracy, and percentage of successful solutions, over a large number of test problems. Based on the work of Biggs [65], Han [66], and Powell [67, 68], the method enables the user to closely mimic Newton's method for constrained optimization as it is done for an unconstrained optimization. An approximation is made of the Hessian or of the Lagrangian function using a quasi-Newton updating method at each major iteration. This approximation is then used to generate a Quadratic Programming (QP) sub-problem and the solution is used to form a search direction for a line search procedure. The main advantage of the formulation consists of the formulation of a QP sub-problem, based on a quadratic approximation of the Lagrangian function.

1.5 The Objective and the Layout of the Thesis

Owing to unreasonable safety risks associated with relatively lower roll stability

limits of partly-filled tank vehicles, considerable efforts have been made to enhance an understanding of the load shift within the tank. These studies have contributed to identification of optimal cross-section of the tanks to limit the fluid slosh in the roll plane under a lateral acceleration field, and the operating practices that could yield a higher rollover risk. The fluid slosh and the associated load shift are known to be far more severe in the longitudinal plane under applications of braking and steering maneuvers, particularly for clean-bore tanks. The analyses of such vehicles under simultaneous braking and steering inputs, however, have been addressed in a single study. The fluid slosh in the longitudinal plane could be limited by designing tanks with alternate geometry, which could yield improved braking and steering performance, and thus jackknife limits.

The main objective of this dissertation research is to derive cross-section of a tank in the roll and pitch planes to achieve minimal load shift caused by the liquid motions under braking and steering inputs. While the primary focus is to derive the optimal geometry to minimize the load shift in the longitudinal direction under braking, a total of five-different cases of load shift are considered. The detailed objectives can be summarized as follows:

a. Development of a two dimensional (2D) generic model of the cargo tank in longitudinal direction as generated by eight circular arcs;

b. The formulation of five cases of three dimensional tank models which combine with the circular cross-section and the reported optimum cross-section in the roll plane [30], while subject to identical load carrying capacity and overall dimensions.

c. Analyze the load shift properties of different cross-section tanks under constant levels of lateral and longitudinal accelerations.

d. Develop a three-dimensional vehicle model incorporating a partly-filled tank

of optimal geometry to study the directional dynamic response.

e. Examine the validity of the model on the basis of the results reported in the published studies.

f. assess the performance potentials of optimal tanks by comparing the response with those of the conventional tank vehicles.

1.5.1 Layout of the Thesis

In chapter 2, the design standards and relative regulations involving the liquid cargo are briefly discussed. A two dimensional model of liquid tank created by eight circular elements in the longitudinal section is described. The independent design variables are defined along with the definitions of the coordinates of the center of gravity (cg), moments, and mass moments of inertia. The optimization functions are formulated to minimize the dynamic load shift and the results attained from simulations are discussed.

In chapter 3, the generalized three-dimensional models of the tank are formulated and analyzed to determine the dynamic characteristics of the partially filled tank. A total of five different cases are identified for the analyses of load shift. The cg coordinates and the trajectories of the moving cg are evaluated under braking/acceleration for the five different models. The variations in the mass moments of inertia about the x-, y-, and z-axes are further evaluated.

In chapter 4, an analytical model of an articulated vehicle equipped with a partly-filled tank and subject to braking and steering if formulated. The coordinate systems are defined in accordance with the SAE standard, and the coordinate transformations are performed to utilize the body-fixed axes systems. The equations of motion for the vehicle model are formulated upon considerations of reported models of the tires, suspension and

the constraint.

In Chapter 5, a Matlab/SIMULINK program is developed for the directional response analysis of the liquid tank vehicle. The directional dynamic responses of the vehicle are evaluated for the 5 different tanks identified in the previous chapters, while subject to braking and/or steering inputs. The simulation results are discussed in relation to those attained for a conventional tank vehicle, and the potential performance benefits of the optimal geometry are further discussed.

In Chapter 6, the major conclusions drawn from this work and the recommendations for future work are summarized.

CHAPTER 2 TWO DIMENSIONAL MODELING AND OPTIMIZATION OF THE LIQUID TANK

2.1 Introduction

The operational safety of partially filled tank trucks is strongly affected by the interactions of the moving liquid cargo with the vehicle. The longitudinal and lateral slosh forces caused by vehicle maneuvers may adversely affect the vehicle stability, controllability and maneuverability, and impose relatively higher local pressures and stresses on the tank structure [69]. A Canadian survey [70] has shown that 45% of the accidents involving transportation of dangerous liquids were due to the roll-over and 72% of the accidents occurred while negotiating a curve. More recently, statistics from the U.S. Department of Transportation have shown that roll-over crashes account for about one half of the 700 heavy-duty truck fatalities that occur annually [71]. There are approximately 15,000 roll over accidents involving commercial heavy vehicles every year in the U.S.A. [72, 73]. Such accidents could have dramatic environmental and financial consequences. In U. K., The average costs of an accident have been estimated between £75,000 and £100,000, which includes recovery and repair of the vehicle, road surface repair and product replacement [74].

Kusters [75] has identified three major causes of highway accidents that involve mostly articulated vehicles, namely: a sudden course deviation, often combined with abrupt braking and high initial speed, excessive speed on curves or a shifting of the load. The shifting of load is known to be most severe in partly filled tank trucks [30]. The likelihood of vehicle rollover is strongly related to the rollover threshold acceleration, also referred to as the overturning limit of the vehicle in steady turning. The rollover threshold mostly depends upon the vehicle geometry and inertia, suspension

characteristics, and tire properties [29]. In case of tank trucks, the overturning moment caused by liquid load shift contributes strongly to the rollover threshold. The liquid load shift and thus the roll stability strongly depend upon the tank geometry, apart from the fill level and the severity of the maneuver.

The roll dynamics of partly-filled tank vehicles have been investigated in many studies using pendulum analogy, mechanical equivalent model, kineto-static and dynamic fluid slosh models [20, 21, 30, 76, 77]. The role of tank cross-section in the roll plane has also been investigated one study in view of the roll plane dynamics and roll stability, and optimal tank cross-section has been defined to enhance the vehicle roll stability [78]. This chapter presents a pitch-plane model of the tank to study the longitudinal load shift caused by constant deceleration arising from a braking maneuver. Optimal tank geometry is defined to reduce the magnitude of pitch plane load shift.

2.2 Pitch Plane Model of a Tank

The motion of the free surface of liquid within a partially filled tank can lead to significant longitudinal and vertical load shift, as well as the alteration of the mass moment of inertia during straight-line braking [4, 30]. The resulting load shift cause excessive disparity in the normal forces acting on the vehicle tires and thus the braking force distributions. The magnitude of the longitudinal and vertical load shifts strongly depend on the braking deceleration, fill condition, and the tank geometry. The braking performance and stability limits of partly-filled tank trucks could be enhanced by limiting the magnitude of dynamic load shift along the longitudinal axis. Transverse baffles with a large central orifice are often used to limit the longitudinal load shift and to enhance the structure integrity [31, 32]. Cargo tanks, employed in general purpose transportation of

liquid cargoes, however, are clean bore designs to facilitate cleaning. The performance characteristics of such vehicles could be enhanced by limiting the load shift through alternate tank geometry.

A generic longitudinal section of a tank is proposed, as shown in Figure 2.1. The geometry consists of eight circular arcs in the longitudinal plane, symmetrical about the vertical centerline. The proposed geometry also consists of uniform cross-section in the lateral plane, which may be circular or modified-oval.

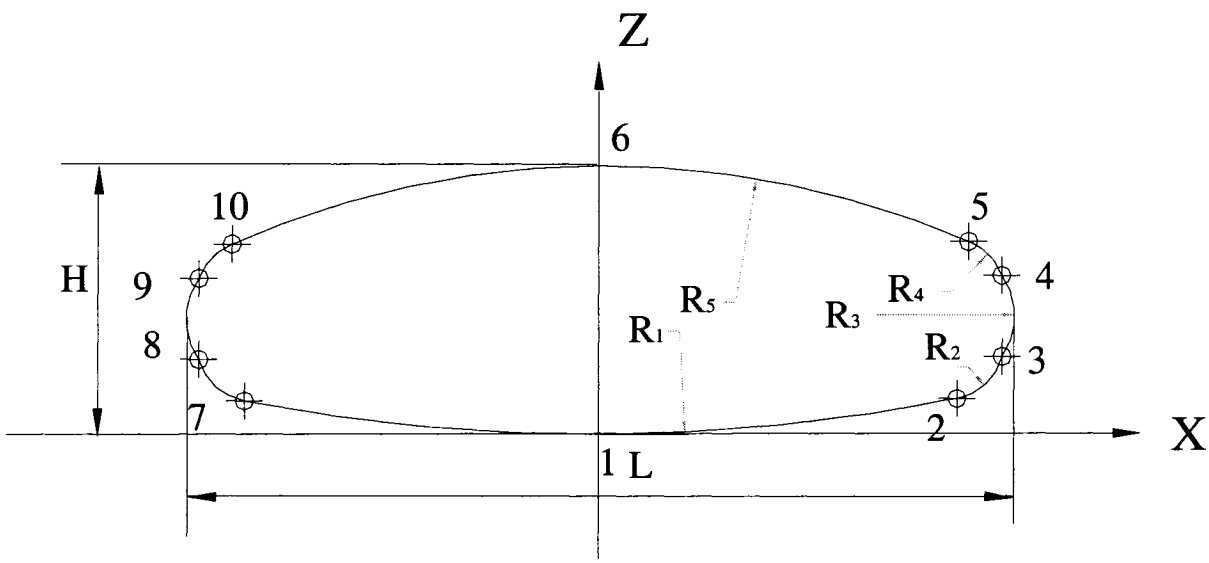

Figure 2.1: Illustration of 8 circular arcs of the proposed tank in the longitudinal section

It is vital that the tank geometry conform with the current weights and dimensional regulations. The design height H is thus limited to 2.04 m, while the length L must be chosen to conform to the local weight and dimension regulations. As shown in Figure 2.1, the radii R_1 to R_5 represent the different circular arcs, while the origin is

located at point *1*. The maximum height is determined from the coordinate of *6*, and points *2* to *10*, with the exception of point *6*, are the intersection points of the adjacent segments, named as segment (*i*) for arc *7-1-2*, segment (*ii*) for arc *2-3*, segment (*iii*) for arc *3-4*, segment (*iv*) for arc *4-5*, segment (*v*) for arc *5-6-10*, segment (*viii*) for arc *10-9*, segment (*vii*) for arc *9-8*, and segment (*vi*) for arc *8-7*, respectively. The coordinates of the intersection points can be determined from the geometric analysis assuming that two adjacent arcs possess identical slope at the intersection point. The proposed generic geometry is applied to identify the arc radii that would yield reduced magnitudes of the longitudinal and vertical load shifts (ΔX and ΔZ) under a particular braking operation, which forms the first step for the optimal design of the liquid tank. Limiting the variation in the pitch mass moment of inertia under braking forms the second objectives.

2.2.1 Identification of Independent and Dependent Variables and Constraints.

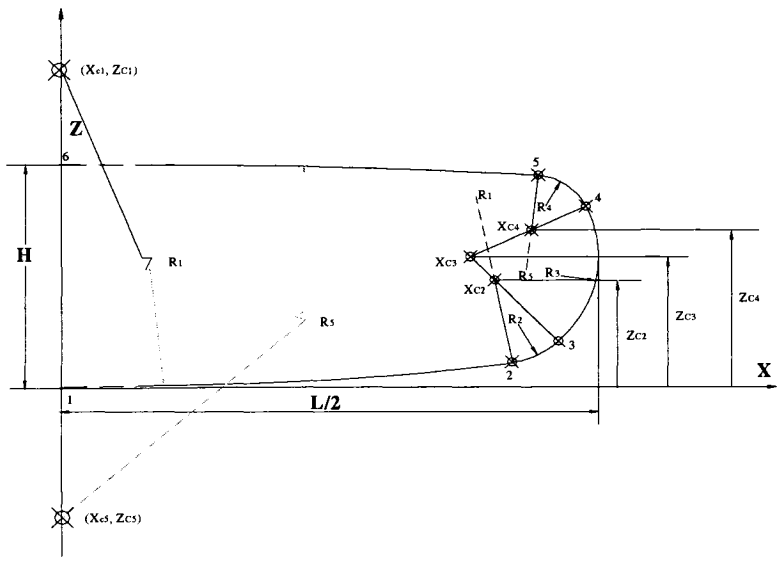

Figure 2.2: Illustration of tank geometry parameters

Figure 2.2 further illustrates the centers of different arcs and the arc radii, where the center coordinate of segment (*i*) and segment (*v*) will locate at the *Z* axis, i.e.:

$$Z_{C1} = R_1,\ X_{C1} = 0; \quad Z_{C5} = H - R_5, X_{C5} = 0; \tag{2.1}$$

The center coordinate of arc (*ii*), (X_{C2}, Z_{C2}) will lay on the line projected from point *2* to the center of segment (*i*) and another line from point *3* to the center of segment (*iii*) (X_{c3}, Z_{c3}), such that the coordinate of the intersection point *2* can be related as:

$$Z_2 = R_1 - \sqrt{R_1^2 - X_2^2} \tag{2.2}$$

$$\frac{Z_2 - Z_{C2}}{R_2} = \frac{Z_2 - Z_{C1}}{R_1}, \quad \frac{X_2 - X_{C2}}{R_2} = \frac{X_2 - X_{C1}}{R_1} \tag{2.3}$$

Similarly, the coordinates of intersection point 3 can be expressed as:

$$X_3 = X_{C3} + \sqrt{R_3^2 - (Z_3 - Z_{C3})^2} \tag{2.4}$$

$$\frac{Z_3 - Z_{C3}}{R_3} = \frac{Z_3 - Z_{C2}}{R_2}, \quad \frac{X_3 - X_{C3}}{R_3} = \frac{X_3 - X_{C2}}{R_2} \tag{2.5}$$

$$X_{C3} + R_3 = \frac{L}{2} \tag{2.6}$$

Coordinates of intersection points 5 and 4 can also be derived as:

$$Z_5 = H - R_5 + \sqrt{R_5^2 - X_5^2} \tag{2.7}$$

$$\frac{Z_5 - Z_{C5}}{R_5} = \frac{Z_5 - Z_{C4}}{R_4}, \quad \frac{X_5 - X_{C5}}{R_5} = \frac{X_5 - X_{C4}}{R_4} \tag{2.8}$$

and:

$$X_4 = X_{C3} + \sqrt{R_3^2 - (Z_4 - Z_{C3})^2} \tag{2.9}$$

$$\frac{Z_4 - Z_{C3}}{R_3} = \frac{Z_4 - Z_{C4}}{R_4}, \quad \frac{X_4 - X_{C3}}{R_3} = \frac{X_4 - X_{C4}}{R_4} \tag{2.10}$$

The above relationships, (2.2) to (2.10), suggest a total of 13 independent equations and 21 variables, therefore the minimum independent variables of above

equations are 8. These independent variables are required to uniquely define the tank construction. A design variable study generally involves the systematic examination of a range of designs carried out in order to choose a good or the best design from among all those examined. Generally the performances of these variables are studied and compared to reach the most suitable values [6]. For a cargo tank, the overall height H and length L are limited by the regulations on the maximum dimensions. Consequently, H and L can be considered as two of the independent variables, which will involve producing a rectangular frame that involves all the intersections associated with the shape of the liquid tank. Moreover, the vertical coordinate of the center of the segment (*iii*) (Z_{c3}) would lie between the origin (*1*) and height (*H*), which represents a good intermediate reference to reduce the number of variables when working out the relations between the variables. Furthermore, Z_4 and R_3 form two of the independent variables.

As illustrated in Figure 2.2, it is also observed that the height of intersection point *2* must be less than or equal to that of the point *3* ($Z_2 \leq Z_3$), while the same would also apply for points *4* and *5* ($Z_4 \leq Z_5$). The intersection points *2* and *5* will mainly determine the form of the tank, while points *3* and *4* will determine the exact geometry. Moreover, the height of point *3* (Z_3) will be less than or equal to the coordinate Z_{c3}, while the height Z_4 will be greater than or equal to Z_{c3}. Consequently, Z_3 and Z_{c3} can thus be considered as two other independent design variables.

From the structural integrity and construction point of view, the minimum radius of any arc is constrained to 0.39 m [1]. In fact, the available ranges for R_2 and R_4 would be far smaller than R_1 and R_5, the radii R_2 and R_4 are thus considered to be more suitable as the last two of the independent design variables. The 8 independent design variables

are thus H, L, R_3, Z_{C3}, Z_3, R_2, Z_4, and R_4.

On the basis of the above 8 independent design variables, Equations (2.2) to (2.10) can be solved to derive the 13 dependent variables (X_2, X_3, X_4, X_5, X_{C2}, X_{C3}, X_{C4}, Z_2, Z_5, Z_{C2}, Z_{C4}, R_1, and R_5). Equations (2.4), (2.5) and (2.6) yield following relationships for X_{C3}, X_{C2}, and Z_{c2}, respectively:

$$X_{C3} = \frac{L}{2} - R_3 \; ; X_{C2} = \frac{X_3(R_3 - R_2) + R_2 X_{C3}}{R_3} \tag{2.11}$$

$$Z_{C2} = \frac{Z_3(R_3 - R_2) + R_2 Z_{C3}}{R_3} \tag{2.12}$$

Equation (2.2) and (2.3) yield following relations for R_1, X_2 and Z_2:

$$R_1 = \frac{R_2^2 - X_{C2}^2 - Z_{C2}^2}{2(R_2 - Z_{C2})} \tag{2.13}$$

$$X_2 = \frac{X_{C2}(X_{C2}^2 + Z_{C2}^2 - R_2^2)}{(R_2 - Z_{C2})^2 + X_{C2}^2} \text{; and } Z_2 = R_1 - \sqrt{R_1^2 - X_2^2} \tag{2.14}$$

Similarly Equations (2.7), (2.8) and (2.10) yield:

$$X_{C4} = \frac{R_4 X_{C3} + X_4 R_3 - R_4 X_4}{R_3} \tag{2.15}$$

$$Z_{C4} = \frac{R_4 Z_{C3} + Z_4 R_3 - R_4 Z_4}{R_3} \tag{2.16}$$

$$R_5 = \frac{X_{C4}^2 - R_4^2 + (H - Z_{C4})^2}{2(H - R_4 - Z_{C4})} \tag{2.17}$$

$$X_5 = \frac{R_5 X_{C4}}{R_5 - R_4}; \quad Z_5 = H - R_5 + \sqrt{R_5^2 - X_5^2} \tag{2.18}$$

Equations (2.2) through (2.18) are solved in conjunction with a number of limit constraints to ensure a feasible design. An equality constraint is imposed to ensure that

the volume of the tank is equal to that of a standard modified-oval tank DOT 406; cross section area = 3.2586 m^2, length = 14.6302 m, such that the design tank volume V_t = 47.6740 m^3. It is also essential to limit the tank weight to not to exceed that of the standard tank. The design surface of the generic tank should be therefore less than or equal to that of the standard modified-oval tank (DOT 406). Considering the perimeter of the DOT 406 tank as 6.63m, the maximum tank surface area is limited to $S_t \leq 103.5168$ m^2. Furthermore, the overall tank width is limited to 2.44 m in accordance with the current dimensional regulations [78].

2.2.2 CG Coordinates and Mass Moment of Inertia

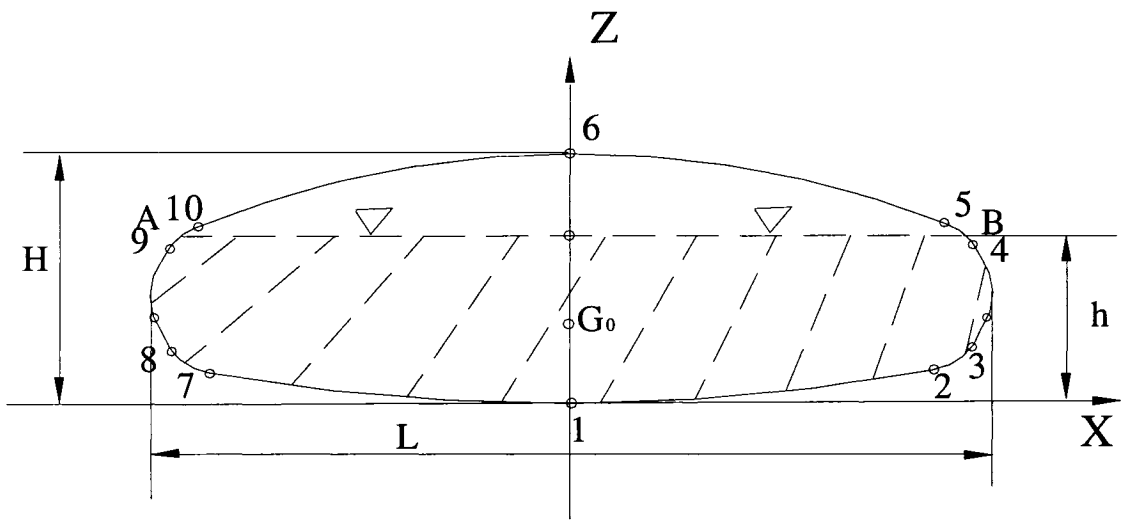

Figure 2.3: The static cg of the liquid in the pitch plane.

Liquid motion in partially filled containers generates slosh forces and moments that affect the directional behavior and stability of the fluid cargo trucks [37]. For the proposed 2D model, shown in Figure 2.3, a rectangular cross section is assumed with overall width in the lateral direction as 2.44 m. The total design area A_l, which will form

one of the constraints for the proposed tank is derived from: $A_l = 2\int_{Z_m}^{Z_u} x dz$, where Z_u and Z_m represent the maximum and minimum vertical coordinates of the tank envelope corresponding to a given x coordinate, which relates to the vertical coordinate z, as:

$$x = X_{ci} + \sqrt{R_i^2 - (z - Z_{ci})^2} \quad (i = 1,2,...,5) \tag{2.19}$$

The instantaneous coordinates G (X_l, Z_l), of the cg of the liquid bulk under a braking deceleration a_x, are then derived from the equation of the liquid free surface and tank geometry as:

$$X_l = \frac{1}{A_f}\iint_Q x dx dz; \quad Z_l = \frac{1}{A_f}\iint_Q z dx dz; \tag{2.20}$$

Where Q defines the domain of the area integral, A_f is the liquid area under the free surface line AB, which is calculated from:

$$A_f = \iint_Q dx dz \tag{2.21}$$

The limits of x and z are identified from the intersection of the free surface and the tank periphery, using the method described in section 2.2.1. The mass moment of inertia of liquid cargo in the partially filled tanks is an important parameter in the tank design, since it directly affects the directional dynamic response and follows the changes in the patterns of the liquid cargo. The mass moment of inertia in the roll, pitch, and yaw planes, (I_x, I_y, and I_z), can be computed from:

$$I_x = \rho\iiint_V (y^2 + z^2) dx dy dz \tag{2.22}$$

$$I_y = \rho\iiint_V (x^2 + z^2) dx dy dz \tag{2.23}$$

$$I_z = \rho \iiint_V (y^2 + x^2) dxdydz \tag{2.24}$$

where ρ represents the mass specific weight of the liquid.

It is obvious that the domain of integration Q is an important parameter in the calculation of the characteristics of the liquid tank, and it is determined from the fill condition, tank geometry, and braking deceleration.

2.3 Static CG Coordinates (X_{lo} Z_{lo})

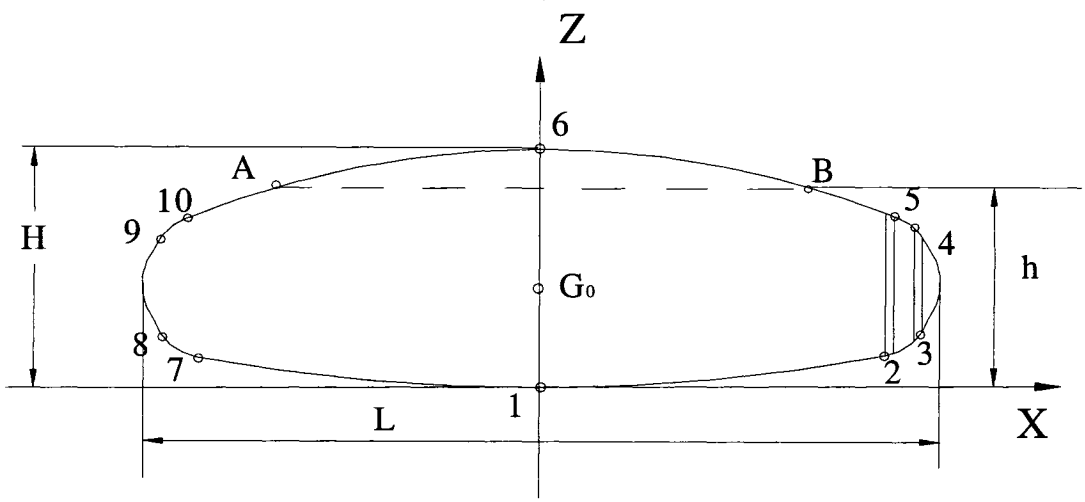

Figure 2.4: Divisions of the partly filled liquid.

For a given static fill height h, as shown in Figure 2.3, the hatched region indicates the domain of area integral Q, and points A and B are the intersection points of the liquid free surface with the tank periphery. On the right side of the tank, there are 4 construction adjectives points: *2, 3, 4*, and *5*, and two center points *1* and *6*, as shown in Figure 2.4. The fill level determines the segment, where the free surface intersects the tank periphery. Rearranging the coordinates of these 6 points (1, 2, 3, 4, 5, B) in sequence from smallest to largest, for the case shown in Figure 2.4, can yield 5 different volumes.

The sum of these compartment volumes is equal to half the total volume of the liquid.

The numbers of segments to be considered in the geometric formulations are determined by considering the liquid elements shown in Figure 2.5, where Z_{x1} and Z_{x2} represent the lower and upper vertical coordinates of a vertical line passing through a fluid element located at a longitudinal distance x from the origin. The coordinates Z_{x1} and Z_{x2} are defined as follows:

For $Z_{x2} > Z_{C3}$, the arc segment where Z_{x2} lies is named as *ih*. Similarly for $Z_{x1} < Z_{C3}$, the lower segment is named as *il*. The segments *il* or *ih* can be determined from the following:

For $x \geq X_k$ and $x < X_{k+1}$, $il = (i), (ii)$, for segment $k = i, ii$.

For $x \geq X_3$ and $x < L/2$, $il = (iii)$;

For $x \geq X_{k+1}$ and $x < X_k$, $ih = (iv), (v)$, for segment $k = iv, v$.

For $x \geq X_4$ and $x < L/2$, $ih = (iii)$.

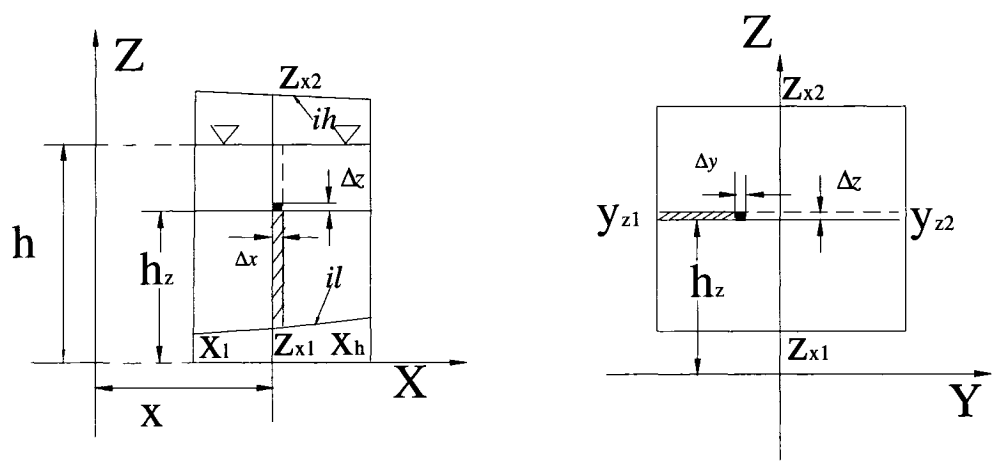

Figure 2.5: The liquid element in the partially-filled tank

The vertical coordinates for a segment enveloped by X_l and X_h (Figure 2.5) can be expressed as:

$$Z_{x1} = Z_{C(il)} - \sqrt{R_{il}^2 - (x - X_{C(il)})^2} \tag{2.25}$$

$$Z_{x2} = Z_{C(ih)} + \sqrt{R_{ih}^2 - (x - X_{C(ih)})^2} \tag{2.26}$$

where *il* and *ih* represent the segment number.

y_{z1} and y_{z2} are the intercepts of free surface of liquid in the roll plane, for the proposed 2D model, such that $y_{z1} = -1.22m$ and $y_{z2} = 1.22m$

Definition of the Domain of the Integral Q.

The vertical boundary of the domain of integration Q in Equation (2.20) is determined by the static fill height and the coordinates Z_{x1} and Z_{x2}, named as the lower and upper bounds in the vertical direction, such that $Z_l = Z_{x1}$, and $Z_h = Z_{x2}$. For varying fill heights, the integral limit in the vertical direction can be derived from one of the follows three cases:

1) For $h < Z_{x1}$, the upper bound Z_h can be considered as Z_{x1}.

2) For $h \geq Z_{x2}$, the region is completed filled, $Z_h = Z_{x2}$;

3) For $Z_{x1} \leq h < Z_{x2}$, the segment is partly filled, $Z_h = h$.

It is possible that the partly and completed filled areas occur within the same segment at the same time. In this situation, the domain is divided into two parts consisting of a partly filled section and a completely filled section. The longitudinal coordinate (x_f) of the section bordering the completely filled segment can be derived from the following by letting $z = h$:

$$x_f = X_{ci} \pm \sqrt{R_i - (h - Z_{ci})^2} \tag{2.27}$$

The liquid area A_k in a particular segment with partly and completely filled zones under static condition is thus calculated from:

$$A_k = \int_{Z_l}^{Z_h} \int_{x_l}^{x_f} dxdz + \int_{Z_i}^{Z_h} \int_{x_f}^{x_h} dxdz \tag{2.28}$$

The moment of the liquid about Z axis can be calculated as:

$$M_z = 2\left[\sum_{k=i}^{v} \int_{z_l}^{z_h} \int_{x_l}^{x_f} zdxdz + \int_{z_l}^{Z_h} \int_{x_f}^{x_h} zdxdz\right] \tag{2.29}$$

Consequently, the coordinates of cg of the liquid under static state, $G_o(X_{l0}, Z_{l0})$, can be derived from:

$$X_{l0} = 0; \quad Z_{l0} = \frac{M_z}{A_f} \tag{2.30}$$

where (i) is the number of the segment of intersection of the liquid free surface with the tank.

2.3.1 Formulation for the CG Coordinates under a Constant Deceleration

Assuming inviscid fluid flow and negligible contribution due to slosh frequency, the gradient of the fluid bulk subject to a uniform deceleration a_x can be derived from [9]:

$$\theta = \tan^{-1}(a_x / g) \tag{2.31}$$

where θ is the gradient of the free surface, as shown in Figure 2.6, for a particular segment.

The equation of the inclined free surface of the liquid cargo due to vehicle longitudinal deceleration can be expressed in terms of its gradient and the longitudinal coordinate, as [4]:

$$h = \tan(a_x / g)x + h_0 \tag{2.32}$$

where h_0 represents the intercept of the liquid surface with the Z axis.

The calculation of h_0 is based on the assumption of the constant volume of liquid under both static and deformed states. The free surface may assume different configuration depending upon the fill height h_0, as shown in Figure 2.7, the submerged surface can be classified into three patterns: 1) A-B-6-D-F-F'-E-1-C-A; 2) C- D-F-F'-E-1-C; and 3): E-F-F'-E, as illustrated in Figure 2.7. For the first pattern, the volume and the mass moment of inertia of the liquid is equal to the sum of half the tank volume, volume and moment of liquid segments B'-B-6-1-B', and partly filled part A-B-B'-C-A.

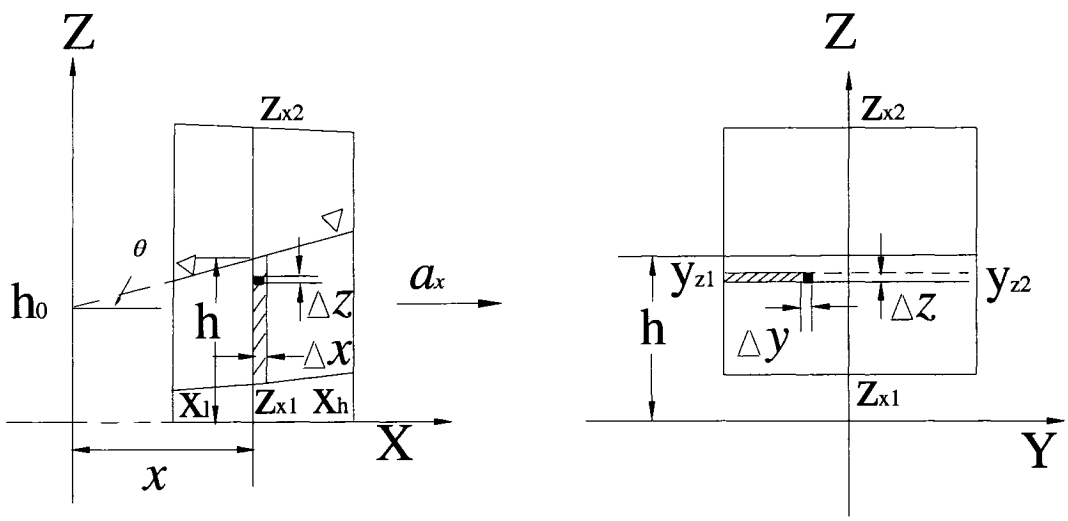

Figure 2.6: The free surface of a liquid element during a constant deceleration.

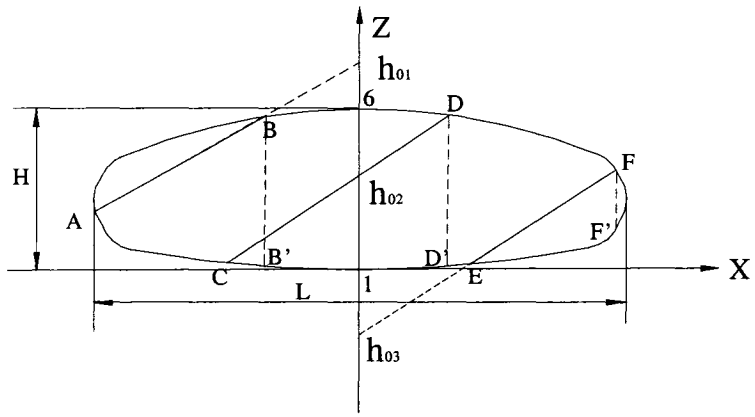

Figure 2.7: Free surface patterns in the pitch plane

In the second pattern, the volume and the mass moment of inertia of the liquid consist of three parts: C-h_{02}-1-B'-C, 1-h_{02} D-D'-1-h_{02}, and D-F-F'-E-D'-D. The volume and the mass moment of inertia of the third pattern includes the region of E-F-F'-E. As illustrated in Figure 2.7, the pattern 3 could cause considerable cg shift in the longitudinal direction under the application of a deceleration. The fill conditions corresponding to patterns 2 and 3, however would yield lesser degree of longitudinal load shift.

The instantaneous coordinates of the liquid bulk cg $G(X_l, Z_l)$ under application of a constant deceleration a_x, can be derived from Equation (2.20) and (2.21). The domain of area integral Q is expressed by 10 different compartments of the tank, labeled as c_j (j = 1...5) at the right side of the Z axis and (j = 10...6) at the left side of the Z axis, sequenced from left to right. The x coordinate and height of the liquid free surface h within each segment can be calculated from Equation (2.32), $h = \tan(a_x / g)x + h_0$, while the limits of integration are computed as described above from the domain Q. Thus the area of liquid in each compartment in a partly filled tank can be calculated from:

$$A_k = \int_{X_{l(k)}}^{X_{h(k)}} \int_{Z_{xl(k)}}^{Z_h} dzdx \qquad (2.33)$$

The total area of liquid in a partly filled tank is computed from summation over the 10 compartments:

$$A_f = \sum_{k=1}^{10} \int_{X_{l(k)}}^{X_{h(k)}} \int_{Z_{xl(k)}}^{Z_h} dz dx \tag{2.34}$$

Where $X_{h(k)}$ and $X_{l(k)}$ are maximum and minimum longitudinal coordinates of the compartment k along the X axis.

The moments of liquid within each compartment about the X and Z axes are expressed by:

$$M_{xk} = \int_{X_{l(k)}}^{X_{h(k)}} \int_{Z_{xl(k)}}^{Z_h} x dz dx; \quad M_{zk} = \int_{X_{l(k)}}^{X_{h(k)}} \int_{Z_{xl(k)}}^{Z_h} z dz dx; \tag{2.35}$$

The total moment of liquid along X and Z axes are calculated from:

$$M_x = \sum_{k=1}^{10} M_{xk}; \quad M_z = \sum_{i=1}^{10} M_{zk}; \tag{2.36}$$

Finally, the instantaneous coordinates of the liquid bulk cg under the application of a braking deceleration a_x, $G(X_l, Z_l)$, can be expressed as:

$$X_l = \frac{M_x}{A_f}; \quad Z_l = \frac{M_z}{A_f} \tag{2.37}$$

2.4 Target Parameters and Results

The generic tank geometry is used to define target design parameters that would yield minimal longitudinal load shift under a constant deceleration. Four different minimization functions are formulated to determine the optimal parameters of the longitudinal-section of the tank in the two-dimensional model. These are based upon minimization of: (*i*): longitudinal load shift; (*ii*): vertical load shift; (*iii*) overall cg height;

and (*iv*): weighed sum of vertical and longitudinal load shifts. The first optimization function, $U_x(\chi)$, is formulated based upon the longitudinal load shift alone, corresponding to a particular liquid fill volume ratio β, defined as the ratio of the wetted longitudinal-sectional area to the total longitudinal sectional area (A_f / A_l). The contribution due to the shift in the vertical coordinate of the cg is considered negligible, such that:

$$U_x(\chi) = \min(\Delta X_{a_x \beta}) \tag{2.38}$$

Where $\Delta X_{a_x \beta}$ is the longitudinal shift of the cargo cg under a straight line braking deceleration a_x and the specified fill ratio β, χ represents the vector of design variables. As described in section 2.2.1, a generic tank geometry can be uniquely described by eight independent variables, i.e., $\chi = \{H, L, R_2, R_3, R_4, Z_3, Z_4, Z_{c3}\}^T$, where '^{T}' indicates the transpose.

The optimization problem, subject to constraints imposed by the perimeter, overall width and height, is solved using a MATLAB function under the constraint imposed by the current regulations. These constraints are further summarized below:

Overall height, H≤ 2.04 m

Overall width = 2.44 m

Perimeter≤ 6.63 m

Tank surface area ≤103.52 m^2

Volume = 47.674 m^3

Maximum length ≤ 16.20 m

Minimum radius ≥ 0.39 m

The solutions are obtained for different fill levels ($0.4 \leq \beta \leq 0.9$) and acceleration magnitudes ranging from 0.3 to 0.7g. Table 2.1 summarizes the design parameters

derived corresponding to each fill level and acceleration magnitude that would yield minimal longitudinal load shift. Figure 2.8 illustrate the trajectories of longitudinal coordinate of the cargo cg (Δx) as a function of the fill ratio β and the deceleration magnitude. The results clearly show larger shift corresponding to lower fill ratios, while the change in the load shift increases only slightly as the deceleration magnitude is increased beyond 0.3 g. The results further show that the blend radii R_2 and R_4 converge towards their minimum value of 0.39 m. The radius of arc at the extremity, R_3, also converges to its minimum to limit the load shift along the longitudinal direction. These three radii converge to their minimum values, irrespective of the fill and acceleration levels. The bottom arc radius R_1 converges to values in the 41.9 to 45.4 m range, depending upon the fill ratio, while the effect of acceleration is relatively small. A larger fill volume tends to converge towards a higher bottom radius. The radius of the top arc also converges to a narrow range of 20.8 m to 25.2 m over the entire range of fill ratio and acceleration levels considered.

The movement of the free surface under application of a constant deceleration also causes changes in the vertical coordinate of the cargo. A second minimization problem is formulated and solved to minimize the shift in the vertical direction (ΔZ), while subject to identical constraints as described for the previous minimization function. The optimization function corresponding to a given condition (fill level and deceleration) is formulated as:

$$U_z(\chi) = \min(\Delta Z_{a_x \beta}) \tag{2.39}$$

Where $\Delta Z_{a_x \beta}$ is the cg shift in vertical direction corresponding to given acceleration a_x and fill ratio β.

Table 2.1 The optimal design parameters identified upon minimization of cg shift in the longitudinal direction under varying levels of fill and acceleration.

β	a_x (m/s^2)	ΔX(m)	H(m)	L(m)	R_1(m)	R_2(m)	R_3(m)	R_4(m)	R_5(m)
0.4	0.3	2.494	2.040	12.480	41.899	0.390	0.390	0.390	20.770
0.4	0.4	2.570	2.040	12.479	42.037	0.390	0.390	0.390	20.876
0.4	0.5	2.646	2.040	12.478	42.178	0.394	0.390	0.390	20.977
0.4	0.6	2.682	2.040	12.477	42.203	0.399	0.390	0.390	20.979
0.4	0.7	2.748	2.040	12.629	43.204	0.390	0.390	0.390	21.509
0.5	0.3	2.023	2.040	12.477	42.309	0.390	0.390	0.390	20.935
0.5	0.4	2.130	2.040	12.481	42.655	0.390	0.415	0.390	20.962
0.5	0.5	2.186	2.038	12.489	40.218	0.390	0.390	0.390	21.555
0.5	0.6	2.203	2.038	12.532	37.986	0.390	0.390	0.390	22.021
0.5	0.7	2.231	2.040	12.583	36.207	0.390	0.390	0.390	22.328
0.6	0.3	1.638	2.040	12.596	43.163	0.390	0.390	0.390	21.347
0.6	0.4	1.733	2.040	12.615	43.304	0.390	0.390	0.390	21.414
0.6	0.5	1.784	2.040	12.627	43.393	0.390	0.390	0.390	21.458
0.6	0.6	1.793	2.040	12.478	42.318	0.390	0.390	0.390	20.940
0.6	0.7	1.798	2.040	12.478	42.318	0.390	0.390	0.390	20.940
0.7	0.3	1.250	2.040	12.626	43.071	0.390	0.390	0.390	21.525
0.7	0.4	1.313	2.040	12.478	42.151	0.390	0.390	0.390	20.979
0.7	0.5	1.352	2.040	12.479	42.014	0.390	0.390	0.390	21.011
0.7	0.6	1.373	2.040	12.479	42.014	0.390	0.390	0.390	21.011
0.7	0.7	1.390	2.040	12.478	42.147	0.390	0.390	0.390	20.980
0.8	0.3	0.863	2.040	12.590	42.951	0.390	0.390	0.390	21.363
0.8	0.4	0.920	2.040	12.602	43.040	0.390	0.390	0.390	21.406
0.8	0.5	0.947	2.040	12.609	43.083	0.390	0.390	0.390	21.430
0.8	0.6	0.960	2.040	12.612	43.104	0.390	0.390	0.390	21.444
0.8	0.7	0.974	2.040	12.615	43.123	0.390	0.390	0.390	21.451
0.9	0.3	0.487	1.946	12.930	45.419	0.390	0.390	0.390	25.213
0.9	0.4	0.507	1.968	12.840	44.788	0.390	0.390	0.390	24.200
0.9	0.5	0.522	1.976	12.810	44.563	0.390	0.390	0.390	23.823
0.9	0.6	0.527	1.982	12.791	44.430	0.390	0.390	0.390	23.590
0.9	0.7	0.532	1.985	12.781	44.357	0.390	0.390	0.390	23.461

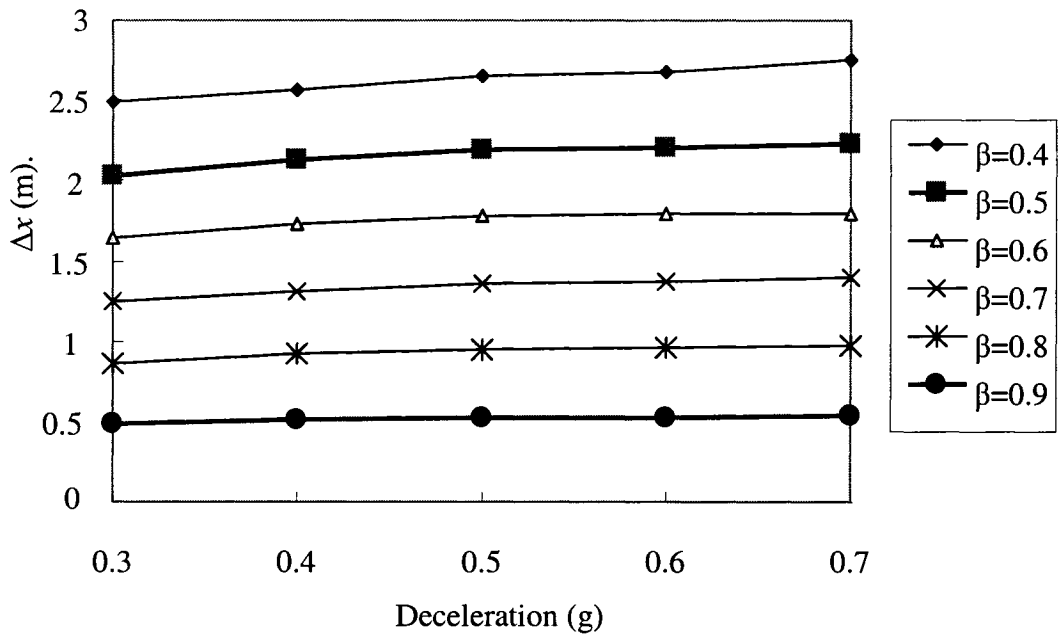

Figure 2.8: Shift in the longitudinal coordinate of the cargo cg as functions of the fill ratio and deceleration magnitude

Table 2.2 summaries the design parameters derived from the solution of Equation (2.39) corresponding to different fill ratios and deceleration magnitudes. Figure 2.9 illustrates the variation in ΔZ with varying fill condition and deceleration magnitudes.

The results show that a lower fill volume yields higher vertical cg shift, which tends to increase with increasing deceleration level. The magnitudes of the vertical shifts, however, are significantly smaller than those in the longitudinal direction. While the blend radii, R_2 and R_4, converge to the minimal value of 0.39m as observed in the previous case, the other design parameters are significantly different from those identified upon minimization of the longitudinal load shift (ΔX). Both the top and bottom radii, R_1 and R_5, converge to significantly higher values, resulting in relatively flat bottom arc. The end cap radius, R_3, is also larger than that derived from minimization of ΔX. The results further show that the optimal solution is strongly dependent upon the fill ratio and only

marginally dependent upon the deceleration magnitude.

Considering that the roll and yaw stability limits of heavy vehicles are most strongly affected by the cg height, a tank geometry that yields lower overall cg height would be beneficial to enhance the stability limits. A third optimization is thus formulated to seek longitudinal-section geometry that would yield lower overall cg height for different fill conditions and deceleration levels. The initial height of the cg in this case is determined from the fill level, and the initial tank design parameters. The optimization function is formulated as:

$$U_{zcg}(\chi) = \min(Z_{cga_x,\beta}) \tag{2.40}$$

Where $Z_{cgax,\beta}$ is the overall cg height corresponding to a static fill ratio β and deceleration a_x.

The optimization problem, subject to identical constraints, is solved to determine the optimal design variables corresponding to fill ratio ranging from 0.1 to 0.9. The results summarized in Table 2.3 show that the arc radii converge to considerably different values. The optimal solutions are strongly dependent upon the operating conditions, i.e.,deceleration and fill level. Each solution is thus considered suitable for a particular condition. From a practical point of view, a compromise solution is desired for the operating conditions encountered in general transportation.

It should be pointed out that the shape of the optimal tank will depend on the optimization objective. As an example, Figure 2.10 illustrates the optimal solutions for $\beta = 0.8$ and $a_x = 0.6$, derived from the three minimization functions. A tank with a smaller length would yield lower longitudinal load shift (ΔX), which would also yield higher tank to satisfy the volume constraint and thus higher Z_{cg}. The minimal vertical cg shift

Table 2.2 The optimal design parameters identified upon minimization of cg shift in the vertical direction under varying fill levels and deceleration magnitudes

β	a_x(m/s^2)	Zcgo(m	ΔZcg(m)	H(m)	L(m)	R_1(m)	R_2(m)	R_3(m)	R_4(m)	R_5(m)
0.4	0.3	0.440	0.279	1.796	13.153	65.792	0.390	0.518	0.390	38.406
0.4	0.4	0.435	0.319	1.785	13.114	70.340	0.390	0.540	0.390	40.036
0.4	0.5	0.432	0.346	1.776	13.111	73.467	0.390	0.553	0.390	41.479
0.4	0.6	0.430	0.366	1.772	13.104	75.127	0.390	0.559	0.390	42.038
0.4	0.7	0.427	0.376	1.767	13.101	77.214	0.390	0.567	0.390	42.904
0.5	0.3	0.497	0.247	1.752	13.062	86.632	0.390	0.577	0.390	45.481
0.5	0.4	0.498	0.274	1.745	13.054	90.192	0.390	0.594	0.390	47.002
0.5	0.5	0.491	0.301	1.735	13.053	94.570	0.390	0.612	0.390	49.305
0.5	0.6	0.492	0.310	1.736	13.043	94.623	0.390	0.616	0.390	48.882
0.5	0.7	0.490	0.322	1.733	13.043	96.308	0.390	0.620	0.390	49.498
0.6	0.3	0.546	0.205	1.665	13.049	140.794	0.394	0.708	0.420	73.542
0.6	0.4	0.540	0.230	1.638	13.058	169.795	0.397	0.744	0.429	91.078
0.6	0.5	0.535	0.245	1.624	13.062	188.110	0.400	0.763	0.434	104.420
0.6	0.6	0.532	0.255	1.614	13.066	201.561	0.401	0.777	0.437	116.590
0.6	0.7	0.530	0.261	1.607	13.068	213.243	0.403	0.786	0.440	127.070
0.7	0.3	0.635	0.134	1.721	13.029	124.113	0.390	0.687	0.409	56.446
0.7	0.4	0.635	0.156	1.785	13.042	154.303	0.390	0.734	0.418	50.613
0.7	0.5	0.638	0.169	1.684	13.040	121.968	0.390	0.687	0.418	65.433
0.7	0.6	0.632	0.171	1.710	13.025	122.295	0.390	0.682	0.407	57.688
0.7	0.7	0.632	0.169	1.710	13.027	126.863	0.390	0.691	0.409	58.535
0.8	0.3	0.715	0.088	1.725	13.013	102.122	0.390	0.641	0.405	52.168
0.8	0.4	0.714	0.104	1.721	13.015	104.266	0.390	0.647	0.406	53.414
0.8	0.5	0.715	0.108	1.723	13.015	103.030	0.390	0.644	0.406	52.905
0.8	0.6	0.714	0.110	1.720	13.016	104.537	0.390	0.648	0.407	53.756
0.8	0.7	0.714	0.110	1.720	13.016	104.537	0.390	0.648	0.407	53.756
0.9	0.3	0.772	0.038	1.720	13.009	103.788	0.390	0.646	0.407	52.918
0.9	0.4	0.792	0.045	1.725	13.008	103.520	0.390	0.643	0.405	52.214
0.9	0.5	0.794	0.051	1.729	13.008	101.049	0.390	0.638	0.404	51.145
0.9	0.6	0.795	0.057	1.734	13.007	98.730	0.390	0.632	0.402	50.024
0.9	0.7	0.796	0.056	1.735	13.007	97.958	0.390	0.630	0.402	49.737

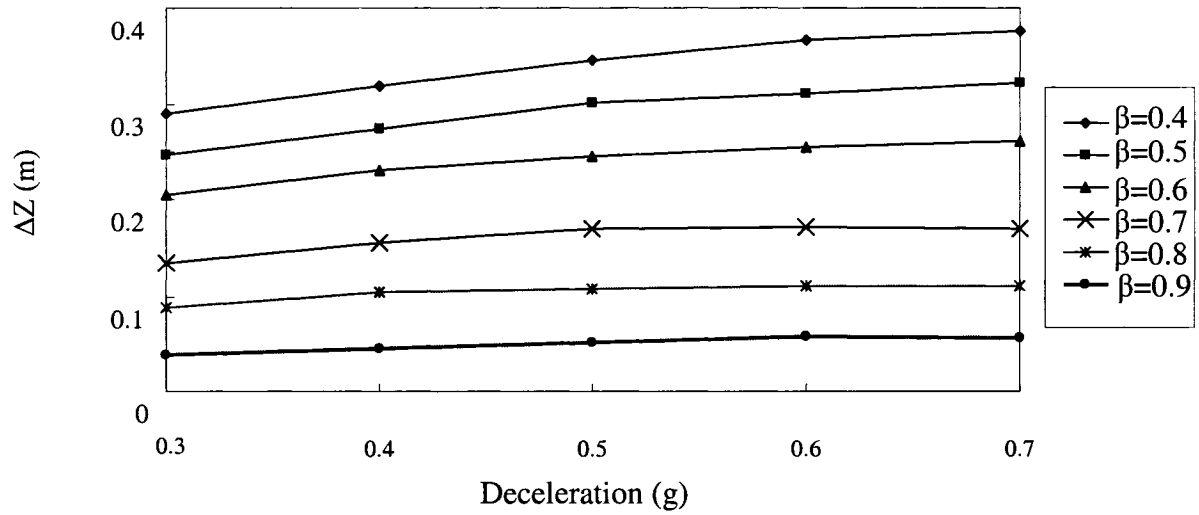

Figure 2.9: Shift in the vertical coordinate of the cargo cg as functions of the fill ratio and deceleration magnitude

and the overall cg height, on the other hand, could be realized by a longer and flat tank. The optimization problem is solved subject to identical constraints and different values of weighting factors, while the magnitude of deceleration is hold constant at 0.6g. This magnitude would represent the typical straight-line braking deceleration of tank trucks under driving condition.

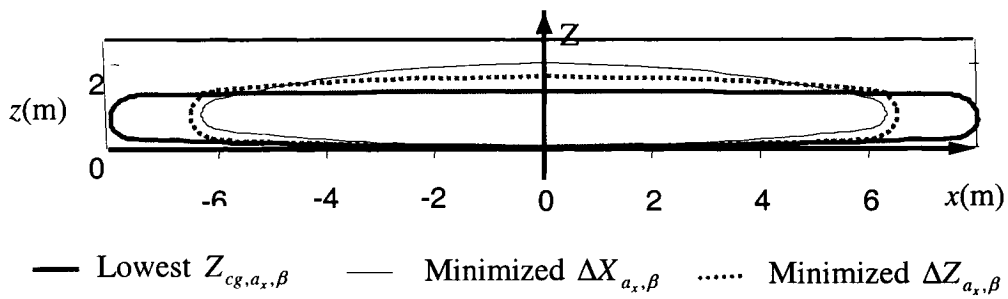

Figure 2.10: Comparisons of pitch-plane cross-section realized from three different minimization objections. (β =0.8, a_x = 0.6g)

Table 2.3 The optimal design parameter identified upon minimization of cg height under static condition.

β	Z_{cg} (m)	H(m)	L(m)	R_1(m)	R_2(m)	R_3(m)	R_4(m)	R_5(m)
0.1	0.092	1.437	15.955	77.530	0.390	0.485	0.390	158.251
0.2	0.177	1.425	15.961	80.417	0.390	0.505	0.390	178.140
0.3	0.257	1.410	15.966	91.390	0.390	0.530	0.390	177.463
0.4	0.327	1.397	15.971	99.412	0.396	0.550	0.390	193.259
0.5	0.393	1.382	15.976	109.063	0.414	0.566	0.390	221.318
0.6	0.456	1.368	15.981	119.596	0.429	0.580	0.390	254.954
0.7	0.508	1.357	15.986	131.652	0.443	0.592	0.390	277.092
0.8	0.570	1.348	15.991	142.875	0.454	0.601	0.390	323.950
0.9	0.633	1.350	15.993	161.938	0.461	0.592	0.390	249.746

The fourth optimization problem is thus formulated based upon the weighted sum of both the primary contributing factors at a particular fill volume, namely ΔX and ΔZ. Considering that the ΔX and ΔZ strongly depend upon the overall dimension of the tank, the dynamic load shifts along the two axes are normalized with respect to those encountered for a conventional cylindrical tank of identical volume, but corresponding to same fill and deceleration levels. The minimization problem is thus formulated as:

$$U_{xz}(\chi) = \min(\lambda_1 \frac{\Delta X_{a_x,\beta}}{\Delta X^*_{a_x,\beta}} + \lambda_2 \frac{\Delta Z_{a_x,\beta}}{\Delta Z^*_{a_x,\beta}}) \tag{2.41}$$

Where $\Delta X^*_{a_x,\beta}$ and $\Delta Z^*_{a_x,\beta}$ are the longitudinal and vertical shifts, respectively, for a uniform cylindrical tank corresponding to deceleration a_x and fill ratio β . λ_1 and λ_2 are the weighting factors, such that $\lambda_1 + \lambda_2 = 1$. A higher value of λ_1 would emphasize the contribution of ΔX , while λ_2 relates to the relative contribution of ΔZ. The optimal tank geometry with the different longitudinal sections can be obtained by setting various combinations of λ_1 and λ_2. While a higher value of λ_2 can lead to the optimal design with

low cg shift in vertical direction, larger values of λ_1 yields to smaller cg shift in the longitudinal direction.

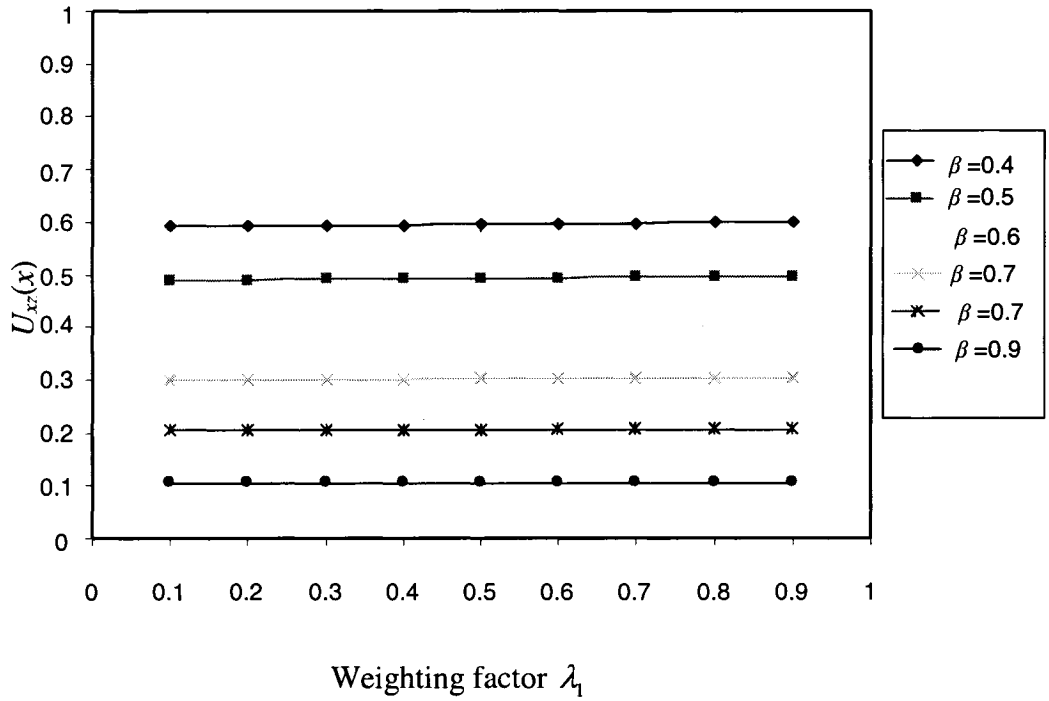

Figure 2.11: The optimal coefficient trajectories of cg shift corresponding to the weighting factors (a_x = 0.6g)

Figure 2.11 illustrates the optimal solution for minimization problem involving weighted sum of both the longitudinal and vertical cg shifts under a deceleration of 0.6g and different fill conditions, with respect to those encountered for a conventional cylindrical tank of identical volume. The results suggest that under a_x = 0.6g, the minimization function in insensitive to λ_1. A higher fill ratio yields a lower value of $U_{xz}(\chi)$, which suggests that the optimal geometry can effectively limit the cg shifts in both the longitudinal and vertical axes.

2.5 Summary

A longitudinal section of a generic tank is characterized by 8 circular arcs, which yields a total of 8 independent design variables. The cg coordinates of the partly-filled generic tank are formulated from its geometry and the equation of the free-surface derived assuming kineto-static motion of the fluid bulk. Four different optimization problems are formulated and solved to identify an optimal tank geometry that would yield minimal longitudinal load shift and cg height.

CHAPTER 3 DEVELOPMENT AND ANALYSIS OF GENERALIZED THREE DIMENSIONAL MODELS

3.1 Introduction

The pitch and roll moments caused by the shift in the cg coordinates and the corresponding variations in the mass moments of inertia of liquid in a partially filled tank, are the essential parameters related to the safety dynamics of a party-filled tank vehicle and thus the tank design. These parameters directly affect the vehicle directional and stability performance of the vehicle under braking and steering maneuvers [2, 10, 30, 80-81]. Tank vehicles employ tanks of uniform cross-sections along the longitudinal axis to facilitate the fabrication. These tanks also utilize curved end caps, while the cross-section may vary from circular to modified-oval shapes. It has been shown that tank cross-section in the roll plane directly influences the vehicle roll stability. On the basis of relative merits and limitations of different cross-sections, an optimal cross-section in the roll plane has been proposed to enhance the vehicle roll-stability limits [5, 26, 28, 30].

The load shift in the longitudinal plane and thereby the braking performance of the vehicle could be limited by defining tank geometry in the longitudinal plane that would limit the braking-induced fluid motion, as discussed in the previous chapter. The addition of baffles within the tank also limits the longitudinal fluid slosh. Clean-bore tanks, employed in transportation of general purpose liquid bulks, however, yield excessive load shift in the longitudinal plane under the application of braking. The cargo load shift under such conditions could be limited by employing alternate non-uniform longitudinal section of the tank. A generic section tank geometry is formulated by sections, integrated the roll as well as pitch proposed in the previous chapter. The

methodologies described in [7, 9, 26, 61, 72] are applied to derive an optimal tank geometry in both the longitudinal and lateral planes of the tank.

3.2 The Generalized Tank Geometry in the Roll and Pitch Planes

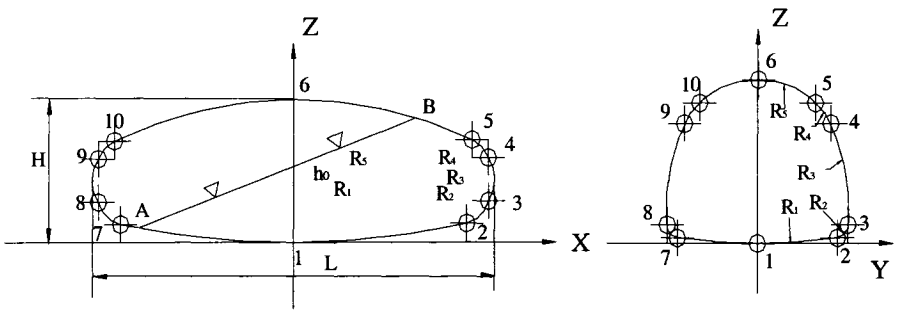

(a) longitudinal section (b) lateral section

Figure 3.1: Illustration of 8 circular arcs of the proposed tank in the longitudinal and lateral section

The proposed generic longitudinal section of the tank, described in the previous chapter, is extended to incorporate a similar generic section in the lateral plane, as proposed by Kang et al. [30]. The resulting generic tank geometry can thus be observed as a combination of eight circular arcs symmetric about the vertical axis in each of the lateral and longitudinal planes. These cross-sections are considered to be sufficiently general to describe many possible tank shapes. As illustrated in Figure 3.1, the bottom arc (R_1) and top arc (R_5) of the liquid tank will play a dominant role in determining the dynamic performances of the liquid tank. The other three arcs R_2, R_3, and R_4, form the

end caps in the longitudinal plane, and the side walls in the lateral plane. The proposed generalized section could be manipulated to derive different tank designs. A longitudinal section with $R_1 = R_2 = R_3 = R_4 = R5 = \infty$ coupled with a lateral section $R_1 = R_2 = R_3 = R_4 = R_5$ would yield a conventional cylindrical tank. The same longitudinal section coupled with a lateral section, where $R_1 = R_5$ and $R_2 = R_4$ would yield a modified oval tank. In this study, five different geometries are realized to investigate the dynamic load shifts and the directional dynamic responses of a party-filled tank vehicle. These five geometrics are derived from the following cases and as shown in Figure 3.2.

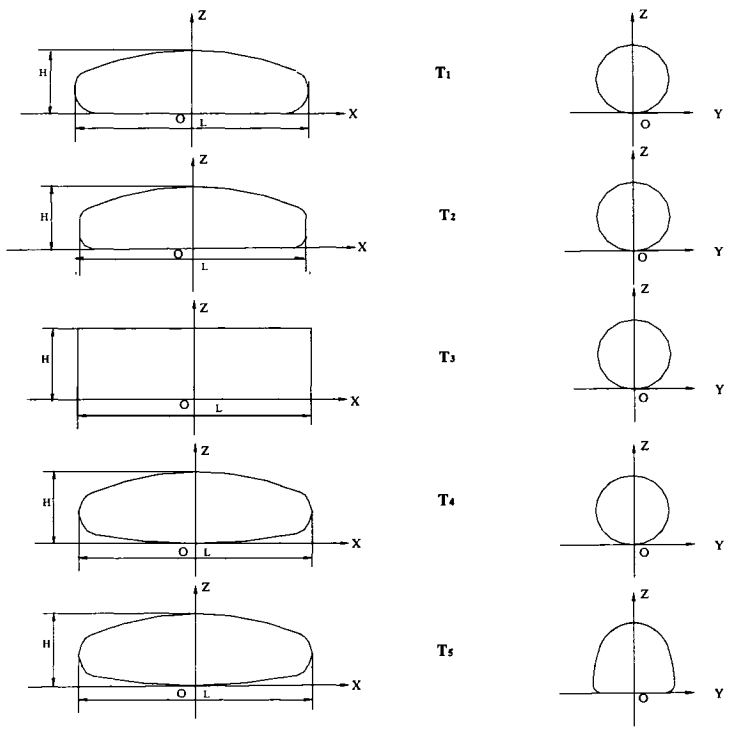

Figure 3.2: An illustration of five tank geometries considered for analyses

Case I: $R_1 = \infty$ and $R_4 = 0$ in the longitudinal plane (point 4 and 5 coincide) coupled with a circular roll-plane section (T_1).

Case II: $R_1 = R_3 = \infty$ in the longitudinal plane coupled with a circular roll-plane

section (T_2).

Case III: $R_1 = R_2 = R_3 = R_4 = R5 = \infty$ in the longitudinal plane coupled with a circular roll-plane section (T_3).

Case IV: All the radii in the longitudinal plane are permitted to vary, with a circular roll plane cross-section (T_4).

Case V: All the radii in both the planes are permitted to vary (T_5).

3.3 Free Surface Gradient

The magnitude of liquid motion within a tank depends on the tank construction, the fill level, and the gradient of the free surface caused by angular motions of the tank (roll and pitch) and lateral and longitudinal acceleration. The lateral and longitudinal load transfer levels of the vehicle are significantly affected by the tank geometry [21]. Assuming steady-state condition, the entire fluid bulk in the tank trailer is considered to move as a rigid body. The vehicle roll and pitch motions coupled with accelerations cause the motion of the free surface of liquid, as shown in the longitudinal and lateral planes in Figure 3.3. The center of mass of the liquid experiences a shift due to the motion of the free surface of the liquid, and thus a load transfer occurs in both planes.

The gradient of the free surface can be determined assuming inviscid fluid motion due to the pressure variations in a static fluid. The pressure variation, dP at the center of an element of the liquid bulk in the tank-fixed coordinate system, $XYZO$, can be expressed as:

$$dP = \frac{\partial P}{\partial x}dx + \frac{\partial P}{\partial y}dy + \frac{\partial P}{\partial z}dz \tag{3.1}$$

where P is the fluid pressure.

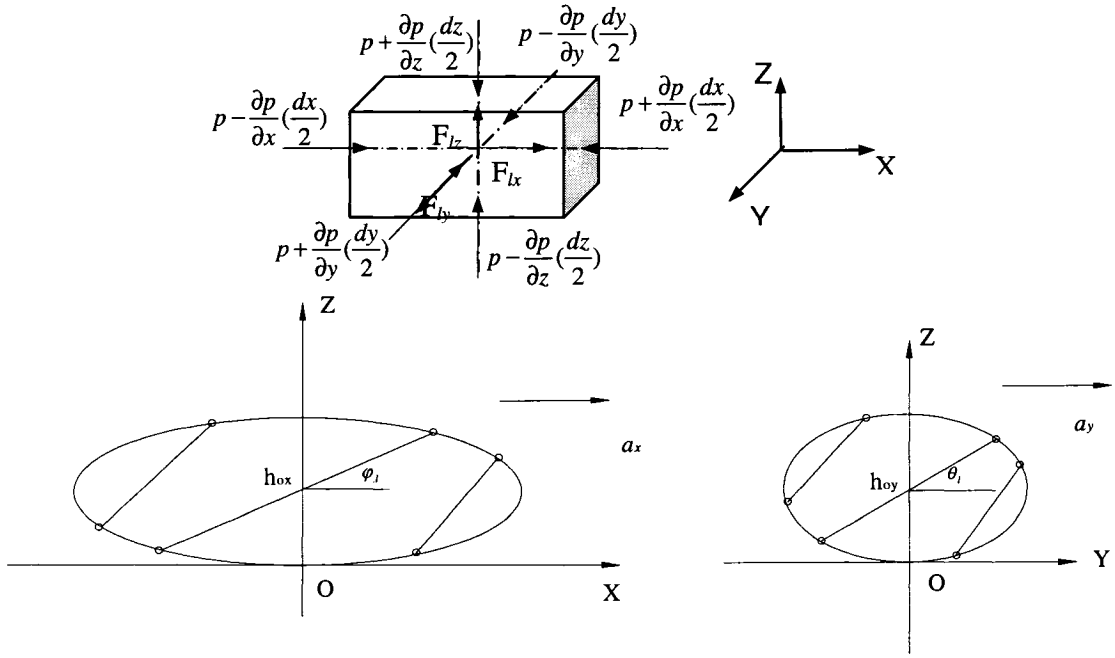

Figure 3.3: Liquid free surface gradient in the longitudinal and lateral planes and force acting on a fluid element

The forces acting on the element can be expressed by the following equilibrium Equations [32]:

$$\frac{1}{\rho}\frac{\partial P}{\partial x} = F_{lx};\ \frac{1}{\rho}\frac{\partial P}{\partial y} = F_{ly};\ and \frac{1}{\rho}\frac{\partial P}{\partial z} = F_{lz} \tag{3.2}$$

Where F_{lx}, F_{ly} and F_{lz} represent the body forces per unit mass of the liquid element along the *OX*, *OY* and *OZ* directions, respectively, and ρ is the mass specific weight of the liquid cargo. Equations (3.1) and (3.2) yield the following expression for the pressure differential of the element:

$$dP = \rho(F_{lx}dx + F_{ly}dy + F_{lz}dz) \tag{3.3}$$

The pressure differential *dP* at the free surface must vanish. Equation (3.3) thus

reduces to:

$$F_{lx}dx + F_{ly}dy + F_{lz}dz = 0 \tag{3.4}$$

The above equation can be expressed as:

$$F_{lx}x + F_{ly}y + F_{lz}z = c_0 \tag{3.5}$$

Where c_0 is a constant.

The coordinates of the mass of fluid in a roll plane could be expressed as:

$$y = \frac{(c_0 - F_{lx}x - F_{lz}z)}{F_{ly}};\ z = \frac{(c_0 - F_{lx}x - F_{ly}y)}{F_{lz}} \tag{3.6}$$

Under the application of a lateral acceleration alone ($F_{lx} = 0$), Equation (3.1) can be simplified as [28, 31]:

$$\frac{1}{\rho}\frac{\partial P}{\partial y} = F_{ly} = a_{ly}\cos\theta_{s2} + \sin\theta_{s2} \tag{3.7}$$

$$\frac{1}{\rho}\frac{\partial P}{\partial z} = F_{lz} = -a_{ly}\sin\theta_{s2} + \cos\theta_{s2} \tag{3.8}$$

Where a_{ly} is the lateral acceleration (in g unit) imposed on the fluid due to the centrifugal acceleration of tank, and θ_{s2} is the tank roll angle.

The gradient of the free surface of liquid thus is derived as:

$$\tan\theta_l = -\frac{dz}{dy} = \frac{\partial P/\partial y}{\partial P/\partial z} \tag{3.9}$$

where θ_l is the free surface gradient in the roll plane.

Substitute Equation (3.6) to (3.9) yield following expression for the lateral coordinate of the cargo cg, where (F_{lx}=0):

$$y = \frac{a_{ly} + \tan\theta_{s2}}{1 - a_{ly}\tan\theta_{s2}}z + \frac{c_0}{1 - a_{ly}\tan\theta_{s2}} \tag{3.10}$$

Under the application of a pure braking or acceleration maneuver (F_{ly}=0), Equations (3.1) to (3.5) can be solved to yield the longitudinal coordinate of cargo cg:

$$x = \frac{a_{lx} + \tan\varphi_{s2}}{1 - a_{lx}\tan\varphi_{s2}} z + \frac{h_{0x}}{1 - a_{lx}\tan\varphi_{s2}} \tag{3.11}$$

Where a_{lx} is the longitudinal acceleration or deceleration, φ_{s2} is the pitch angle of the tank, h_{0x} is the intercept of liquid free surface with the X-axis, as shown in Figure 3.3.

For small roll angle and free surface gradient, the relationship (3.10) reduces to a simplified form similar to that developed by Rakheja et al. [4]:

$$f_s(z) = \frac{a_{ly} + \theta_{s2}}{1 - a_{ly}\theta_{s2}} z + h_{0y} \tag{3.12}$$

Where the constant term $h_{0y} = \frac{c_0}{1 - a_{ly}\theta_{s2}}$, represents the interception of the liquid free surface with the Z-axis in the roll plane.

In the pitch plane, Equation (3.11) can be reduced to an expression similar to that developed by Rakheja et al. [81] and Ranganathan et al. [82]. Considering that the pitch angle of heavy vehicles is significantly smaller than the roll angle, further simplification involving $\varphi_{s2} \approx 0$, yields

$$f_s(x) = a_{lx}x + h_{0x} \tag{3.13}$$

3.4 Determination of Instantaneous CG Coordinates and Mass Moments of Inertia

The coordinates of the liquid cargo cg and the mass moments of inertia are strongly affected by the gradients of the free surface in both planes, tank geometry, fill condition, and magnitudes of lateral and longitudinal accelerations. Since the variation in the cg coordinates and the mass moments of inertia of the cargo directly influence the

directional dynamics of the vehicle, the essential formulations are derived to determine these parameters as a function of the fill condition, tank geometry, and magnitudes of a_{lx} and a_{ly}. Following subsections present a systematic methodology to determine the cg position and the mass moments of inertia for a generic tank geometry.

3.4.1 Possible Free Surface Patterns in the Partially Filled Liquid Tank

The analyses of the cg coordinates of the deformed fluid requires the knowledge of the fluid volume. The formulations presented in the previous chapter are thus applied in both the planes to derive the total fluid volume for a given static fill height *h*, while a_{lx} = a_{ly} =0. Under application of a longitudinal deceleration (a_{ly} =0), the fluid free surface yields two intersection points with the tank periphery in the pitch plane, as shown in Figure 3.4. The free surface of liquid in a partly-filled tank, is deflected in both the roll plane and pitch planes, when the vehicle is subject to braking and steering. Based on the position of intersection of the free surface with the *Z* axis, the patterns of liquid in the longitudinal plane could be defined in three possible categories, as shown in Figure 3.4: Pattern 1, A-B-6-D-F-F'-E-1-C-A; Pattern 2: C-h_{02}-D-F-F'-E-1-C; and Pattern 3: E-F-F'-E.

In Pattern 1, the parameters of the deflected liquid, with respect to the geometric origin of the tank, are determined from the fully filled section on the right side of B'-B and the partially filled section on the left side of B-B`. In Pattern 2, the parameters of the partly-filled liquid consist of three parts: C-$h_{02}$- 1- C, $h_{02}$-D-D`-1, and D-F-E-D`-D. In Pattern 3, Parameters of the partly-filled liquid are based on the region formed by E-F-F`-E. From the three patters considered, it is evident that the longitudinal shift and the cargo

cg is dependent upon the fill level and thus the pattern. It should be noted that many other patterns of the free surface are possible depending upon the fill height and the magnitude of deceleration. A wide range of possible patterns in the roll plane have been presented in [30].

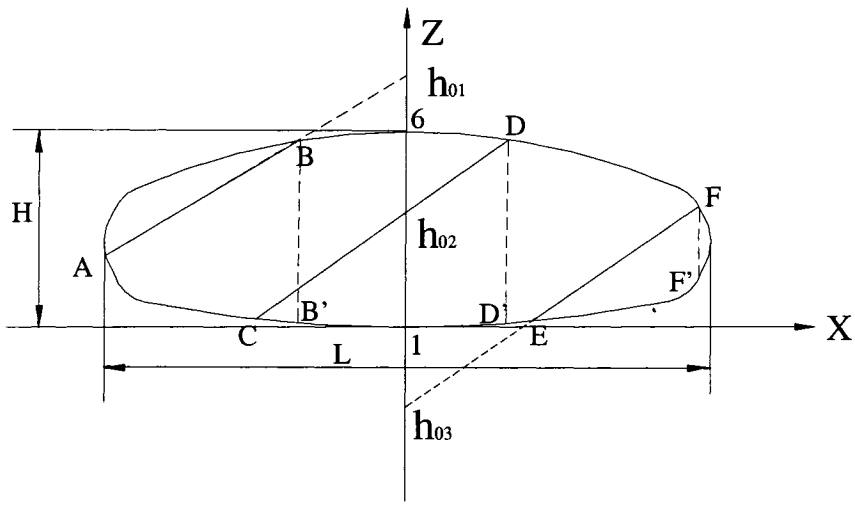

Figure 3.4: Illustration of some of the free surface patterns in the pitch plane

3.4.2 Computations of Volume and Mass Moment of Inertia

The total fluid volume, and the roll, pitch and yaw moments of the deflected liquid in a partially filled tank can be computed from the following:

$$V_f = \iiint_V dV \tag{3.14}$$

$$M_x = \iiint_V x dV \tag{3.15}$$

$$M_y = \iiint_V y dV \tag{3.16}$$

$$M_z = \iiint_V z dV \tag{3.17}$$

Where V defines the domain of the volume, and M_x, M_y and M_z are the roll, pitch and yaw moments of the fluid, respectively, about the origin.

The coordinates of the liquid cargo cg (X_l, Y_l, Z_l), depend on the fill level and free surface gradient, and are derived from:

$$X_l = \frac{1}{V_f}\iiint_V x dV;\ Y_l = \frac{1}{V_f}\iiint_V y dV;\ and\ Z_l = \frac{1}{V_f}\iiint_V z dV \tag{3.18}$$

The shifts in the coordinates of the liquid cargo cg under applications of braking and steering accelerations can be expressed as:

$$\Delta X_l = X_l;\ \Delta Y_l = Y_l;\ and\ \Delta Z_l = Z_l - Z_{l0} \tag{3.19}$$

Where Z_{l0} is the static cg theigh with respect to the origin.

The corresponding values of the mass moments of inertia are further computed from the following integrals:

$$I_{xl} = \rho\iiint_V (y^2 + z^2)dv;\ I_{yl} = \rho\iiint_V (x^2 + z^2)dv;\ \ I_{zl} = \rho\iiint_V (x^2 + y^2)dv \tag{3.20}$$

The equations of the liquid free surface in the pitch plane and the roll plane are expressed by Equation (3.11) and (3.12), respectively. The volume of fluid can be computed by considering a liquid element in the 3D space, as illustrated in Figure 3.5. The variables d_x, d_y, and d_z are the increments of volume element in the X, Y, and Z, directions respectively. The left illustration represents the volume element section of the tank in longitudinal direction; the middle and right-side illustrations represent the element in the roll planes of a circular and a generic section tank.

3.4.3 Integration Limits for the Partially Filled Tank

The integration limits for computation of the fluid volume and the mass moments of inertia in the pitch plane have been defined in section 2.4.4. The integration limits for

the roll plane can able be established in a similar manner. As illustrated in Figure 3.5, the coordinates of the limiting intersection points on the tank periphery, under static condition, (Z_{xl}, Z_{x2}, Y_{zl} and Y_{z2}) can be related to the coordinates of center of the arc containing the disc formed by the element. The vertical limits of the disc enveloping a fluid element in the roll plane are derived from the arc radii in the pitch plane upon consideration of the segment, where the disc may lie, as shown in Figure 3.5.

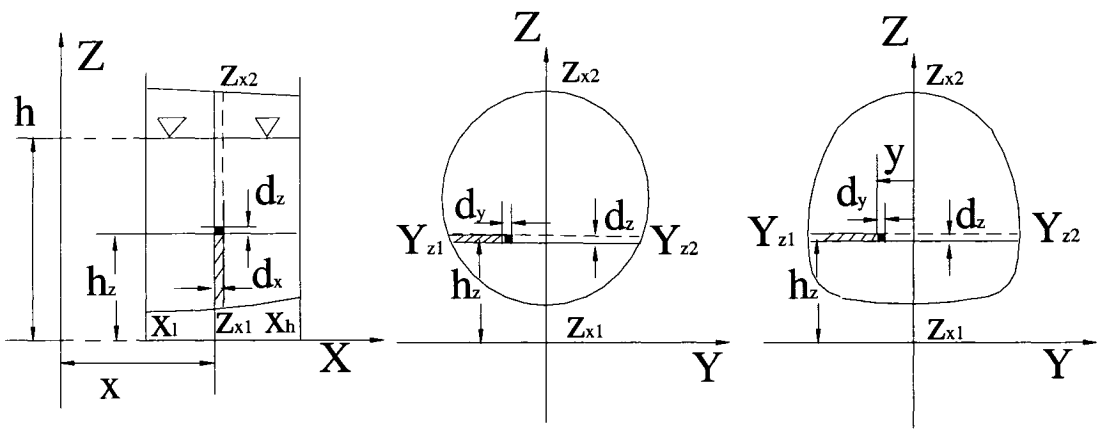

Figure 3.5: The liquid volume element in the partially-filled tank

$$Z_{x1} = ZC(il) - \sqrt{R(il)^2 - (x - XC(il))^2}\ ; \tag{3.21}$$

$$Z_{x2} = ZC(ih) + \sqrt{R(ih)^2 - (x - XC(ih))^2}\ ;\ i=1, \ldots, 5 \tag{3.22}$$

where *il* and *ih* refer to the lower and upper segments, as described in section 2.3, and $R(il)$ and $R(ih)$ refer to the respective arc radii. *ZC* and *XC* define the coordinates of the arc center, *il* and *ih*. For the circular cross-section tank, the integration limits (Y_{zl}, Y_{z2})

depend upon the radius of the circular disc $R_y(x)$, such that:

$$Y_{z1} = -\sqrt{R_y^2(x) - [h - R_y(x)]^2} \tag{3.23}$$

$$Y_{z2} = \sqrt{R_y^2(x) - [h - R_y(x)]^2} \tag{3.24}$$

For a generic cross-section in the roll plane, these limits depend upon the radius of arc intersecting the free surface and the coordinates of its center $((YC_x(i), ZC_x(i))$, such that:

$$Y_{z1} = -YC_x(i) - \sqrt{RY_x(i)^2 - (h_z - ZC_x(i))^2} \tag{3.25}$$

$$Y_{z2} = YC_x(i) + \sqrt{RY_x(i)^2 - (h_z - ZC_x(i))^2} \tag{3.26}$$

Where $YC_x(i)$ and $ZC_x(i)$ are the coordinates of the center of arc i in the roll plane, and $RY_x(i)$ is the radius of arc i.

In the above formulation, the coordinates of arcs centers vary along the X- axis. Considering the proportional change in the radii of the arcs and their center coordinates, these are computed from:

$$YC_x(i) = YC(i) \cdot \varepsilon;\ \ ZC_x(i) = ZC(i) \cdot \varepsilon;\ \ \ RY_x(i) = RY(i) \cdot \varepsilon \tag{3.27}$$

Where $YC(i)$ and $ZC\ (i)$ are the coordinates of the arcs centers for the section defined at $x = 0$, and ε is constant of proportionality, defined as section height $(Z_{x2} - Z_{x1})$ to the maximum height, H:

$$\varepsilon = \frac{Z_{x2} - Z_{x1}}{h_k} \tag{3.28}$$

Under the applications of longitudinal and lateral accelerations, the integration limits of the fluid domain vary significantly and are far more complex. The equations of the free surface of fluid in the pitch and roll planes have been defined in Equation (3.11)

and (3.12), respectively. Let h_{0x} be the height of the intersection point of the free surface at $x = 0$ in the pitch plane, and $h_{0y}(x)$ be the height of the intersection point in the roll plane section located at x. Let $h(x)$ be the free surface height in the pitch plane, as shown in Figure 3.6. Depending upon the fill level and the magnitudes of accelerations, the free surface $h(x)$ may exceed the upper bound Z_{x2} or it may be less than the lower bound Z_{x1}. The same would be applicable in the roll plane, as illustrated in Figure 3.7 for a few cases of the free surface deflections.

The volume and mass moments of inertia of the deflected fluid are computed by considering a fluid element located at a height h_z, as shown in Figure 3.6 in the pitch plane. For $h(x) > Z_{x2}$, the domain (Z_{x1}, Z_{x2}) defines the integration limit in the roll plane. For $Z_{x1} < h_{0x} \leq Z_{x2}$, the integration limit would be Z_{x1} to $h(x)$. In the roll plane, the integration limits depend upon the height of the intersection point $h_{0y}(x)$ of the free surface and the central vertical axis. For $h_{0y} > Z_{x2}$, the integration limits are (Z_{x1}, Z_{x2}) and (Y_{z1}, Y_{z2}), as shown in Figure 3.7 (b). For $Z_{x1} < h_{0y} \leq Z_{x2}$, the fluid domain is bounded by $(Z_{x1}, h_{0y}(x))$ and (Y_{z1}, Y_{z2}). For $h_{0y} > Z_{x1}$, the bounds are given by the coordinates of the intersection points with the tank periphery (Z_{x1}, Z_{x2}) and (Y_{z1}, Y_{z2}).

3.5 Identification of Optimal Longitudinal Sections

Optimal longitudinal section of the generic tank is identified using the five different cases described in section 3.2, while the optimal roll cross-section defined in [30] is considered for the cases involving generic cross-section. The minimization problem, defined in section 2.4, is used to identify optimal longitudinal section to realize minimal longitudinal load shift:

$$U_x(\chi) = \text{Minimize}(\Delta X)_{a_x\beta} \tag{3.29}$$

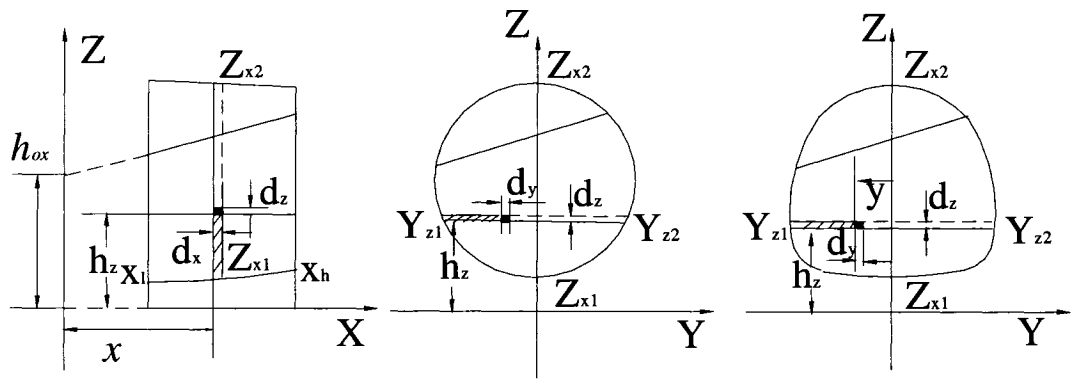

Figure 3.6: The integration limits of the fluid domain in the pitch and roll planes.

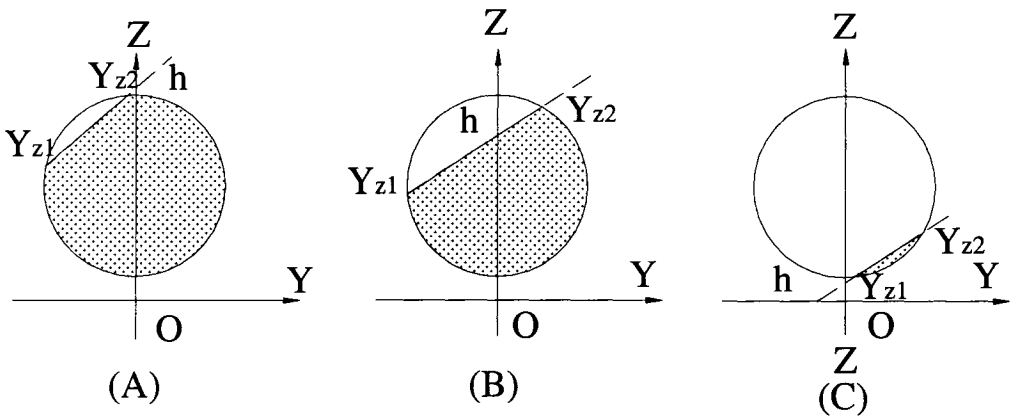

Figure 3.7: The integration boundaries of the fluid domain in the roll plane.

The above minimization problem is subject to the constraints imposed on the total volume and the perimeter, as described in section 2.4, while the tank length is limited to a maximum of 16.02 m. Moreover, the lateral cross-section of the tank in each case is

related to the longitudinal section parameters. For configurations T_1 to T_4, the maximum diameter in the roll plane is equal to the maximum tank height. For the T_5 configuration, the peak design parameters for the related section are taken as those reported by Kang [30]. These parameters are varied proportionally along the x-axis. Moreover, the configuration T_3 represents the conventional circular cross-section tank. This configuration is thus considered as the reference and is not subjected to the minimization. The solution of the minimization problem, yields the design parameters that are listed in Table 3.1 for the five cases considered. (excluding T_3).

Table 3.1 Optimal design parameters of the longitudinal section

Configuration	Parameters (m)						
	R_1	R_2	R_3	R_4	R_5	H	L
T_1	∞	0.584	1.39	0	1033.48	2.04	15.63
T_2	∞	0.39	∞	0.79	1108.03	2.04	14.89
T_4	6251.78	0.39	5.39	0.39	529.70	2.04	15.33
T_5	2130.20	1.39	5.39	0.39	439.17	2.04	15.83
T_3	∞	∞	∞	∞	∞	2.04	14.63

As illustrated in Table 3.1, some similar characteristics of the optimal design parameters appear for configuration T_1, T_2, T_4 and T_5 in the longitudinal section: the overall length of optimal tanks are longer than T_3 because of the varying cross-section along the longitudinal direction. The heights of these tanks are identical as 2.04 m, while the top and bottom arcs of the tanks assume larger volumes, and the end arcs R_2, R_3 and R_4 are relatively small. It is noted that the surface areas for the optimal shapes are smaller than that of T_3, while the volumes are identical. For example, the surface area of T_2 is 94.787 m^2, which 8 % less than that of T_3.

The performance characteristics of the identified optimal sections are evaluated in

terms of shifts in the longitudinal cg coordinate and the instantaneous vertical cg coordinate, as functions of the fill level and magnitudes of deceleration. The results obtained for the T_1, T_2, T_4 and T_5 optimal configuration are compared with those for the conventional T_3 configuration to assess the potential gains. For this purpose, the performance characteristics of the T_3 design are initially evaluated and discussed in the following section.

3.5.1 Load Shift and Mass Moment of Inertia Characteristics of Conventional T_3 Design.

T_3 is the most commonly used tank design in general purpose liquid cargo fleets [72]. Consequently, this particular design has been the focus of the majority of the reported studies on steering and braking responses. The dynamic characteristics of T_3 at different fill levels are compared with the identified design tanks under different levels of a_{lx} and a_{ly}, and the fill levels of 30%, 60%, and 90%. Figure 3.8 to 3.9 illustrate the longitudinal, lateral and vertical cg coordinates shifts as functions of a_{lx} and a_{ly}, and the fill level. The results show that ΔX is primarily dependent upon the fill level and the magnitude a_{lx}. The dependence on a_{lx}, however, diminishes as it approaches 0.3g. The influence of a_{ly} on ΔX may be considered insignificant. The application of a low level a_{lx} yields considerable load shift in the longitudinal plane and the fluid assumes a nearly steady shape as a_{lx} exceeds 0.3g. Low fill volumes, obviously yield higher load shift under a relatively low braking deceleration. The cg shift in the lateral plane mainly depends on the magnitude of lateral acceleration and fill level. It is interesting to note that the magnitude of ΔY decreases with increasing a_{lx}, which is attributed to the clustering of the fluid within one part of the tank. The vertical coordinate of the cg, Z, is mostly

dependent upon the fill height, as shown in Figure 3. 9. The variation in the vertical cg

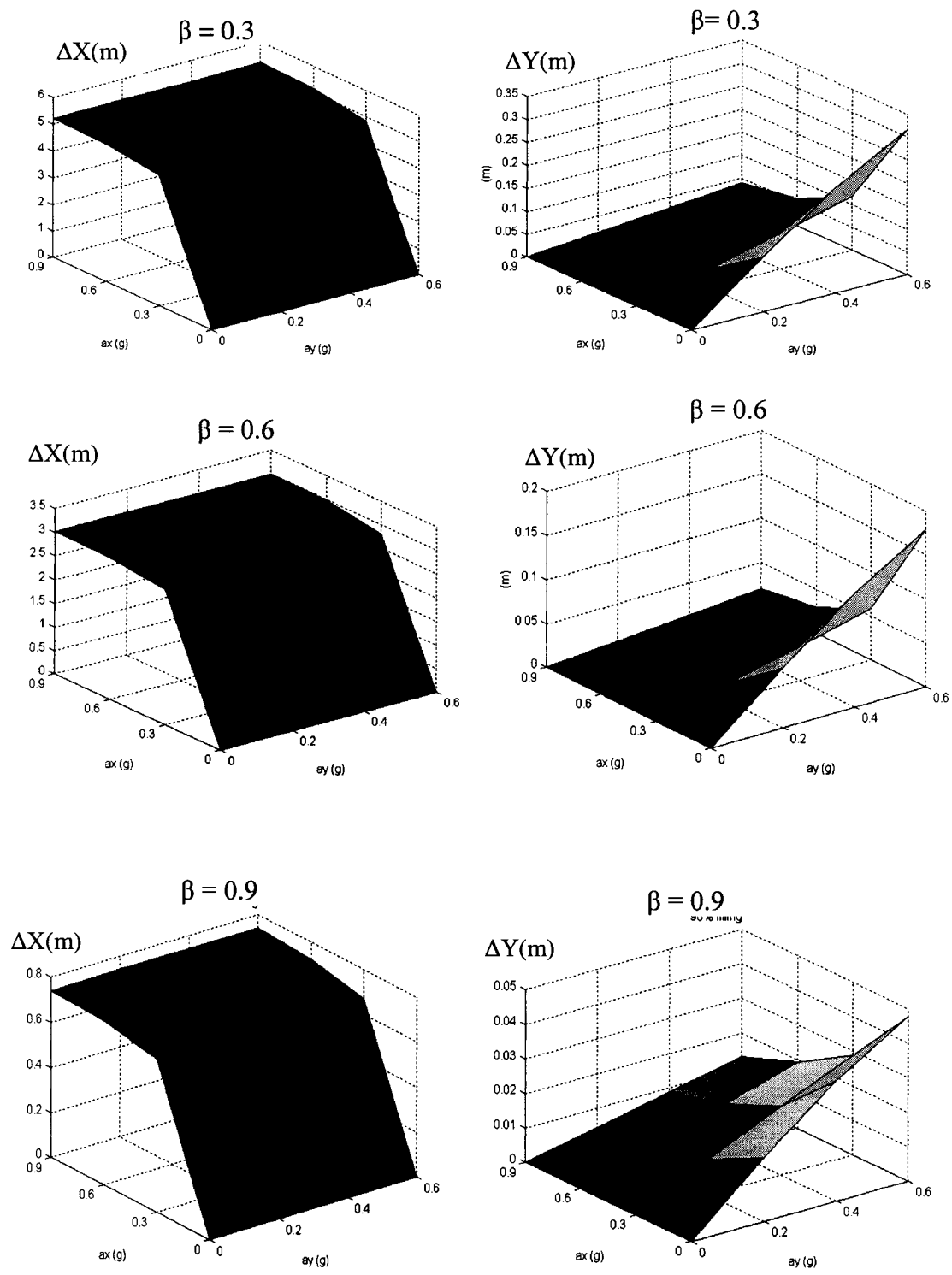

Figure 3.8: Variations in longitudinal (Δ X) and lateral (Δ Y) cg coordinates of the liquid cargo in the pitch and roll planes as function of a_{lx}, a_{ly} and β (configuration T_3).

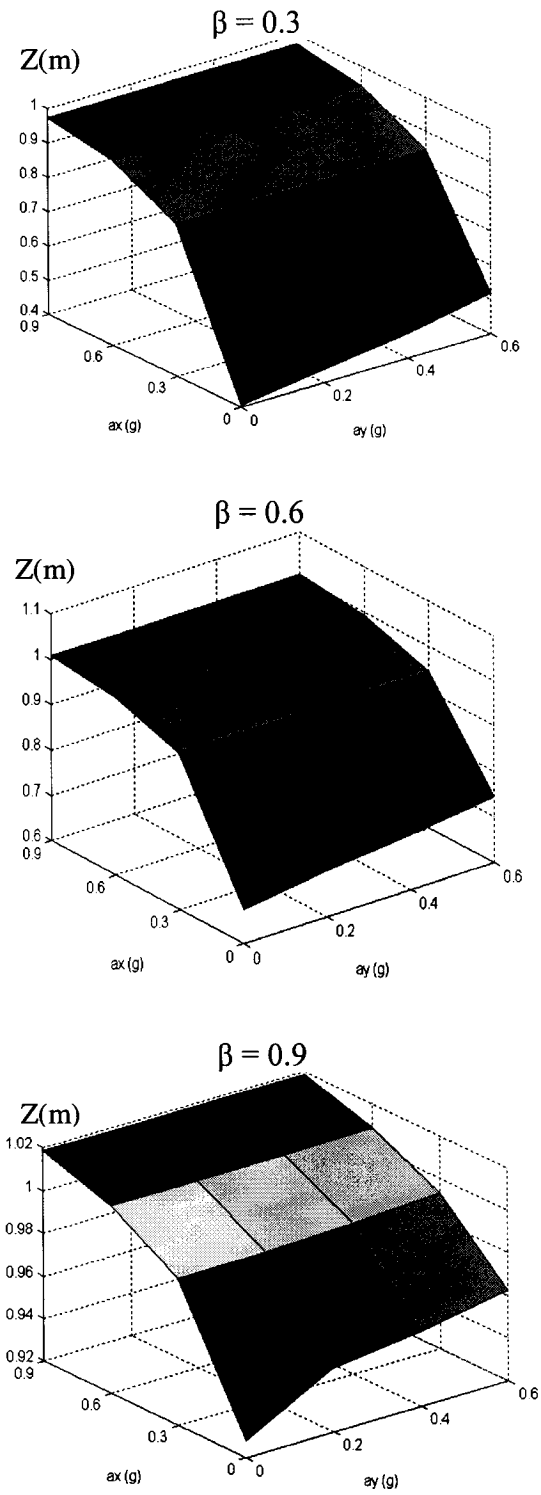

Figure 3.9: Trajectories of vertical cg coordinate of the liquid cargo in a roll plane as function of a_{lx}, a_{ly} and β (configuration T_3).

coordinate could be significantly large under lower fill volume, when lateral and longitudinal acceleration fields are applied.

Figure 3.10 and 3.11 illustrate the variations in the roll, pitch and yaw mass moment of inertia of the cargo as functions of the fill level, a_{lx} and a_{ly}. The roll mass moment of inertia of the fluid, I_x, increase most significantly with increasing a_{lx} but moderately with increasing a_{ly}, irrespective of the fill level. The pitch mass moment of inertia, however, decrease rapidly with increasing a_{lx} for fill levels of 60% and 90%. An opposite trend, however, is observed for the 30% fill condition, which is most likely attributed to clustering of the fluid bulk towards on end plate. The influence of a_{ly} on I_y is very small, as evident in Figure 3.10. The yaw mass moment of inertia of the fluid bulk also reveals trends similar to those observed for I_y, but the effect of a_{ly} is more notable. These results clearly show that the mass moment of inertias of the fluid cargo are strongly dependent upon both the magnitudes of acceleration fields and fill level, which would further affect the directional dynamic responses of a partly-filled tank combination.

3.5.2 Relative Performance Characteristics of Different Optimal Tanks

The directional dynamics of articulated vehicles under simultaneous braking and steering have been addressed in a few studies [84-89], while ever fewer studies have considered the liquid movement within the partly-filled tanks [90-91]. The combination of variable speed operations, together with cornering, is one of the most commonly encountered highway maneuvers, which has been associated with most vehicle accidents. During variable speed directional maneuvers, the load transfer in the longitudinal direction coupled with the lateral load transfer due to steering, including the variation of moment of inertia, can lead to wheel lock-up, resulting in possible yaw instability and/or

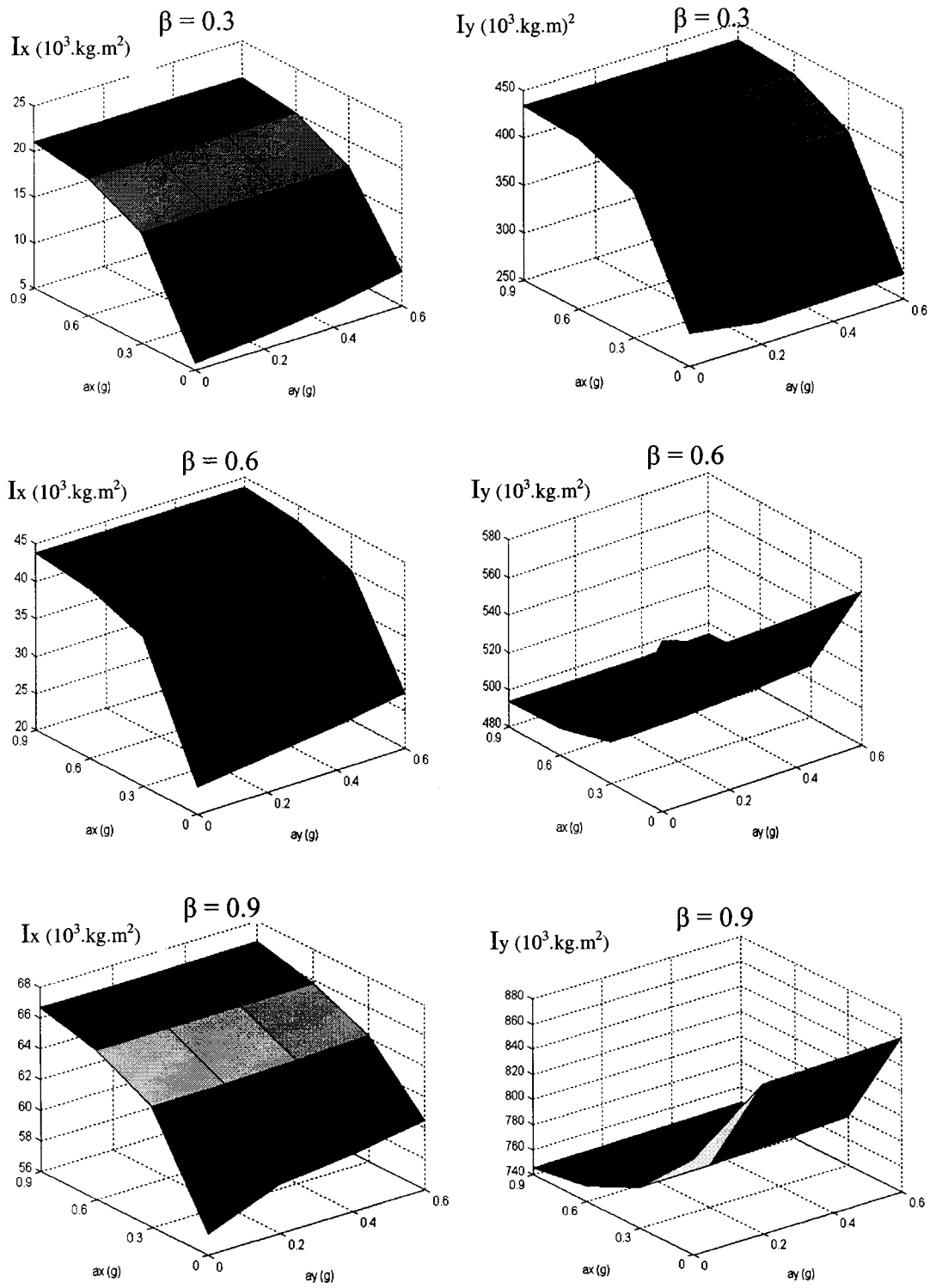

Figure 3.10: Variations of I_x and I_y of the liquid cargo in the pitch and roll planes as function of a_{lx}, a_{ly} and β (configuration T_3).

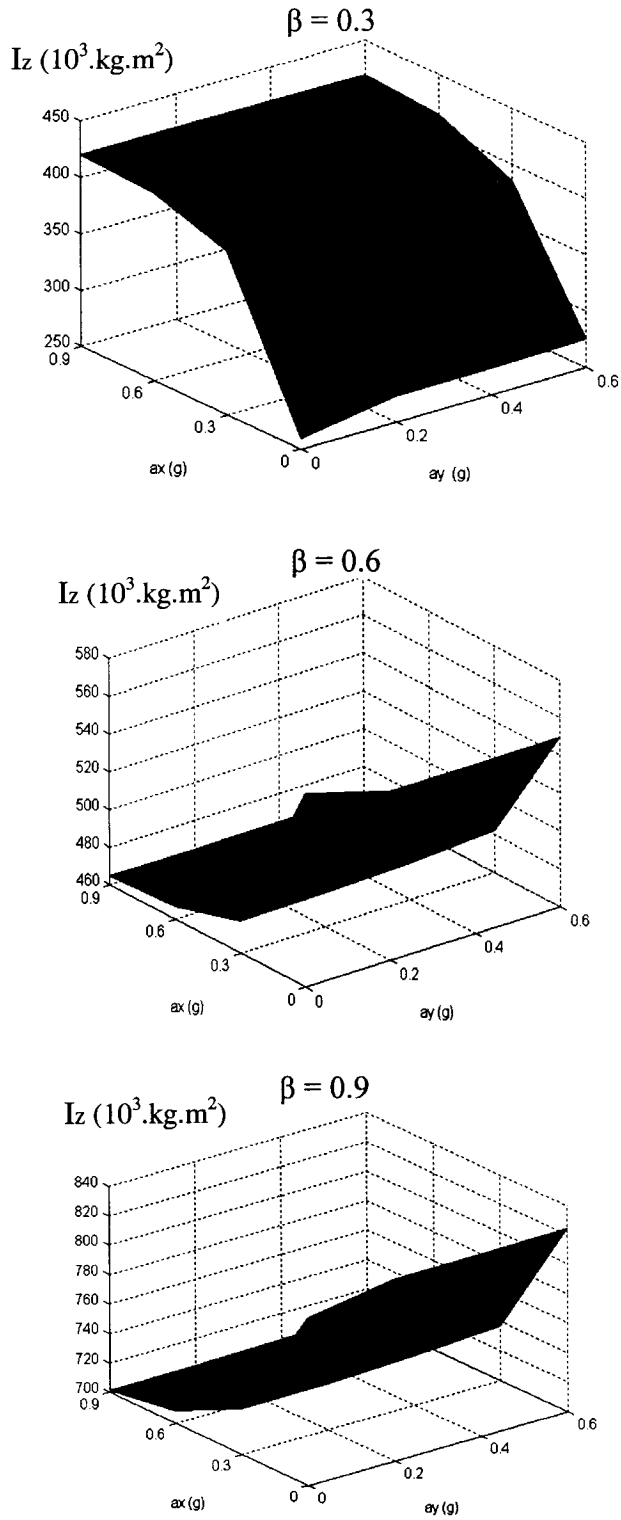

Figure 3.11: Variations I_z of the liquid cargo in a roll plane as function of a_{lx}, a_{ly} and β (configuration T_3).

loss of directional control of the vehicle [92]. The load transfer in the longitudinal and lateral directions is further exaggerated in the case of partially filled tank vehicles due to unrestricted liquid cargo movement in the roll and pitch planes. This may cause considerable reduction in stability limits and safety performance of the vehicle [30]. Tank designs with identified optimal geometries could be applied to limit the dynamic load shift and thus enhance the directional stability limits. The relative properties of the identified geometries are evaluated in terms of longitudinal and lateral load shifts, and variations in mass moment of inertia.

Figure 3.12 to 3.14 illustrate the variations in the X, Y, and Z coordinates of the fluid bulk cg, respectively, for the T_1 to T_5 designs, as function of a_{lx}, a_{ly} and fill level. The shifts in the longitudinal and vertical coordinates are presented for varying levels of a_{lx}, while that in the lateral coordinate is evaluated for different magnitudes of a_{ly}. The responses of the different configurations are also normalized with respect to corresponding response parameters of the conventional design (T_3) in order to evaluate the relative performance of a particular design. The results show that the configuration T_1, despite its longer design, yields considerably lower load shift in the longitudinal plane for 30% and 60% fill levels. The conventional design yields highest load shift (ΔX) for these fill conditions, as observed in Figure 3.12. The conventional design, however, yields lowest load shift for higher fill level (90%), which is attributed to its relatively smaller length. Considering that the longitudinal load shift is most significant for lower fill volumes, the proposed configurations T_1, T_4 and T_5 may be considered to attain improved performance.

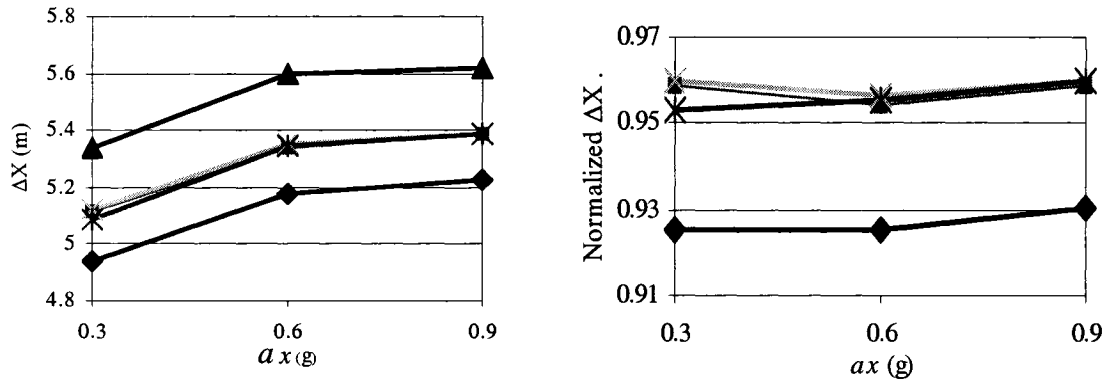

(a) β =0.3

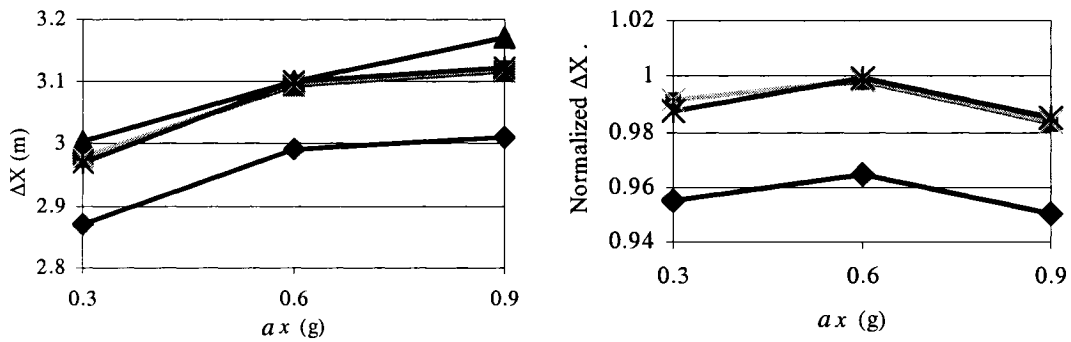

(b) β =0.6

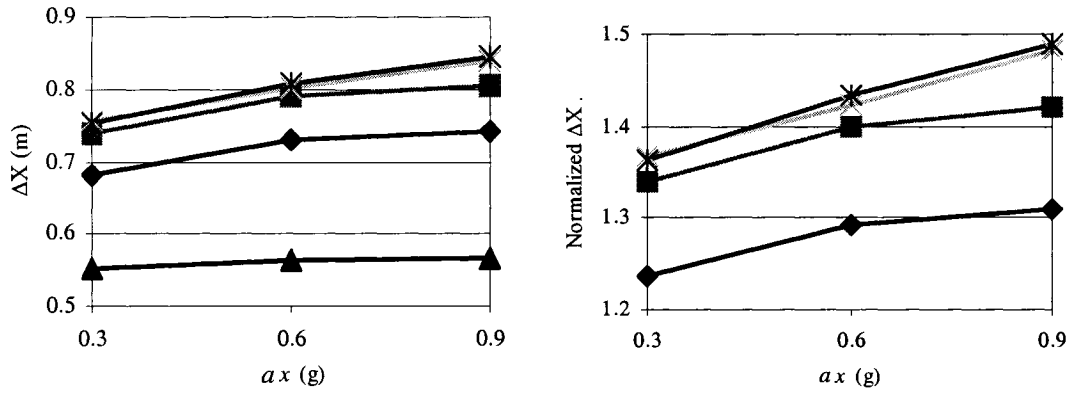

(c) β=0.9

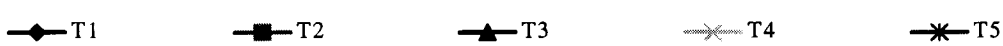

Figure 3.12: The cg trajectory and the normalized values in the longitudinal direction.

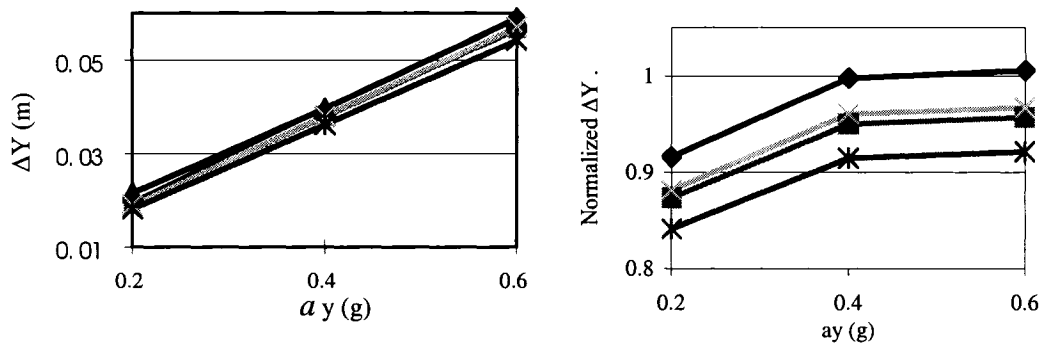

(a) β=0.3

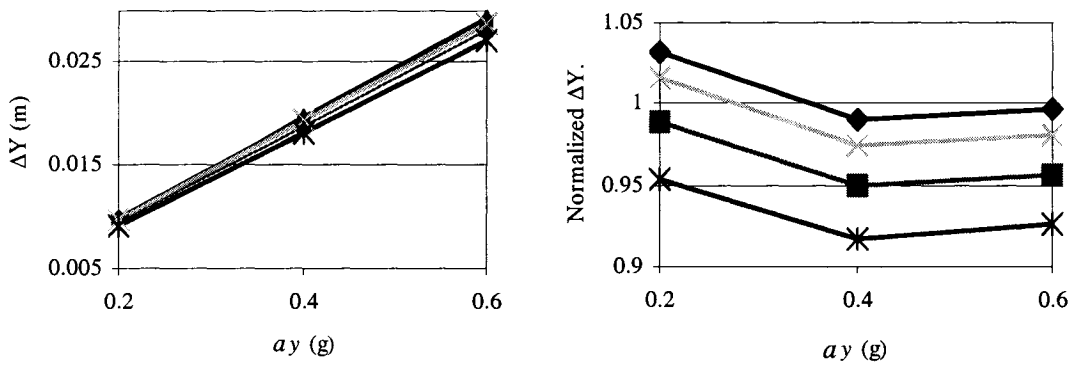

(b) β=0.6

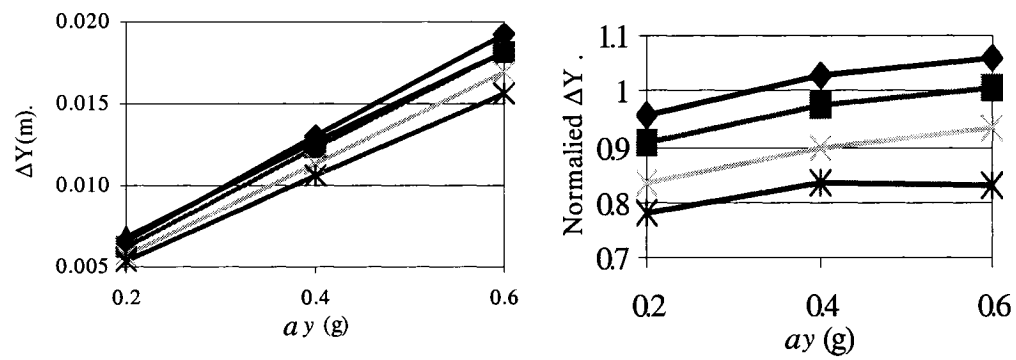

(c) β=0.9

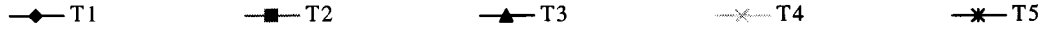

Figure 3.13: The cg shift and normalized value in the lateral direction, a_x = 0.6g.

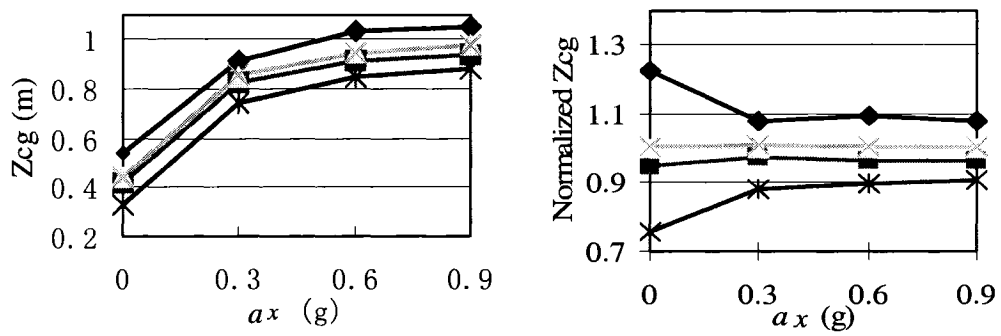

(a) β=0.3

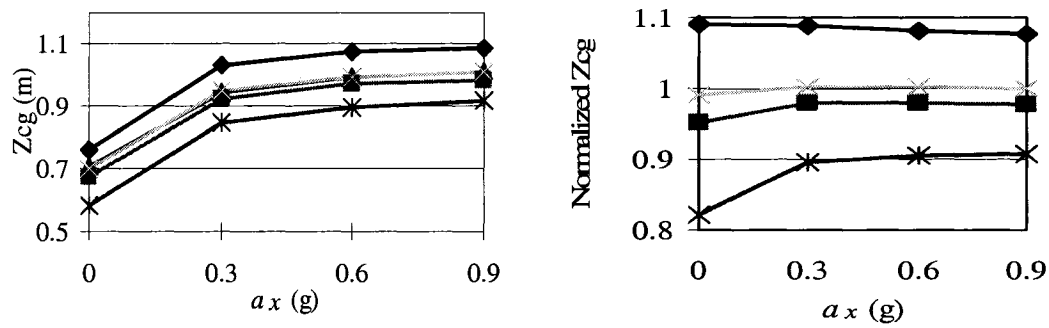

(b) β=0.6

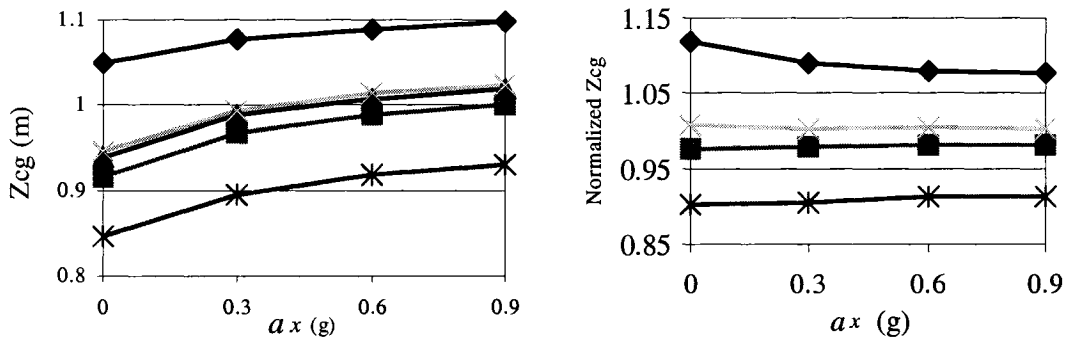

(c) β=0.9

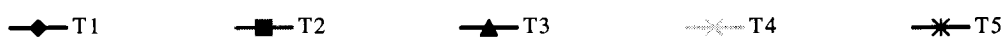

Figure 3.14: The cg trajectories and the normalized values in the vertical direction.

The relative performance characteristics of different geometries in terms of lateral load shift (ΔY) , show only minimal influence of the tank cross-section. The effect of the geometry, however, is more evident when the response is normalized with respect to that of T_3. The results suggest that configuration T_5, comprising the optimal roll-plane section, could be most beneficial in limiting the lateral load shift. The T_2 and T_4 designs also yield lower lateral load shift, even thought the cross-section is circular. The T_5 geometry also yields lower static cg height, and lowest shift in the vertical coordinate of the fluid bulk, irrespective of the magnitude of a_x, as shown in Figure 3.14.

Figure 3.15 to 3.17 illustrate the relative variation in mass moments of inertia of the fluid bulk, I_x, I_y and I_z, respectively, of the five tank configurations. Owing to relatively smaller effect of a_y, as evident in Figure 3.9 to 3.11, the analyses are performed with varying level of a_x and fill level. The results show that the roll mass moment of inertia of the liquid increases with increasing a_x, irrespective of the fill level, and it approaches nearly steady values at a_x exceeds 0.3g. The figures also show variations in I_x, I_y and I_z, normalized with respect to those of the conventional design T_3. The results shown in Figure 3.15 clearly illustrate the potential benefits of configuration T_5 in limiting the variation in roll mass moment of inertia, while the conventional design yields highest values of I_x for all fill condition. The conventional design also yields highest values of I_y and I_z, irrespective of the fill condition, as evident in Figure 3.16 and 3.17. The configuration T_1 yields lowest values of I_y and I_z for all fill levels and deceleration magnitudes considered.

3.6 Identification of Optimal Longitudinal Sections

A three - dimensional kineto - static model of a partly filled tank with generic

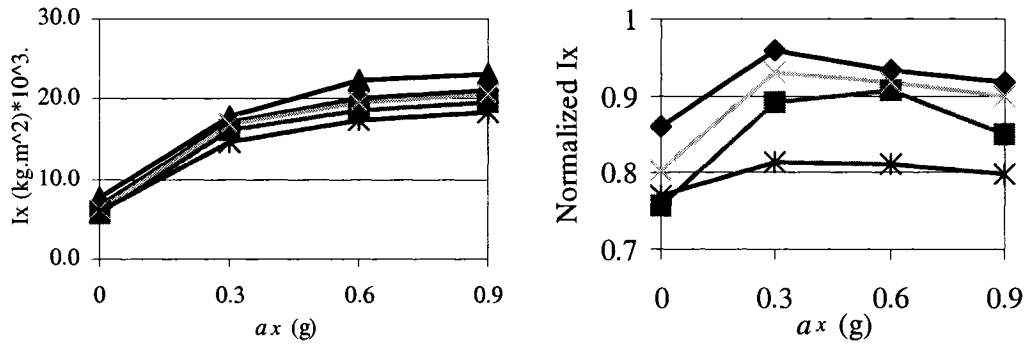

(a) β=0.3

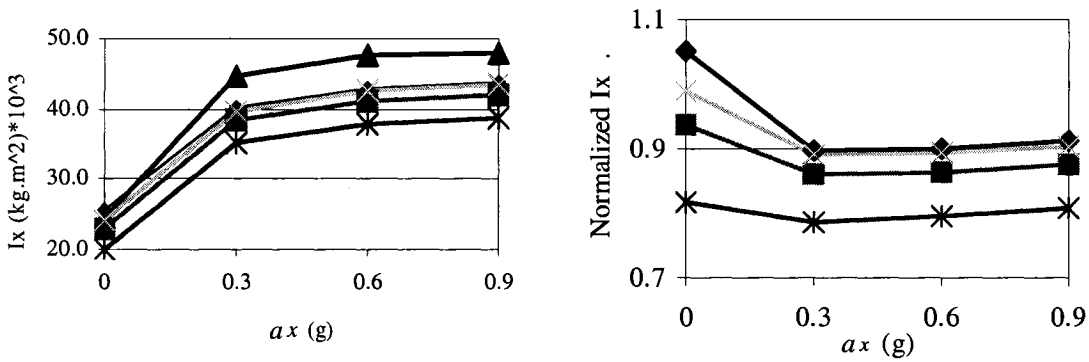

(b) β=0.6

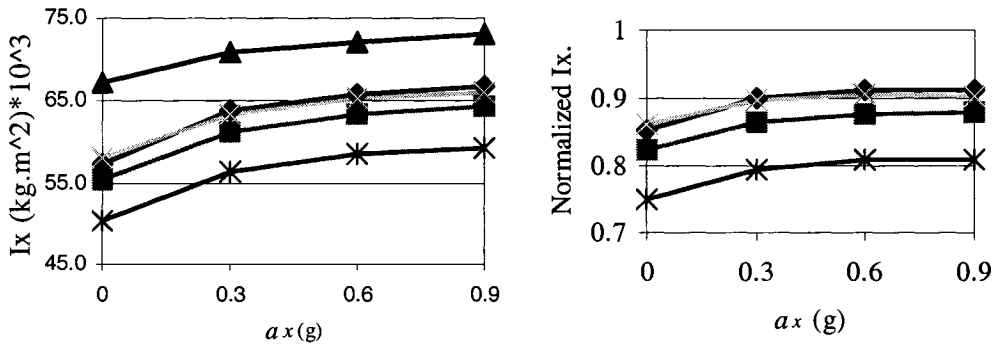

(c) β=0.9

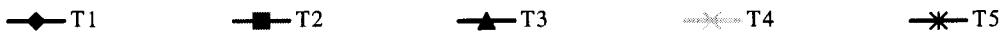

Figure 3.15: The variation and normalized figures of I_x.

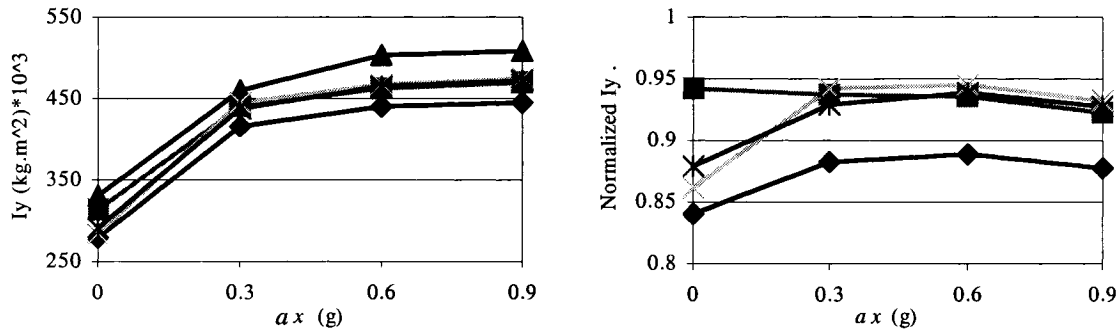

(a) β=0.3

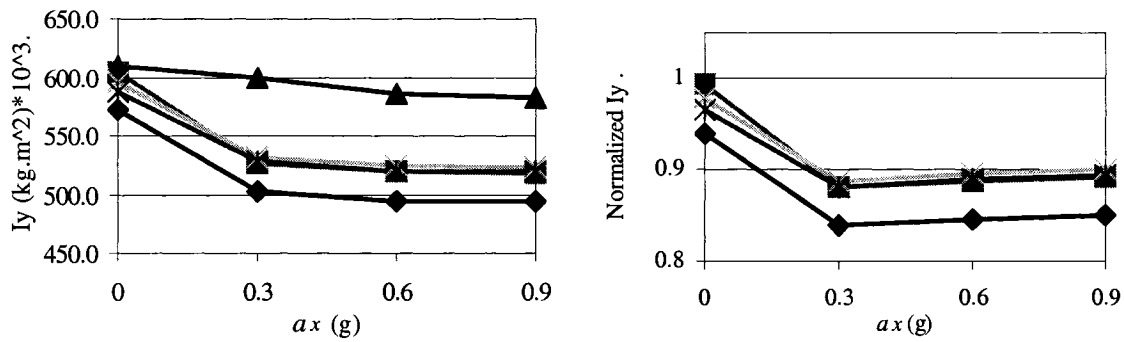

(b) β=0.6

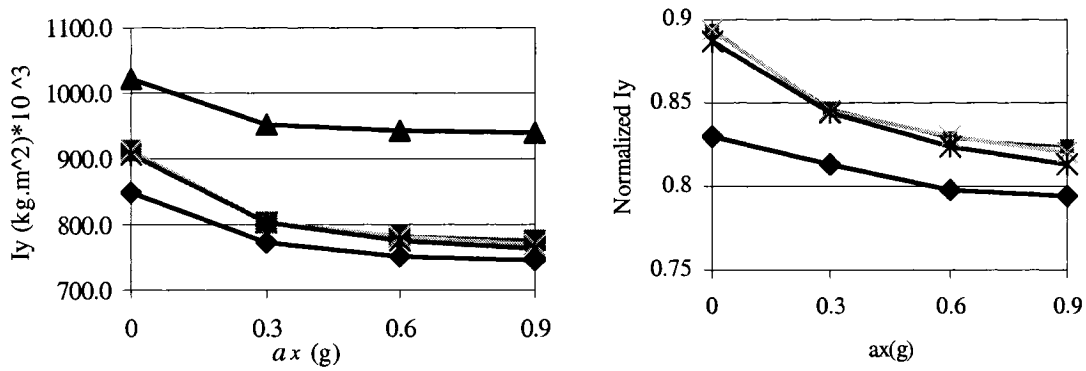

(c) β=0.9

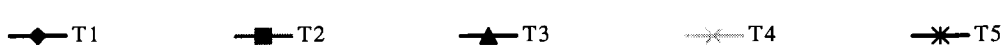

Figure 3.16: The variation and normalized figures of I_y.

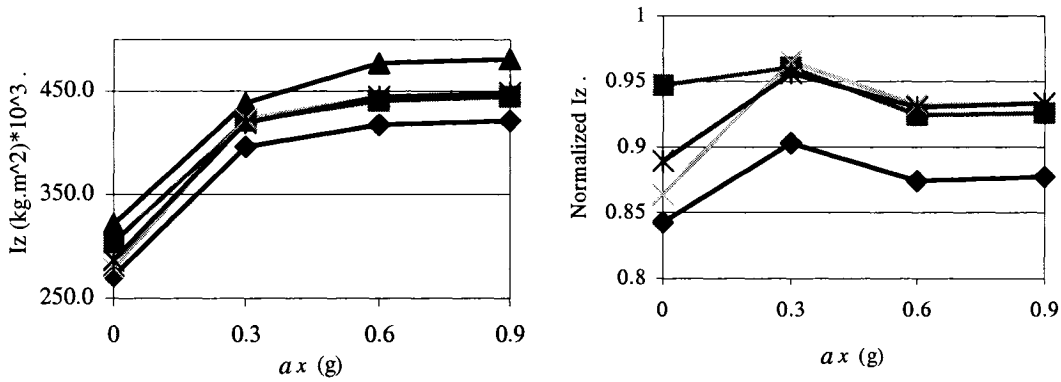

(a) β=0.3

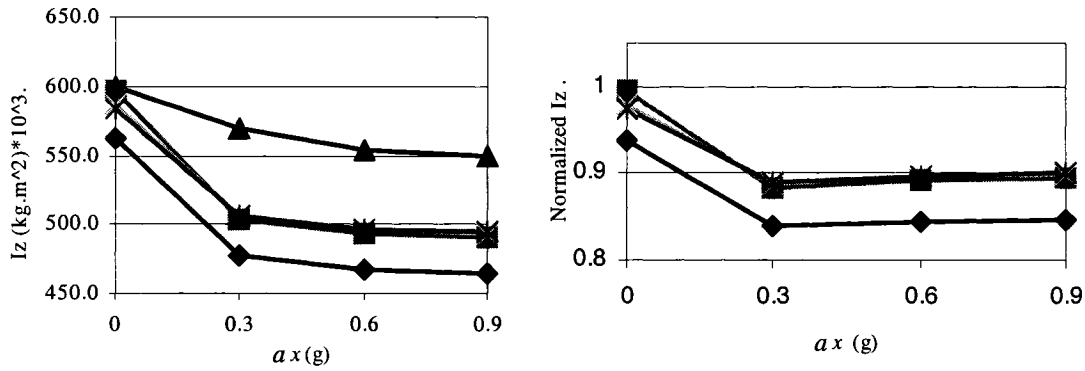

(b) β=0.6

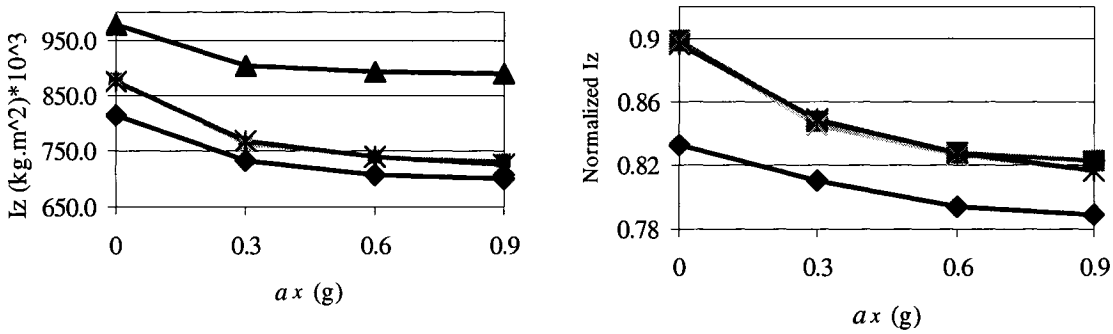

(c) β=0.9

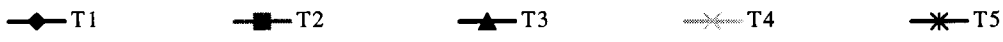

Figure 3.17: The variation and the normalized values of I_z.

longitudinal and lateral sections is formulated to study the dynamic load shift and mass moments of inertia variation of the fluid bulk as function of lateral and longitudinal acceleration fields, and fill level. A multi-parameter optimization problem is formulated and solved to identify the longitudinal section parameters that would yield minimal longitudinal load shift, while the lateral section is retained as either circular or the conical.

3.7 Summary

A total of four optimal configurations are identified and their performance characteristics are assessed with respect to those of a conventional cylindrical tank. The results suggest that the configuration T_5 comprising the optimal lateral section yields relatively lower shift in the cg coordinates and the mass moment of inertia. This particular configuration is integrated to the vehicle model in the following chapters to further explore its potential performance benefits.

CHAPTER 4 VEHICLE MODEL DEVELOPMENT

4.1 Introduction

The directional dynamic responses and stability characteristics of a vehicle combination with a partly-filled liquid tanker are dependent upon many vehicle-, tank- and environment related factors. The influence of the fluid load shift and the tank design factor on the vehicle performance can thus be evaluated upon consideration of the total tank-vehicle combination. The different optimal tank designs described in Chapter 3 are thus integrated to the directional dynamic model of a five-axle tractor-semitrailer vehicle combination to study its performance characteristics. The resulting analytical model thus permits for analyses of load shifts in the lateral and longitudinal planes, variations in the mass moments of inertias, and various directional response measures under the application of steering or braking or combined steering and braking inputs. A vehicle model is initially described in this chapter on the basis of those reported in the literature [30, 32, 80]. The subsystem models, such as those of the tires, suspensions, and the steering system, are taken from the published studies while the tank model presented in the previous chapter is integrated to the vehicle model.

4.2 Development of the Vehicle Model

A five-axle tractor-semitrailer combination, comprising a three-axle tractor and a two-axle semitrailer coupled through a conventional fifth wheel, is considered for the model development. The choice of this particular configuration is justified by its reltively high population in Canada and the USA [80]. A three-dimentional model of the vehicle is developed to simulate for braking and steering responses. The model formulations

involving the component models and the coordinate systems are described in the following sections.

4.2.1 The Coordinate Systems

A set of body-fixed coordinate systems are defined to describe the translational and rotational motions of different sprung and unsprung bodies of the tractor-semitrailer vehicle, as shown in Figures 4.1 and 4.2 [30]. In the figures, (i_n, j_n, k_n) defines the fixed inertial coordinate system, and (i_{sf}, j_{sf}, k_{sf}; f=1, 2) define the locations and attitude of the sprung masses with respect to the inertial coordinate system, where f = 1 refers to the tractor sprung weight and f = 2 to the trailer sprung weight. The axis system, (i_{ui}, j_{ui}, k_{ui}; i =1, 2,.., 5) describes the motions of the unsprung masses of the combination relative to the respective sprung mass-fixed coordinate system.

The origin of the inertial coordinate system is placed at the tractor sprung mass cg at the beginning of the simulation. The motions of sprung mass along its body-fixed axis system can be related to the inertial coordinate system by the following transformation:

$$\begin{Bmatrix} \vec{i}_n \\ \vec{j}_n \\ \vec{k}_n \end{Bmatrix} = D_{sf} \begin{Bmatrix} \vec{i}_s \\ \vec{j}_s \\ \vec{k}_s \end{Bmatrix}_f \quad (f=1, 2) \tag{4.1}$$

Where the transformation matrix D_{sf} can be derived using three sequential steps of rotations (roll, pitch and yaw) [30, 81, 93, 94], such that:

$$D_{sf} = D_{yawf} D_{pitchf} D_{rollf} \tag{4.2}$$

Where D_{rollf}, D_{pitchf} and D_{yawf} represent roll, pitch, and yaw rotation matrices, respectively, and are given by:

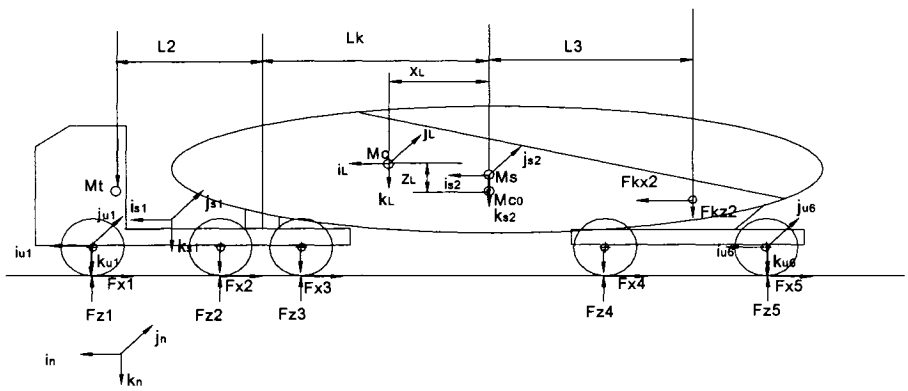

Figure 4.1: The coordinate systems.

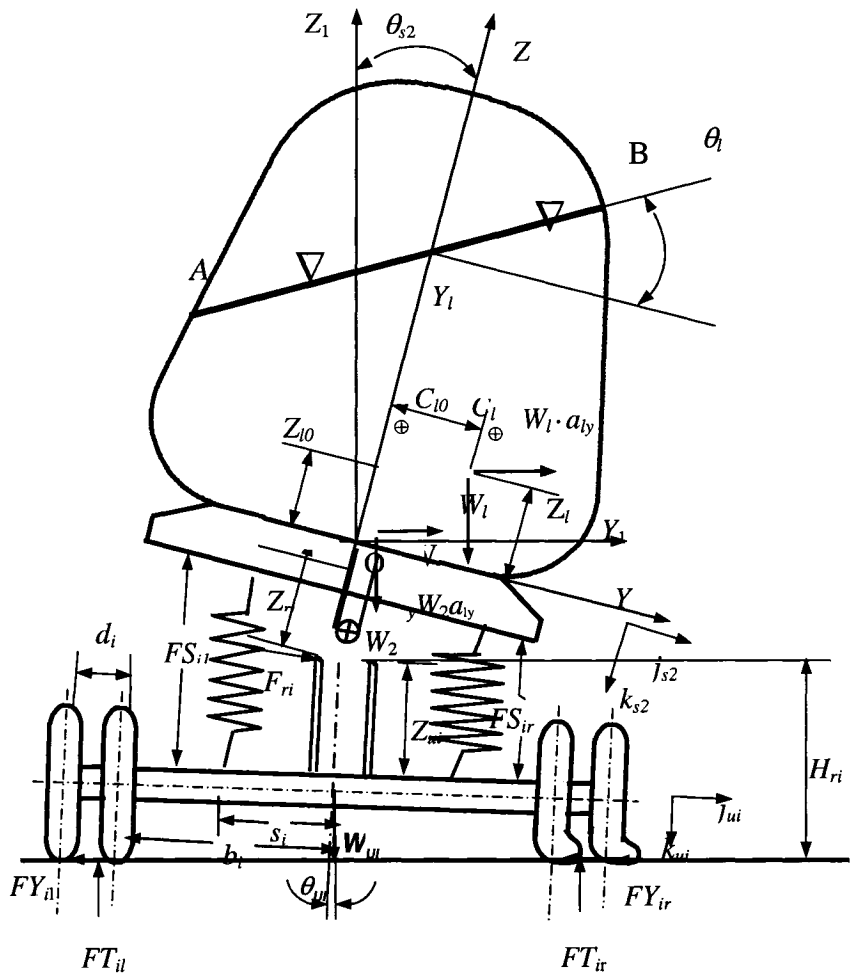

Figure 4.2: Vehicle model representation in the roll plane.

$$D_{roll_f} = \begin{bmatrix} 1 & 0 & 0 \\ 0 & \cos\theta_s & -\sin\theta_s \\ 0 & \sin\theta_s & \cos\theta_s \end{bmatrix}_f$$

$$D_{pitch_f} = \begin{bmatrix} \cos\alpha_s & 0 & \sin\alpha_s \\ 0 & 1 & 0 \\ -\sin\alpha_s & 0 & \cos\alpha_s \end{bmatrix}_f$$

$$D_{yaw_f} = \begin{bmatrix} \cos\varphi_s & -\sin\varphi_s & 0 \\ \sin\varphi_s & \cos\varphi_s & 0 \\ 0 & 0 & 1 \end{bmatrix}_f \qquad (4.3)$$

where θ_{sf}, α_{sf} and φ_{sf} are the roll, pitch and yaw angles, respectively, of the sprung unit f. Assuming small pitch angles ($\sin\alpha_{sf} \approx \alpha_{sf}$ and $\cos\alpha_{sf} \approx 1.0$) of the sprung masses, matrix D_{pitchf} can be simplified to yield:

$$D_{sf} = \begin{bmatrix} \cos\varphi_s & -\sin\varphi_s\cos\delta_s + \alpha_s\cos\varphi_s\sin\delta_s & \sin\varphi_s\sin\delta_s + \alpha_s\cos\varphi_s\cos\delta_s \\ \sin\varphi_s & \cos\varphi_s\cos\delta_s + \alpha_s\sin\varphi_s\sin\delta_s & -\cos\varphi_s\sin\delta_s + \alpha_s\sin\varphi_s\cos\delta_s \\ -\alpha_s & \sin\delta_s & \cos\delta_s \end{bmatrix}_f \qquad (4.4)$$

The unsprung mass will roll and bounce with respect to the sprung mass to which it is attached. The orientation of the unsprung mass fixed system ($\vec{i}_u$, $\vec{j}_u$, $\vec{k}_u$) with respect to the sprung mass axis system can be defined by the following transformation:

$$\begin{Bmatrix} \vec{i}_s \\ \vec{j}_s \\ \vec{k}_s \end{Bmatrix}_f = D_{fi} \begin{Bmatrix} \vec{i}_u \\ \vec{j}_u \\ \vec{k}_u \end{Bmatrix}_i \quad (f = 1,\ i = 1, 2, 3;\ \text{and}\ f = 2,\ i = 4, 5) \qquad (4.5)$$

Where the transformation matrix D_{fi} is defined by roll (θ_{sf} and θ_{ui}) and pitch (α_{sf}) angles, given by :

$$D_{fi} = \begin{bmatrix} 1 & -\alpha_{sf}\sin\theta_{ui} & -\alpha_{sf}\cos\theta_{ui} \\ \alpha_{sf}\sin\theta_{sf} & \cos(\theta_{sf}-\theta_{ui}) & \sin(\theta_{sf}-\theta_{ui}) \\ \alpha_{sf}\cos\theta_{sf} & -\sin(\theta_{sf}-\theta_{ui}) & \cos(\theta_{sf}-\theta_{ui}) \end{bmatrix} \quad (4.6)$$

4.2.2 Equations of Motion

Having completely defined the coordinate systems, the differential equations of motion for each sprung mass can be derived by applying Newton's second law of motion.

Longitudinal force equations:

$m_f a_f \vec{i}_f + m_{lf} a_{lf} \vec{i}_{lf}$ = (Longitudinal components of constraint forces) + (Longitudinal components of suspension forces) + Longitudinal components of forces due to gravity; (f=1, 2) (4.7)

Lateral force equations:

$m_f a_f \vec{j}_f + m_{lf} a_{lf} \vec{j}_{lf}$ = (Lateral components of constraint forces) + (Lateral components of suspension forces) + (Lateral components of forces due to gravity); (f=1, 2) (4.8)

Vertical force equations:

$m_f a_f \vec{k}_f + m_{lf} a_{lf} \vec{k}_{lf}$ = (Vertical components of constraint forces) + (Vertical components of suspension forces) + (Vertical components of forces due to gravity); (f=1, 2) (4.9)

where m_f and m_{lf} are the sprung and liquid cargo masses, respectively, of unit f, while m_{ll}=0, and a_f is the acceleration vector of cg of the sprung mass f, expressed by:

$$a_f = (\dot{u}_f + q_f w_f - r_f v_f)\vec{i}_{sf} + (\dot{v}_f + r_f u_f - p_f w_f)\vec{j}_{sf} + (\dot{w}_f + p_f v_f - q_f u_f)\vec{k}_{sf} \quad (4.10)$$

a_{lf} (f = 2) is the acceleration vector of the liquid bulk cg, $a_{l2} = a_{lx}\vec{i}_{s2} + a_{ly}\vec{j}_{s2} + a_{lz}\vec{k}_{ls2}$, derived as:

$$\begin{aligned} a_{l2} = &\{a_{x2} + \dot{q}_2 Z_{l2} - \dot{r}_2 Y_{l2} + q_2(p_2 Y_{l2} - q_2 X_{l2}) - r_2(r_2 X_{l2} - p_2 Z_{l2})\}\vec{i}_{s2} \\ &+ \{a_{y2} + \dot{r}_2 X_{l2} - \dot{p}_2 Z_{l2} + r_2(q_2 Z_{l2} - r_2 Y_{l2}) - p_2(p_2 Y_{l2} - q_2 X_{l2})\}\vec{j}_{s2} \\ &+ \{a_{z2} + \dot{p}_2 Y_{l2} - \dot{q}_2 X_{l2} + p_2(r_2 X_{l2} - p_2 Z_{l2}) - q_2(q_2 Z_{l2} - r_2 Y_{l2})\}\vec{k}_{s2} \end{aligned} \quad (4.11)$$

Where u_f, v_f and w_f are the translational (longitudinal, lateral and vertical) velocities of unit f along its body-fixed coordinate system ($\vec{i}_{sf}$, $\vec{j}_{sf}$, and $\vec{k}_{sf}$), and a_{x2}, a_{y2} and a_{z2} are the components of trailer sprung mass acceleration (a_2) along the trailer body-fixed coordinate system. p_f, q_f, and r_f are the rotational velocities (roll, pitch and yaw rates) of the sprung mass f with respect to the inertial coordinate system, while $\dot{p}_f$, $\dot{q}_f$, and $\dot{r}_f$ are the corresponding angular accelerations. X_{l2}, Y_{l2}, and Z_{l2} are the coordinates of the instantaneous cg of the liquid bulk in terms of tank trailer body-fixed system, which are computed using the kineto-static analyses presented in section 2.3.

The three components of forces due to gravity of the trailer sprung mass and liquid cargo are computed as:

$$\begin{Bmatrix} F_{gx} \\ F_{gy} \\ F_{gz} \end{Bmatrix} = D_{sf}^{-1} \begin{Bmatrix} 0 \\ 0 \\ (m_f + m_{lf})g \end{Bmatrix} = (m_f + m_{lf})g \begin{Bmatrix} -\alpha_{sf} \\ \sin\theta_{sf} \\ \cos\theta_{sf} \end{Bmatrix} \quad (4.12)$$

The equations of rotational motions of each sprung mass are expressed in the following general form:

Roll moment equations:

$$(I_{xf} + I_{xlf})\dot{p}_f - (I_{yl} + I_{lf} - I_{zf} - I_{zlf})q_f r_f = \text{(Roll moment due to constraint) +}$$

(Roll moments due to suspension forces) + (Roll moment due to liquid forces); (f =1, 2) (4.13)

Pitch moment equations:

$(I_{yf} + I_{ylf})\dot{q}_f - (I_{zf} + I_{zlf} - I_{xf} - I_{xlf})p_f r_f$ = (Pitch moment due to constraint) + (Pitch moments due to suspension forces) + (Pitch moment due to liquid forces); (f=1, 2) (4.14)

Yaw moment equation:

$(I_{zf} + I_{zlf} + \sum_{i=N_1}^{N_2} I_{zui})\dot{r}_f - (I_{xf} + I_{xlf} - I_{yf} - I_{ylf})p_f q_f$ = (Yaw moment due to constraint) + (Yaw moments due to tire forces) + (Yaw moment due to liquid forces); (f=1, 2) (4.15)

Where I_{xf}, I_{yf}, and I_{zf} are the roll, pitch, and yaw mass moments of inertia of sprung mass f, and I_{xlf}, I_{ylf} and I_{zlf} are the roll, pitch, and yaw mass moments of inertia of the liquid cargo with respect to the body-fixed system of sprung mass f. I_{zui} is the yaw mass moment of inertia of unsprung mass i. N_1 and N_2 are the number of axles attached to each sprung mass unit, i.e., N_1 = 1 and N_2 = 3 for f = 1; and N_1 = 4 and N_2 = 5 for f =2 respectively.

The three moment components due to inertial forces (liquid load) in the trailer sprung mass axis system are computed from:

$$\begin{Bmatrix} M_{lx} \\ M_{ly} \\ M_{lz} \end{Bmatrix} = \begin{Bmatrix} X_{l2} \\ Y_{l2} \\ Z_{l2} \end{Bmatrix} \times \left[m_{l2} \begin{Bmatrix} a_{lx} \\ a_{ly} \\ a_{lz} \end{Bmatrix} + D_2^{-1} \begin{Bmatrix} 0 \\ 0 \\ m_{l2} g \end{Bmatrix} \right]$$

$$= m_{l2}\begin{Bmatrix} Y_{l2}a_{lz} - Z_{l2}a_{ly} + g(Y_{l2}\cos\theta_{sf} - Z_{l2}\sin\theta_{sf}) \\ Z_{l2}a_{lx} - X_{l2}a_{lz} - g(Z_{l2}\alpha_{sf} + X_{l2}\cos\theta_{sf}) \\ X_{l2}a_{ly} - Y_{l2}a_{lx} + g(X_{l2}\sin\theta_{sf} + Y_{l2}\alpha_{sf}) \end{Bmatrix} \quad (4.16)$$

Where a_{lx}, a_{ly} *and* a_{lz} are components of acceleration vector of the liquid cargo along the trailer sprung mass coordinate system ($\vec{i}_{sf}$, $\vec{j}_{sf}$, $\vec{k}_{sf}$), and M_{lx}, M_{ly} and M_{lz} are the roll, pitch and yaw moments caused by liquid forces about the origin.

Equations of motion for the unsprung masses

The dynamics of each unsprung mass is described by two second-order differential equations in vertical and roll axes, derived using the respective body-fixed coordinate system. The equations describing the motion of each of the unsprung masses are derived in the following form:

$m_{ui}a_{ui}g$ = (Vertical forces due to suspension) + (Vertical forces due to tires) $+m_{ui}g$; (i =1, 2, …, 5) (4.17)

$I_{xui}\dot{p}_{ui}$ = (Roll moments due to suspension forces) + (Roll moments due to tire forces); (i=1, 2, …, 5) (4.18)

Where a_{uzi} is vertical acceleration of unsprung mass i, I_{xui} is its roll mass moment of inertia and p_{ui} is its roll rate.

4.2.3 Tire Forces and Moments

The vehicle tires transmit forces and moments to the vehicle arising form the tire-road interactions. The resulting forces and moment are complex nonlinear function of the normal load, longitudinal shift and side-slip. The majority of studies have employed either liner tire models or three-dimensional look-up tables to characterize lateral and

longitudinal forces, and aligning moment, as function of vehicle speed, normal load, side-slip angle and longitudinal slip[23, 34, 37]. In this thesis, a tire model used by MSC (Mechanical Simulation Corporation) within TruckSim software [24] is applied.

When the tire is subjected to combined cornering and braking maneuvers, the shear forces and aligning moment are limited by the tire-road friction. The "combined slip theory" proposed by Pacejka and Sharp [6] is used to determine the tire forces and moments under combined cornering and braking effects, and to account for ground surface friction that is different from the friction conditions in the laboratory test equipment. Tire vertical stiffness determines how the load varies as the tire bounces on the road. Furthermore, the tires do not immediately generate forces when they develop lateral slip angles and longitudinal slip ratios due to delays associated carcass deflection. It has been suggested that under a step input in slip, the lateral and longitudinal forces build up approximately as first-order lag in the distance traveled [34].

Figure 4.3 illustrates the variations in the longitudinal tire force as a function of the slip ratio and tire vertical force as reported in the MSC model [24]. The corresponding tire/ground friction coefficient for this data is 0.73. The tire model used in MSC assumes that the tire behavior is symmetric about the origin with respect to the longitudinal slip.

The lateral tire force characteristics, as a function of the lateral side-slip angle and tire vertical load, are shown in Figure 4.4. The figures show that both the longitudinal and lateral tire forces are nonlinear function of the longitudinal slip, side-slip angle and the vertical load, when considered independently under braking and turning. Tire aligning moment properties of the tire are illustrated in Figure 4.5 as functions of the normal load

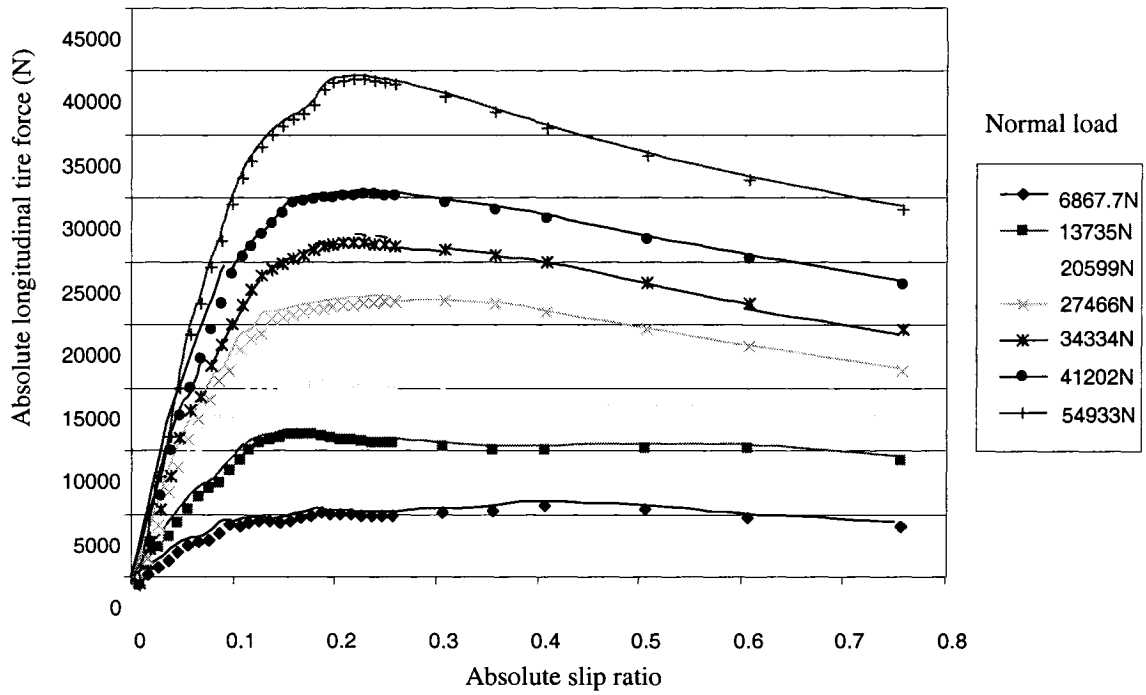

Figure 4.3: Variations in the longitudinal tire force as a function of the slip and normal load.

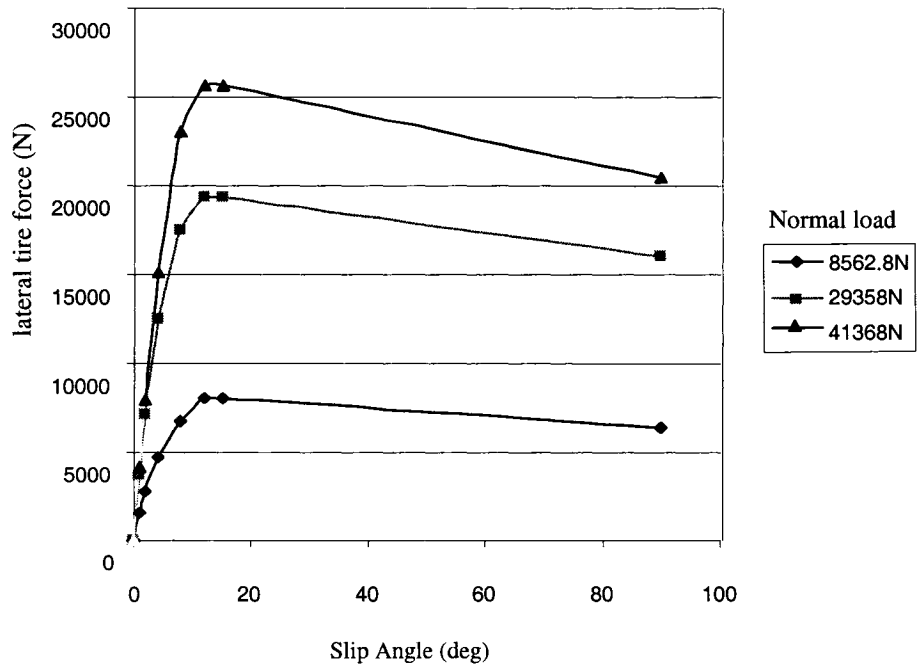

Figure 4.4: Tire cornering characteristics derived from the MSC tire model [24].

and side-slip angle. Such properties in the absence of braking can be expressed by a two-dimensional lookup table of slip angle and vertical load.

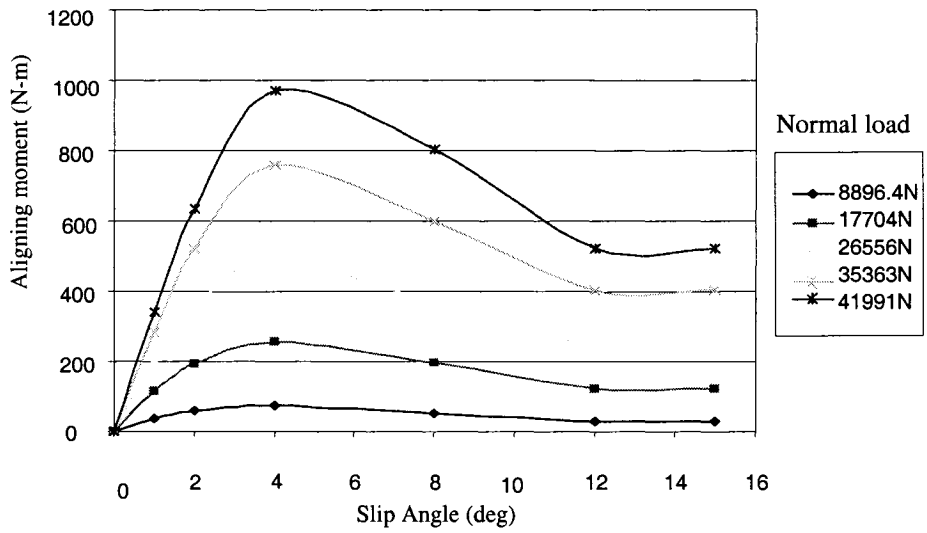

Figure 4.5: Tire aligning moment characteristics derived from the MSC tire model [24]

The cornering forces developed by the tires are evaluated as functions of the side-slip angles. Assuming small levels of longitudinal acceleration, articulated angle, and identical slip angles of the left and right wheels, the slip angle are evaluated from:

$$\alpha_f = \delta - \frac{v_{u1} + l_1\dot{\varphi}_{s1}}{u_{u1}}$$

$$\alpha_r = -\frac{v_{u1} - l_2\dot{\varphi}_{s1}}{u_{u1}}$$

$$\alpha_t = \varphi_{s1} - \varphi_{s2} - \frac{v_{u1} - l_2\dot{\varphi}_{s1} - l_k(\dot{\varphi}_{s1} + (\dot{\varphi}_{s1} - \dot{\varphi}_{s2}))}{u_{u2}} \qquad (4.19)$$

Tire vertical stiffness is an indication of how the load varies as the tire bounces on the road. Assuming linear vertical properties of the tire, as shown in Figure 4.6, the vertical force developed by a tire can be determined directly from the instantaneous tire deflection and effective tire vertical stiffness [93]. The vertical tire force developed by a

tire is thus derived as a linear function of its deflection, provided a tire-road contact exists. As the tire lifts off the ground, the vertical tire force diminishes.

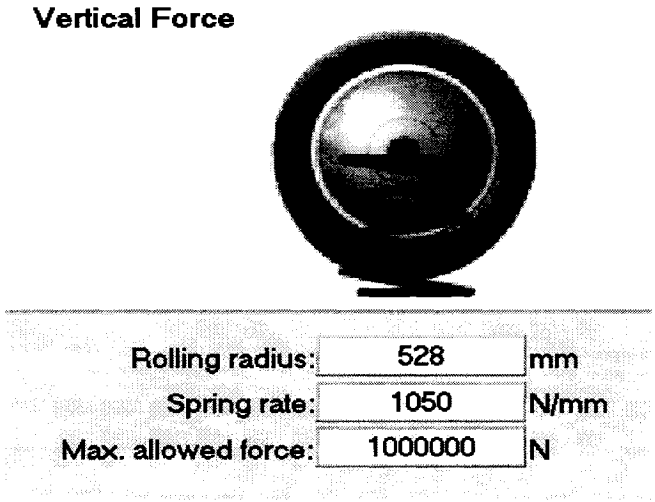

Figure 4.6: Vertical force characteristics of MSC tire model

Simultaneous applications of braking and turning, however, limit the lateral and longitudinal forces developed by a tire due to limited tire-road adhesion. One of the simplest theories for predicting the longitudinal and cornering forces available at a specific slip angle in the presence of a tractive or braking force is based on the friction ellipse concept, as shown in Figure 4.7 [34]. The relationship between the cornering force and the slip angle under free rolling conditions can be determined from the measured data. The cornering forces F_y^M at variables slip angles under free rolling conditions are marked as the minor axis of the friction ellipse, while the maximum tractive or braking force, F_x^M, in the absence of lateral force, constitutes the major axis of the ellipse. The available cornering force F_y at a given side-slip angle and braking force F_x is then determined from the following equation of the friction ellipse:

$$\left(\frac{F_x}{F_x^M}\right)^2 + \left(\frac{F_y}{F_y^M}\right)^2 = 1 \tag{4.20}$$

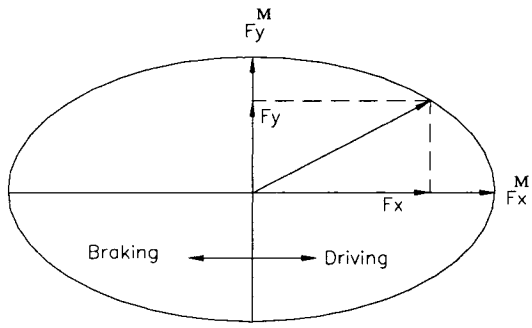

Figure 4.7: The friction ellipse concept relating the maximum cornering force to a given longitudinal force.

4.2.4 Suspension Forces

By far the majority of the commercial vehicle suspensions employ leaf springs as the vertically compliant elements [98]. For the reason of simplicity, instead of using the measured suspension force-deflection data, an analytical approach has been adopted to model the suspension as a combination of a nonlinear spring and a linear damping element, as shown in Figure 4.8. The vertical force acting on the vehicle sprung mass through the suspension system is equal to the static equilibrium force plus the perturbation force, which is denoted as *FS*, from the spring equilibrium point. Furthermore, the suspension springs with a tandem axle group are lumped together assuming small load transfer with the axles in a tandem group. The five-axle vehicle combination is thus represented by a three-composite axle vehicle: (a) front axle; (b) a single composite axle due to rear tandem axle of the tractor; and (c) a single composite axle due to trailer tandem axle. The perturbation force due to the suspension springs of the composite axles can be expressed as [80]:

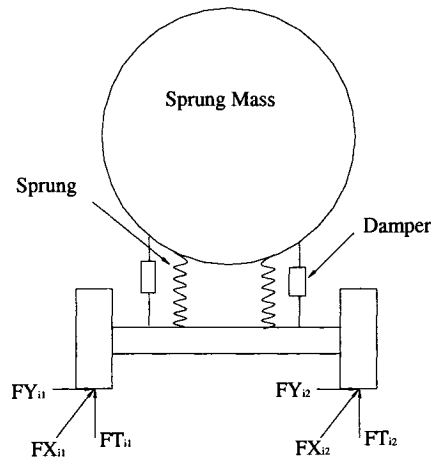

Figure 4.8: The suspension model

$$FS_i = \begin{Bmatrix} K_{f1}e_i + K_{f2}e_i^{\,5} + D_f\dot{e}_i \\ K_{r1}e_i + K_{r2}e_i^{\,5} + D_r\dot{e}_i \\ K_{t1}e_i + K_{t2}e_i^{\,5} + D_t\dot{e}_i \end{Bmatrix} \qquad (4.21)$$

Where K_{f1} and K_{f2} are stiffness constants of the tractor front suspension springs, K_{r1} and K_{r2} are those of the composite tractor rear suspension spring, and K_{t1} and K_{t2} are the constants for the composite trailer suspension spring. D_f, D_r, and D_t are the viscous damping coefficients of the front-, rear- and trailer axle suspensions, respectively. FS_i is the spring force developed by the ith composite axle suspension (i = 1, 2, 3), and e_i is the deflection of the i-th spring from its equilibrium position, which can be expressed in terms of the generalized coordinates:

$$e_{1l} = -s_1\theta_{s1}; \quad e_{2r} = s_1\theta_{s1}$$

$$e_{il} = -s_i\theta_{s1}; \quad e_{ir} = s_i\theta_{s1}; \quad i = 2,\ 3$$

$$e_{il} = -s_i\theta_{s2}\cos\varepsilon_f + (l_i\theta_{s2})\sin\varepsilon_f; e_{ir} = s_i\theta_{s2}\cos\varepsilon_f + (l_i\theta_{s2})\sin\varepsilon_f; i = 3, 4 \quad (4.22)$$

where subscripts 'l' and 'r' refer to left- and right-suspension springs, and ε_f is the articulation angle between the tractor and the trailer, i.e.:

$$\varepsilon_f = \varphi_{s1} - \varphi_{s2} \tag{4.23}$$

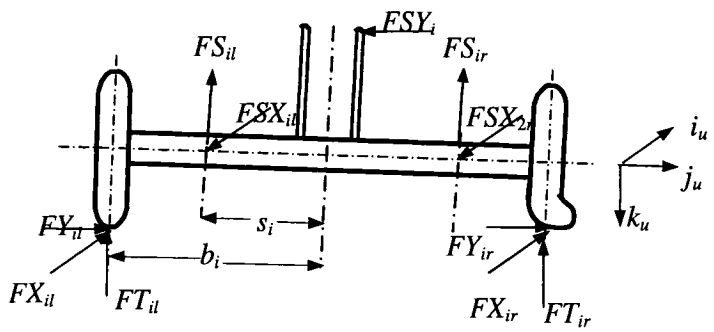

Figure 4.9: Suspension forces on a single axle

The suspension springs generate force components along all the three translational directions. The suspension springs are assumed to remain parallel to an axis normal to the unsprung mass (k_u), as illustrated in Figure 4.9. The lateral component of the suspension force (FSY_i) is assumed to occur at the roll center located at a fixed distance beneath the sprung mass cg [30]. The vertical force component (FS_{ij}, $j = l, r$) acts along the fixed k_u axis, while the longitudinal force component (FSX_{ij}, $j = l, r$) acts along the i_u axis, which also includes the force transferred from the braking. The Figure also shows the three components of the tire forces FX_{ij}, FY_{ij} and FT_{ij} ($j = l, r$) acting along i_u, j_u and k_u axes, respectively, at the tire-road interface of tires on axle i. Many simplifying assumptions have been applied concerning the forces developed between the sprung and unsprung masses, which are detailed in [30, 105-108].

4.2.5 Braking Forces

The braking forces are determined by considering the tire force and wheel inertia torque, as shown in Figure 4.10. For a given tire of radius r subject to angular

velocity ω_k, the dynamic equilibrium of the wheel can be expressed as:

$$J_k \dot{\omega}_k = F_{xk} r - T_{bk} \tag{4.24}$$

Where J_k is the mass moment of inertia of the rolling wheel, ω_k is the angular velocity of a wheel on axle i, F_{xk} is the braking force generated at the tire/ground interface, and T_{bk} is the braking torque applied, and r is the wheel radius. The tire slip ratio is defined as:

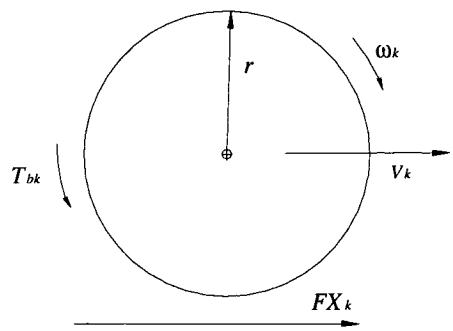

Figure 4.10: Wheel dynamics

$$\lambda_k = \frac{\omega_k r - V_k}{V_k} \tag{4.25}$$

Where, V_k is the forward speed and $\omega_k r$ defines the theoretical forward speed of the wheel.

For a linear brake system model, the attempted brake torque on the *k-th* moving wheel, T_{bk}, is derived from the brake proportion factor and the line pressure, such that: $T_{bk} = B_{tr} \times P_{bk}$, where P_{bk} represents the effective line pressure, minus the push-out pressure, including time lag and rise time, and B_{tr} represents the brake torque coefficient for the wheel [13]. However, if the wheel approaches lock-up condition, the actual brake torque is limited by the tire-road friction. In the case of a brake system model with nonlinear characteristics, a brake force lookup table (treadle pressure versus brake torque) can be used to define the local brake torque coefficient. The longitudinal tire force is a function

of the slip ratio and the tire vertical force, as described in Figure 4.3, which is further modified through consideration of the friction ellipse theory.

4.3 Constraint Forces and Moment

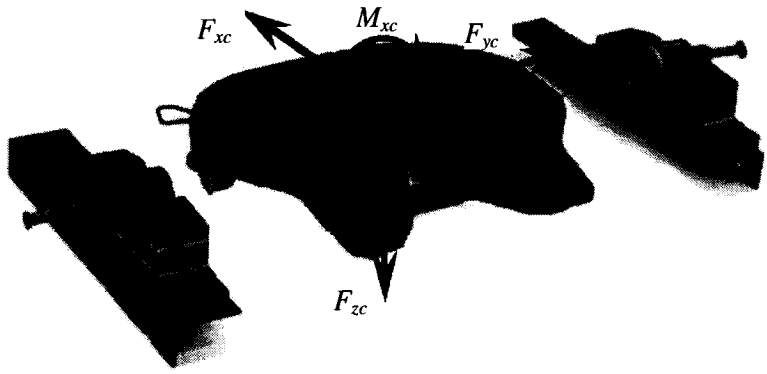

Figure 4.11: Illustration of constraint forces and moment

The constraint forces and moments appearing in the differential equations of motion for sprung masses of the tank vehicle combination, arise from the articulation, as shown in Figure 4.11. Equations (4.7) to (4.9) and (4.13) to (4.15), are derived assuming a parallel spring-damper model of the articulation tractor and the semitrailer [30]. The transmitted force at the fifth wheel can be easily computed based on the spring-dashpot model as:

$$\vec{F}_c = K_c \vec{\delta}_p + C_c \dot{\vec{\delta}}_p \tag{4.26}$$

where $\vec{F}_c$ and $\vec{\delta}_p$ represent constraint force vector and difference in path vector for the fifth wheel position of the tractor and semitrailer. K_c and C_c are constants describing the spring rate and the damping coefficient. The complete computation of $\vec{\delta}_p$ and $\dot{\vec{\delta}}_p$ are presented in reference [102]. The relative roll displacement and velocity between the tractor and semitrailer are used, in conjunction with the torsional stiffness and damping factor of the

constraint to calculate the roll moment transmitted through the fifth wheel, such that:

$$M_{xc} = K_{xc}(\theta_{s1} - \theta_{s2}) + C_{xc}(\dot{\theta}_{s1} - \dot{\theta}_{s2}) \tag{4.27}$$

where K_{xc} and C_{xc} denote roll torsional stiffness and damping coefficients at the fifth wheel.

4.4 Equations of Motion for the Vehicle Combination

The forces and moments developed by the tires, suspension, constraint and fluid cargo are integrated into the generalized equations of motion, presented in Section 4.2, to derive the equations of motion for the partly-filled vehicle combination. The equations of motion for the sprung masses are expressed in the inertial coordinate system (i_n, j_n, k_n), while those for the unsprung masses are formulated in the body-fixed frame (i_s, j_s, k_s). The pitch and yaw angle response of the sprung masses are assumed to be small, such that $\sin\varphi_{sf} \approx \varphi_{sf}$, $\cos\varphi_{sf} \approx 1$, $\sin\alpha_{sf} \approx \alpha_{sf}$, $\cos\alpha_{sf} \approx 1$. The suspension forces developed along the unsprung mass axis system (i_u, j_u, k_u) are expressed in the inertial coordinate system using the transformations described in section 4.2, such that:

$$\begin{Bmatrix} FSX_n \\ FSY_n \\ FS_n \end{Bmatrix} = D_{sf} \begin{Bmatrix} \vec{i}_s \\ \vec{j}_s \\ \vec{k}_s \end{Bmatrix} = \begin{Bmatrix} FSX + (-\phi\cos\theta + \alpha\sin\theta)FSY + (\phi\sin\theta + \alpha\cos\theta)FS \\ \phi FSX + (\cos\theta + \phi\alpha\sin\theta)FSY + (-\sin\theta + \phi\alpha\cos\theta)FS \\ -\alpha FSX + \sin\theta FSY + \cos\theta FS \end{Bmatrix}_{sf} \tag{4.28}$$

Where FSX_n, FSY_n, and FS_n are the suspension forces in the inertial coordinate system. The forces developed due to constraint and the moving liquid are also expressed in the inertial frame in a similar manner. The above forces and moment components are integrated to derive the equations of motion for the vehicle combination assuming three composite axles (1-front axle; 2-tractor rear axle; and 3-trailer-axle). The resulting

equations of motion are presented below:

Equation of longitudinal motion of the tractor:

$$m_1(\ddot{x}_1 + q_1 w_1 - r_1 v_1) = (\alpha_{s1}\cos\theta_i + \phi_{s1}\sin\theta_i)(FS_{1l} + FS_{1r} + FS_{2l} + FS_{2r}) +$$

$$F_{xc} - m_1 g\alpha_{s1} + FSX_{1l} + FSX_{1r} + FSX_{2l} + FSX_{2r} + (-\phi_{s1}\cos\theta_i + \alpha_{s1}\sin\theta_i)\times$$

$$(FSY_{1l} + FSY_{1r} + FSY_{2l} + FSY_{2r}) \qquad (4.29)$$

where:, $\theta_i = (\theta_{s1} - \theta_{ui}), i = 1, 2$; for the front and rear axle suspension forces; and F_{xc} is the longitudinal component of the constraint force reflected into the inertia coordinate system.

Equation of lateral motion of the tractor:

$$m_1(\ddot{y}_1 + r_1 u_1 - p_1 w_1) =$$

$$F_{yc} + m_1 g\sin\theta_i + (-\sin\theta_i + \phi_{s1}\alpha_{s1}\cos\theta_i)(FS_{1l} + FS_{1r} + FS_{2l} + FS_{2r}) +$$

$$\phi_{s1}(FSX_{1l} + FSX_{1r} + FSX_{2l} + FSX_{2r}) + (\cos\theta_i + \phi_{s1}\alpha_{s1}\sin\theta_i)\times$$

$$(FSY_{1l} + FSY_{1r} + FSY_{2l} + FSY_{2r}) \qquad (4.30)$$

where F_{yc} is the lateral component of the constraint force.

Equation of vertical motion of the tractor:

$$m_1(\ddot{z}_1 + p_1 v_1 - q_1 u_1) =$$

$$F_{zc} + \cos\theta_i(FS_{1l} + FS_{1r} + FS_{2l} + FS_{2r}) +$$

$$m_1 g\cos\theta_1 - \alpha_{s1}(FSX_{1l} + FSX_{1r} + FSX_{2l} + FSX_{2r}) +$$

$$\sin\theta_i(FSY_{1l} + FSY_{1r} + FSY_{2l} + FSY_{2r}) \qquad (4.31)$$

where F_{zc} is the vertical component of the constraint force.

Equation of roll motion of the tractor:

$$I_{x1}\dot{p}_1 - (I_{y1} - I_{z1})q_1 r_1 = (FSY_{n1l} + FSY_{n1r})(h_1 - h_{r1}) + (FSY_{n2l} + FSY_{n2r})(h_1 - h_{r2}) -$$

$$F_{yc}(h_1 - h_k) + M_{xc} - [(FS_{n1l} - FS_{n1r})s_1 + (FS_{n2l} - FS_{n2r})s_2] \quad (4.32)$$

Where h_1, h_{r1}, and h_{r2} are the heights of cg, and roll centers of front and rear axle suspensions of the tractor, respectively; s_1 and s_2 are the lateral suspension spreads of the front and rear axles of the tractor; M_{xc} is the roll moment of tractor due to constraint.

Equation of pitch motion of the tractor:

$$I_{y1}\dot{q}_1 - (I_{z1} - I_{x1})p_1 r_1 = -l_1(FS_{n1l} + FS_{n1r}) + l_2(FS_{n2l} + FS_{n2r}) + l_2 F_{zc} +$$

$$(FSX_{n1l} + FSX_{n1r})(h_1 - h_{r1}) + (FSX_{n2l} + FSX_{n2r})(h_1 - h_{r2}) + F_{xc}(h_1 - h_k) \quad (4.33)$$

Equation of yaw motion of the tractor:

$$(I_{z1} + I_{zu1} + I_{zu2})\dot{r}_1 - (I_{x1} - I_{y1})p_1 q_1 =$$

$$(FSY_{n1l} + FSY_{n1r})l_1 - (FSY_{n2l} + FSY_{n2r})l_2) - F_{yc}l_2 + AT_{1l} + AT_{1r} + AT_{2l} + AT_{2r} +$$

$$[(FSX_{n1l} - FSX_{n1r})s_1 + (FSX_{n2l} - FSX_{n2r})s_2] \quad (4.34)$$

Where AT_{ij} are the aligning moment due to tires j (j=1, .., 4) on axle i.

Equation of vertical motion of unsprung masses of the tractor:

$$m_{ui}a_{uzi} = FS_{il} + FS_{ir} - (FT_{il} + FT_{ir})\cos\theta_{ui} - FY_{il} + FY_{ir})\sin\theta_{ui} + m_{ui}g\cos\theta_{ui}$$

$$i = 1, 2. \quad (4.34)$$

Equation of roll motion of unsprung masses of the tractor:

$$I_{xui}\dot{p}_{ui} = (FT_{il} - FT_{ir})b_i - (FS_{il} - FS_{ir})s_i - F_{ri}Z_{ui} -$$

$$[(FT_{il} + FT_{ir})\sin\theta_{ui} + (FY_{il} + FY_{ir})\cos\theta_{ui}](H_{ri} - Z_{ui}\cos\theta_{ui}); \quad (4.35)$$

Where i = 1, 2, and 3; I_{xu1}, I_{xu2}, I_{xu3} are roll mass moments of inertia of each axle of tractor and p_{u1}, p_{u2}, and p_{u3} are their roll velocities; m_{u1}, m_{u2}, and m_{u3} are masses due to

axle *1*, axle *2*, and axle 3; and a_{u1}, a_{u2}, a_{u3} are the vertical accelerations in the respective unsprung mass axis system. Other symbols used in Equations (4.35) and (4.36) are shown below:

F_{ri}: Lateral force acting through the roll center of axle i

FY_{ij}: Lateral force developed at the jth tire-road interface on axle i

H_{ri}: Height of the roll center of axle i from the ground plane

Z_{ri}: Vertical distance between the roll center and cg of the sprung weight

Z_{ui}: Vertical distance between cg of unsprung weight and the roll center

Equation of longitudinal motion of the semi-trailer:

$$m_2(\dot{u}_2 + q_2 w_2 - r_2 v_2) + m_l[a_{x2} + \dot{q}_2 Z_{l2} - \dot{r}_2 Y_{l2} + q_2(p_2 Y_{l2} - q_2 X_{l2}) - r_2(r_2 X_{l2} - p_2 Z_{l2})]$$

$$= -F_{xc} - (m_2 + m_l) g \alpha_{s2} + (\alpha_{s2} \cos\theta_2 + \phi_{s2} \sin\theta_2)(FS_{3l} + FS_{3r}) +$$

$$FSX_{3l} + FSX_{3r} + (-\phi_{s2} \cos\theta_2 + \alpha_{s2} \sin\theta_2)(FSY_{3l} + FSY_{3r}) \qquad (4.37)$$

Equation of lateral motion of the semi-trailer:

$$m_2(\ddot{y}_2 + r_2 u_2 - p_2 w_2) + m_l[(a_{y2} + \dot{r}_2 X_{l2} - \dot{p}_2 Z_{l2} + r_2(q_2 Z_{l2} - r_2 Y_{l2}) - p_2(p_2 Y_{l2} - q_2 X_{l2})]$$

$$= -F_{yc} + (m_2 + m_l) g \sin\theta_{s2} + (-\sin\theta_2 + \phi_{s2}\alpha_{s2} \cos\theta_2)(FS_{3l} + FS_{3r}) +$$

$$\phi_{s2}(FSX_{3l} + FSX_{3r}) + (\cos\theta_2 + \phi_{s2}\alpha_{s2} \sin\theta_2)(FSY_{3l} + FSY_{3r}) \qquad (4.38)$$

Equation of vertical motion of the semi-trailer:

$$m_2(\ddot{z}_2 + p_2 v_2 - q_2 u_2) + m_l[a_{z2} + \dot{p}_2 Y_{l2} - \dot{q}_2 X_{l2} + p_2(r_2 X_{l2} - p_2 Z_{l2}) - q_2(q_2 Z_{l2} - r_2 Y_{l2})]$$

$$= -F_{zc} + (m_2 + m_l) g \cos\theta_{s2} + \cos\theta_2(FS_{3l} + FS_{3r}) -$$

$$\alpha_{s2}(FSX_{3l} + FSX_{3r}) + \sin\theta_2(FSY_{3l} + FSY_{3r}) \qquad (4.39)$$

Equation of roll motion of the semi-trailer:

$$(I_{x2} + I_{xl2})\dot{p}_2 - (I_{y2} + I_{yl2} - I_{z2} - I_{zl2}) q_2 r_2$$

$$= -M_{xc} + m_{l2}[Y_{l2}a_{lz} - Z_{l2}a_{ly} + g(Y_{l2}\cos\theta_{s2} - Z_{l2}\sin\theta_{s2})] -$$

$$(FS_{n3l} - FS_{n3r})s_3 - [F_{yc}(h_3 - h_k) + (FSY_{n3l} + FSY_{n3r})(h_3 - h_{r3})] \qquad (4.40)$$

Equation of pitch motion of the semi-trailer:

$$(I_{y2} + I_{yl2})\dot{q}_2 - (I_{z2} + I_{zl2} - I_{x2} - I_{xl2})p_2 r_2$$

$$= -l_k F_{zc} + l_3(FS_{n3l} + FS_{n3r}) + m_{l2}[Z_{l2}a_{lx} - X_{l2}a_{lz} - g(Z_{l2}\alpha_{s2} + X_{l2}\cos\theta_{s2})] +$$

$$F_{xc}(h_3 - h_k) + (FSX_{n3l} + FSX_{n3r})(h_3 - h_{r3}) \qquad (4.41)$$

Equation of yaw motion of the semi-trailer:

$$(I_{z2} + I_{zu3} + I_{zl2})\dot{r}_2 - (I_{x2} + I_{xl2} - I_{y2} - I_{yl2})p_2 q_2$$

$$= (FSX_{n3l} - FSX_{n3r})s_3 + AT_{3l} + AT_{3r} + F_{yc}l_k - (FSY_{n3l} + FSY_{n3r})l_3 +$$

$$m_{l2}[X_{l2}a_{ly} - Y_{l2}a_{lx} + g(X_{l2}\sin\theta_{s2} + Y_{l2}\alpha_{s2})] \qquad (4.42)$$

Where: l_3 represent the distance from the trailer wheel axle to the tank bottom center; h_k is the height of fifth wheel. s_3 is the distance from suspension width. AT_{3l} and AT_{3r} are the Aligning moments due to tire on semi-trailer axle.

Unsprung mass vertical force

$$m_i a_{uzi} = FS_{il} + FS_{ir} - (FT_{il} + FT_{ir})\cos\theta_{ui} - (FY_{il} + FY_{ir})\sin\theta_{ui} + m_{ui}g\cos\theta_{ui} \qquad (4.43)$$

Unsprung mass roll moment equation:

$$I_{xui}\dot{p}_{ui} = (FT_{il} - FT_{ir})b_i - (FS_{il} - FS_{ir})s_i - F_{ri}Z_{ui} -$$

$$[(FT_{il} + FT_{ir})\sin\theta_{ui} + (FY_{il} + FY_{ir})\cos\theta_{ui}](H_{ri} - Z_{ui}\cos\theta_{ui}); \qquad (4.44)$$

It is assumed that the yaw plane acceleration components of the individual unsprung masses may be estimated from the acceleration of the mass center of the entire vehicle based upon the assumption that the entire vehicle is moving as a single rigid body

in the yaw plane. The estimated lateral and longitudinal acceleration components as well as yaw acceleration are then used to compute the yaw plane constraint forces between the sprung and unsprung masses, FSX_{ij}, FSY_{ij}, based upon the known tire forces. The lateral force acting on the sprung mass from the unsprung mass i is computed from:

$$FSY_i = FY_{i1} + FY_{i2} - m_{ui}a_{uyi} \tag{4.45}$$

Where a_{uyi} denotes the lateral acceleration of unsprung mass i in the yaw plane. The longitudinal forces on the sprung mass from unsprung mass i are derived as:

$$FSX_{i1} + FSX_{i2} = FX_{il} + FX_{ir} - m_{ui}a_{uxi} \tag{4.46}$$

$$FSX_{ir} - FSX_{il} = \frac{1}{s_i}\left[(FX_{ir} - FX_{il})b_i - (AT_{il} + AT_{ir}) - I_{zui}\ddot{\varphi}_{ui}\right] \tag{4.47}$$

where a_{uxi} and φ_{ui} denote longitudinal acceleration and yaw rate of unsprung mass i in the yaw plane system, respectively.

4.5 Summary

The dynamic equilibrium formulations of an articulated vehicle combination comprising a partially filled liquid tank are derived using Newton's second law of motion, which are considered valid until a vehicle tire loses contact with the road. The equations of motion may be solved to determine the vehicle responses to a steering or a braking input or a combination of the two. The analytical model is solved for varying directional inputs and different fill levels of the fluid cargo in the following chapter.

CHAPTER 5 DYNAMIC PERFORMANCE ANALYSIS AND THE SIMULATION PROGRAM

5.1 Introduction

The stability and the dynamic response characteristics of the partly-filled tank vehicles are strongly influenced by the movement of the liquid cargo within the tank. This phenomenon is associated with load shift that may result in instability and/or loss of directional control of the vehicle. During the variable speed directional maneuvers, the transfer of the cg of the liquid load in the longitudinal, lateral, and vertical directions will be affected by the strength of braking, the steering radius and the forward speed of the vehicle, as well as the geometric shape of the liquid tank. Most studies on the dynamic behavior and safety operation performance characteristics of heavy vehicles have focused on the rigid cargos on either the steering or braking inputs. However, the most common operation condition that may yield in an accident of heavy vehicles on the highway is the combinations of steering and braking, which have been addressed in few studies [90, 94, 105-107].

The cargo movement within a partly-filled tank and its influence on the dynamic performance of the vehicle combination under simultaneous steering and braking have not been thoroughly addressed due to the complexities associated with the modeling of the fluid dynamics behavior inside the moving tank [30]. The common analysis of the dynamic performance of a truck-trailer vehicle assumes the cargo to be rigidly attached to the trailer structure.

The first commercial vehicle handling models were developed at the University of Michigan about 20 years ago. The commercial software, however, does not include the

effects of cargo movement on the overall dynamics of the vehicle system. One of the objectives of this work is to overcome this limitation. The optimal design of liquid cargo tank will further be assumed and based upon specific braking and steering maneuvers. The dynamic response of the cargo in the partially filled tank will be evaluated. The overall dynamic performance of the vehicle will be also evaluated and readjusted based on the instantaneous cargo load as per the motion of the fluid in the partially filled tanks. The influence of the liquid dynamics on the vehicle is assumed as a set of comprehensive parameters.

SIMULINK tool box available within Matlab will be used to evaluate the safety performance and the dynamic performance of the partially filled liquid tank vehicles. The approach is very convenient since any modification in the vehicle configuration could be operated of a simple way. However, no Graphic User Interface (GUI) have been yet implemented to make the software more user friendly.

5.2 Performance Evaluations and Simulation Parameters.

5.2.1 The Evaluation Criteria of the Dynamic Response

The evaluation of the dynamic response to the combined braking and steering maneuvers of the articulated freight vehicles are frequently investigated in terms of the lateral Load Transfer Ratio (LTR), vertical Dynamic Load Factor (DLF), and Rearward Amplification Ratio (RAR). The directional response characteristics are expressed in terms of the deviations of the coordinates of the cargo cg (ΔY_l and ΔZ_l), the mass moments of inertia (I_{xl2}, I_{yl2} and I_{zl2}) of the cargo with respect to the tank cg; the roll angle (θ_{s2}), the lateral acceleration (a_{y2}) and the yaw rate (r_2) of the semi-trailer sprung mass; the articulation angle (γ); the wheel dynamic load factor (DLF) and the load transfer ratio

(LTR) of the combination.

The articulated vehicles, especially the multiple articulated vehicles, often exhibit relatively large magnitudes of lateral motion at the rearmost unit during the high-speed directional maneuvers, which may be further amplified by the motion of the liquid cargo within a partly-filled tank trailer. The Rearward Amplification Ratio (RAR), is defined as the ratio of the maximum value of the lateral acceleration (and/or roll angle) at the cg of the sprung mass of the rearmost trailer to that developed at the cg of the tractor sprung mass during a transient directional maneuver, and is expressed as:

$$RAR = \max\left(|RAR_{max}|, |RAR_{min}|\right) \tag{5.1}$$

For a tractor semi-trailer combination:

$$RAR_{max} = \max\left(a_{y2}\right)/\max\left(a_{y1}\right) \tag{5.2}$$

$$RAR_{min} = \min\left(a_{y2}\right)/\min\left(a_{y1}\right) \tag{5.3}$$

Where a_{y1} and a_{y2} are the instantaneous lateral accelerations encountered at the cg of the tractor and the semi-trailer sprung weights, respectively. The RAR describes the vehicle's tendency to amplify the severity of maneuver-induced motions of the tractor. A larger value of RAR indicates an increased likelihood of rollover of the rearmost trailer of a combination [30, 108].

The likelihood of vehicle rollover has also been described in terms of the lateral load transfer trend of the vehicle. This tendency is often expressed in terms of the dynamic load transfer ratio (LTR) and the dynamic vertical load factor (DLF) [87]. The dynamic vertical load factors are defined as the ratio of the instantaneous vertical load on the left or right track of a given axle to the static vertical load on that track and are expressed as:

$$DLF_r = \frac{2F_{zr}}{F_{zr} + F_{zl}} \text{ and } DLF_l = \frac{2F_{zl}}{F_{zr} + F_{zl}} \tag{5.4}$$

Here: F_{zr} and F_{zl} are the instantaneous vertical loads on the right-and left-wheels of an axle respectively. The DLF assumes a unity value under static conditions and will approach zero during a directional maneuver, when tires on the inner track lose contact with the road. The DLF due to the outer track tires under such situation will attain a maximum value of the 2. This measure describes the roll dynamics of a particular axle. The roll dynamic performance of a vehicle combination has also been evaluated in terms of the dynamic load transfer ratio (LTR), defined as the ratio of the sum of instantaneous absolute value, of the difference between right-wheel loads and left-wheel loads, to the sum of all the wheel loads, and is expressed as [107]:

$$LTR = \sum_{i=1}^{N} \frac{|F_{zri} - F_{zli}|}{F_{zri} + F_{zli}} \tag{5.5}$$

where N represents the number of axles of the combination. LTR assumes an initial value of zero and approaches unity when the wheels on the inside track lift off the ground.

5.2.2 Simulation Parameters

The dynamic characteristics of a vehicle are affected by the vehicle construction parameters and their inertia values. The selected vehicle will be referred from the literature and from the previous experimental work [30, 80]. As shown in Table 5.1 to 5.5.

5.2.3 The Simulation Model for the Partly-Filled Tank Vehicle under Simultaneous Braking and Turning Manoeuvres

The dynamic model for the directional response and the stability analysis of a partly - filled liquid tank vehicle under simultaneous braking and turning maneuvers can

Table 5.1 Simulation parameters of the tractor

Type	Three-Axle
Sprung weight m_1 (kg)	8444.0
Distance between tractor cg and front wheel axle l_1 (m)	2.59
Distance between tractor cg and rear wheel axle l_2 (m)	3.29
Tare center of gravity height h_1(m)	1.12 m
Roll mass moment of inertia I_{x1} (kg-m^2)	12446.5
Yaw and pitch mass moment of inertia I_{y1} and I_{z1} (kg-m^2)	65734.6
Front axle track width s_1(m)	1.01
Rear axle track width s_2(m)	0.91
Front axle roll center to ground h_{r1}(m)	0.464
Rear axle roll center to ground h_{r2}(m)	0.838

Table 5.2 Parameters for the semi-trailer

Type	Two-Axle
Trailer axle roll center to ground h_{r3} (m)	0.686
Sprung weight (empty) m_2 (N)	51827
Unsprung weight m_{ui} (N)	13344
Wheel base l_3 (m)	10.41
Tare center of gravity height h_2 (m)	1.52
Roll mass moment of inertia I_{x2} (Nms^2)	9039
Yaw and pitch mass moment of inertia I_{y2} and I_{z2} (Nms^2)	11298

Table 5.3 Parameters for the tractor and semitrailer suspension

Type	Value
Tractor front spring, K_{f1} (N/m)	272,000
Tractor front spring, K_{f2} (N/m^5)	3.36e10
Tractor front and rear damper, D_f, D_r (N.s/m)	9,080
Tractor rear spring, K_{r1} (N/m)	853,000
Tractor rear spring, K_{r2} (N/m^5)	1.05e11
Trailer spring, K_{t1} (N/m)	1.55e6

Table 5.4 Parameters for the fifth wheel

Type	Value
Fifth wheel roll stiffness, I_{cx} (Nm/rad)	6,000,000.0
Height of fifth wheel above ground, h_3 (m)	0.8
Fifth wheel stiffness, K_{xc} (N/m)	20,000,000
Fifth wheel damping coefficient, C_{xc} (N.s/m)	200,000
Distance from tractor cg to fifth wheel, l_2(m)	3.29
Distance from semitrailer cg to fifth wheel, l_k (m)	5.93

Table 5.5 Axles parameters

	Axle 1	Axle 2	Axle 3	Axle 4	Axle 5
Unsprung weight, m_{ui}, (kN)	5.34	11.12	11.12	6.67	6.67
Loaded tire radius r_i, (m)	0.516	0.516	0.516	0.546	0.546
Roll center height, (m)	0.464	0.838	0.838	0.686	0.686
Axle roll mass moment of inertia, (Nms^2)	418	576	576	463	463
Wheel polar moment of inertia, (Nms^2)	23	26	26	26	26
Tire track width, (m)	2.045	1.829	1.829	1.829	1.829
Dual tire spacing, (m)	-	0.330	0.330	0.330	0.330
Suspension spring spacing, (m)	0.827	0.965	0.965	1.118	1.118

be effectively developed by integrating the 3-D quasi-static fluid slosh model, developed in section 4.4, into a variable speed yaw/roll dynamic model of a rigid cargo vehicle [93]. A five-axle articulated tank vehicle combination comprised of a three-axle tractor and a two-axle semi-trailer has been considered in order to study its dynamic characteristics under combined braking and turning maneuvers. The tractor consists of a single front axle with single tires that can be arbitrarily steered. All the other axles on the vehicle combination can be represented as single or tandem axles with single or dual wheel sets.

The articulated tank vehicle combination is modeled as two sprung masses: the

sprung mass of the tractor m_1, and the tare mass of the semi-trailer structure and the empty tank m_2. The liquid cargo mass, m_l, is considered as a constrained floating mass with respect to the cg of the trailer sprung mass. The axles are modeled as three composite independent masses. The two sprung masses of the vehicle are characterized as rigid bodies with 6 DOF, which all: longitudinal, lateral, vertical, roll, pitch and yaw motions. The unsprung masses are free to roll and bounce with respect to the sprung masses to which they are attached. A rotational DOF is defined for each of the composite wheel sets to perform braking analysis. The torsional flexibility of the tractor frame, and the coupling between the tractor and the trailer sprung masses are represented by two lumped torsional springs. The roll stiffness due to the anti-sway bars and linkages is represented by auxiliary roll stiffness between the sprung and the unsprung masses for each axle.

The braking system on each axle of the vehicle combination is represented by the input pressure and output torque applied with the time lag (delay between the time of pedal action and the onset of pressure rise in the brake chamber), rise time (time required to reach 63% of the steady-state step response) and the brake torque ratio (the resulting brake torque per unit of air pressure in the brake chamber). These properties can be described either of a linear fashion, by a brake torque coefficient, or by including their nonlinear characteristics using lookup tables. Although the model development is carried out for pneumatic brake systems commonly used in heavy vehicles, the characteristics of the hydraulic brake systems can also be incorporated through appropriate braking system models, where the brake lag and rise times are considered negligible [97]. In the simulation model, the brake torque is applied to the wheel causing it to decelerate, while

the tire brake force is derived from longitudinal slip in conjunction with the tire model. At a given instant, a portion of the brake torque may thus be devoted to achieving the deceleration of the wheel.

The directional dynamic model of the articulated tank vehicle is developed subject to a number of simplifying assumptions, namely: (*i*) the sprung and unsprung masses move as one rigid body in yaw; however, they experience independent roll and pitch motions; (*ii*) the suspension springs experience deflection along the fixed unsprung mass and roll about the user-defined suspension roll center, located at a fixed distance below the sprung mass cg; the longitudinal and the lateral forces arising from tires are thus applied directly at the spring locations resulting in forces and moments about cg of the sprung mass; (*iii*) the suspension spring forces are modeled as nonlinear functions of suspension deflections and the dissipative properties; (*iv*) sprung mass roll and pitch rotations are assumed to be small in the implementation of the mathematical equations such that the simulations can be considered valid only up to a maneuver limit at which a wheel lift-off occurs; (*v*) the cross-products of mass moments of inertia of the sprung masses are considered negligible to avoid the dynamic coupling among the three rotational-DOF (roll, pitch and yaw).

The articulation is modeled as a force and moment constraint in which the tractor and the semi-trailer are subject to equal and opposing forces and moments, dependent on the difference in the fifth wheel position and orientation, as measured at the tractor and the semi-trailer. Initially the fifth wheel position of the tractor and the semi-trailer are assumed to be identical. As the simulation proceeds, the forces developed at the tire-road interface will cause disparate paths for the fifth wheel position of the tractor and the

semi-trailer. A distance will thus develop between them. The direction of the restraining hitch force is assumed to be along a line through the fifth wheel location of the tractor and the semi-trailer. The fifth wheel restraint moment is similarly represented by a torsional spring-damper connection between the tractor and the semi-trailer. The effects of pitch rotation and the articulation angle are neglected since the most commonly used fifth wheel and inverted fifth wheel couplings permit relative yaw and pitch rotations between the leading and the trailing units, but are considerably stiff in roll. The roll moment transmitted through the fifth wheel is assumed to be applied along the longitudinal axis of the tractor.

The entire liquid cargo within the tank is assumed to move as a rigid body, due to the lateral and the longitudinal accelerations of the tank trailer subject to combined steering and braking maneuver [30]. The motion of the free surface of the liquid creates a new deflected shape of the liquid bulk within the tank, resulting in a shift of the coordinates of the liquid cargo cg from its static position $C_{l0}(L/2, 0, Z_{l0})$ to $C_l(X_l, Y_l, Z_l)$, which are expressed in terms of the tank body-fixed coordinate system, and bears considerable variations in the mass moments of inertia properties.

The entire system of the tractor and the semi-trailer vehicle can be divided into three subsystems: operation system, tractor system, and semi-trailer system. The operating system includes the braking and the steering units. The tractor system consists of the tractor sprung mass m_1, the suspension constructions, and the wheel sets. The semi-trailer system includes the tare mass of the semi-trailer structure along with the empty tank m_2, the liquid cargo mass m_l, the suspension constructions, and wheel sets, as are illustrated in Figure 5.1.

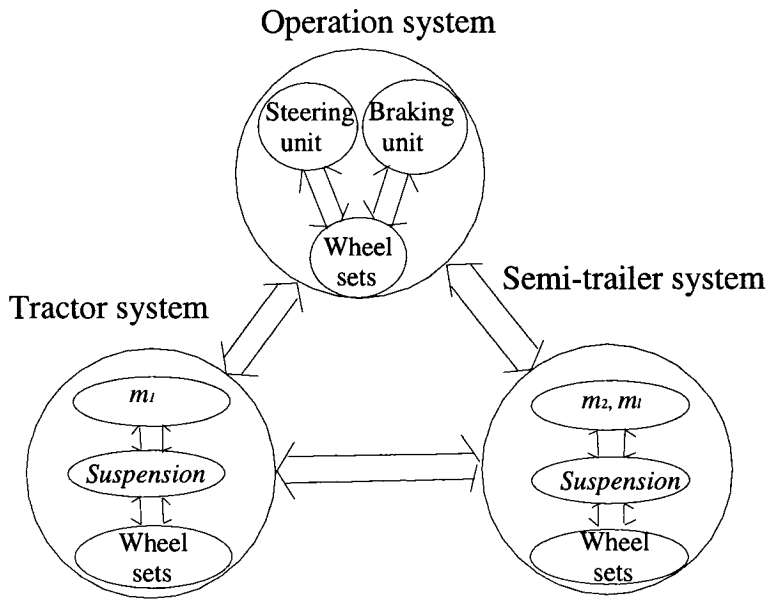

Figure 5.1: The formulation of the vehicle model (SIMULINK)

5.3 Dynamic Simulation of the Trailer System

The trailer system will simulate the dynamic characteristics of the liquid motion in the partially-filled liquid tank and it will output the tire force, the wheel set rotation and bounce, the suspension support and the force transition between sprung and the unsprung mass. Assuming the same dynamic characteristics for each wheel in the tandem construction, the count of the DOF is the following: there are 6 DOF in the sprung mass of the trailer, 3 DOF in the front tandem and 3 DOF in the rear tandem of trailer system. The DOF in the tandem system is: the bounce (vertical motion), the roll rotation and the tire rotation (for braking simulation). The input of the simulation for the trailer system will be changed according to the different steering and braking manoeuvre, to maintain the simulation of the vehicle under stable conditions. The input of the trailer system will be adjusted according to the initial speed of the vehicle, the filling conditions, the steering angle, and the braking strength.

The liquid mass in the simulation of the trailer system will be selected at 50% and 70% filling conditions, or the same weight for the equivalent rigid cargo. Four cases have been considered in the simulation apart from the validation of the simulation model. (1) at 10 psi braking condition and 50% filling condition, simulate two different steering input of 0.5^{o} and 1.0^{o}, and then compare the different responses of liquid cargo for T_5 tanker with and same mass of the rigid cargo; (2) at the steering angle of 0.5°, analyze the braking input as 10 psi and 30 psi, and then compare the dynamic simulation of liquid cargo of T_5 model with the equivalent solid cargo; (3) at 10 psi braking and 70% filling conditions, analyze the vehicle dynamic response of liquid cargo for T_5 model and the equivalent rigid mass for the steering angle of 0.5^{o} and 1.0^{o} respectively; (4) under the same operational conditions, 10 psi braking pressure, 0.5^{o} steering angle, 50 % filling condition, compare the dynamic response of all five models of tanks, T_1 to T_5. In all simulations in which steering and braking are applied, steering is assumed to be applied at time $t = 0$ s, while braking is applied at time $t = 4$s.

5.3.1 Validation of the Simulation Program

The vehicle response characteristics to different steering and braking inputs are initially investigated for the cleanbore cylindrical T_5 trailer as a function of the fill level. The analyses are performed for both partly-filled liquid cargo and an equivalent rigid cargo in a particular vehicle model. Under the same input conditions, the results of the simulation will be validated against Kang's results in Figure 5.2.

As shown in Figure 5.2, the legend Tank5_SOLID0.5 and _SOLID1.0 refer to at the steering $\delta_t = 0.5^{0}$ and 1.0^{0}, SOLID cargo, and T_5 tank, respectively. The DLF on the left side (outside) of the trailer will increase with the steering input; after the application

of braking at t = 4s, the DLF on the left side will decrease, and the trailer with the liquid cargo will respond more extremely than the trailer with rigid cargo.

It should be pointed out that in Kang's work; the variable-speed yaw/roll tank vehicle model is used to simulate the dynamic characteristics of the tank vehicle combination under various steering and braking inputs, fill volumes, road conditions and tank cross-sections. The motion in pitch plane is neglected in the yaw/roll model. The motion in the pitch plane is calculated in this work and a discussion on how this would affect other dynamic parameters is carried out.

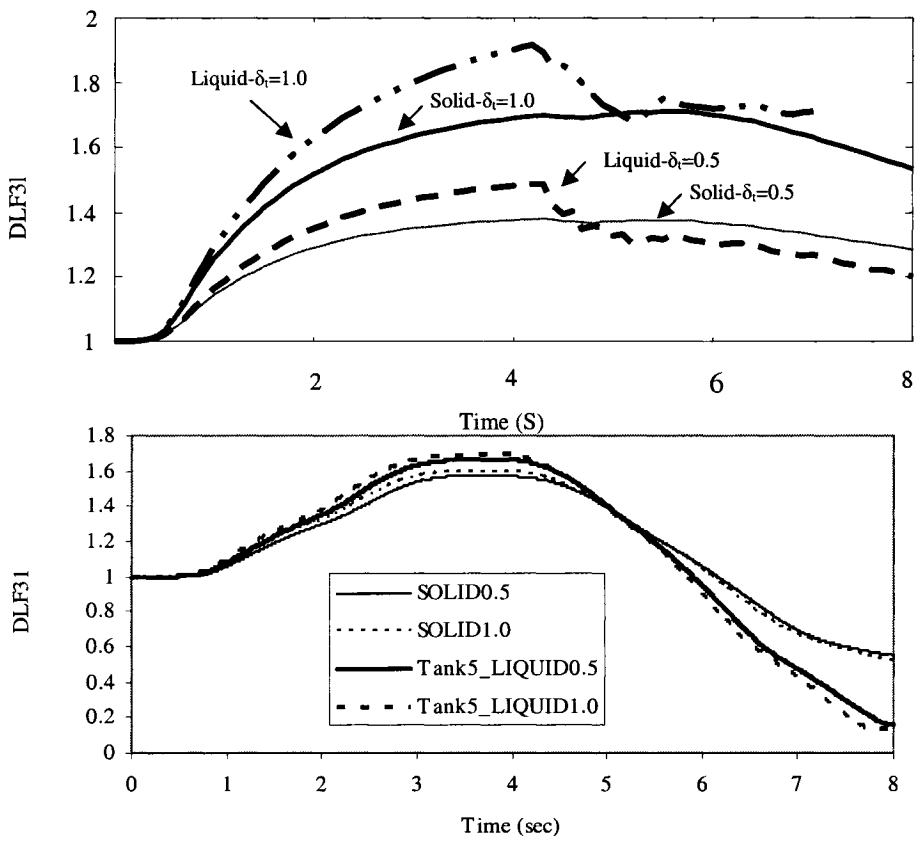

Figure 5.2: The DLF response of trailer left wheel under steering and braking. (T_b=68.95kPa, β=0.5, the above figure represents the result of Kang [30]

5.3.2 The Influence of the Steering Angle

The dynamic load shift properties of a 50% filled (cargo specific weight: 1.357 ton/m^3) tank vehicle equipped with clear bore of T_5 type are evaluated under both steering and braking inputs. The dynamic load shift characteristics are assessed in terms of the dynamic load factors (DLF) of different tires, using equation (5.4). The analyses are performed for 0.5 and 1.0 degree ramp-step steer inputs at the beginning of the simulation and the braking treadle pressure of 68.95 kPa (10 psi) at t = 4 second. The results show the DLF responses of tires of the corresponding equivalent rigid cargo vehicle to illustrate the contributions due to the moving cargo.

Figure 5.3 illustrate that the DLF responses of different tires perform within a slight variation between solid cargo and the equivalent liquid cargo during steering. However, the differences become more significant while vehicle is under braking and steering. This phenomenon would be due to the liquid shift from its static equilibrium position and the change of additional moments of liquid cargo in pitch, yaw, and roll planes, as shown in Figure 5.4. Similar trend is noticed in the variation of the moments along the three principal axles. The solid cargo yields no change in the moment about the above mentioned axes. Moreover, in the yaw-roll model, the pitch motion is neglected. However, the proposed model points out the fact that a significant moment in pitch plane is generated during braking and steering. This finding represents one of the significant contributions of this work. Figure 5.5 represents the variation of the cg with respect to the point "G_0" in Figure 2.4. As for the solid cargo, no cg shift is expected (illustrated in Figure 5.5 by a straight line), the variations of the cg position along the three principle axes are growing mainly after braking is applied during steering maneuver. The cg shifts

in lateral direction, becomes smaller as the vehicle subjected to a constant braking.

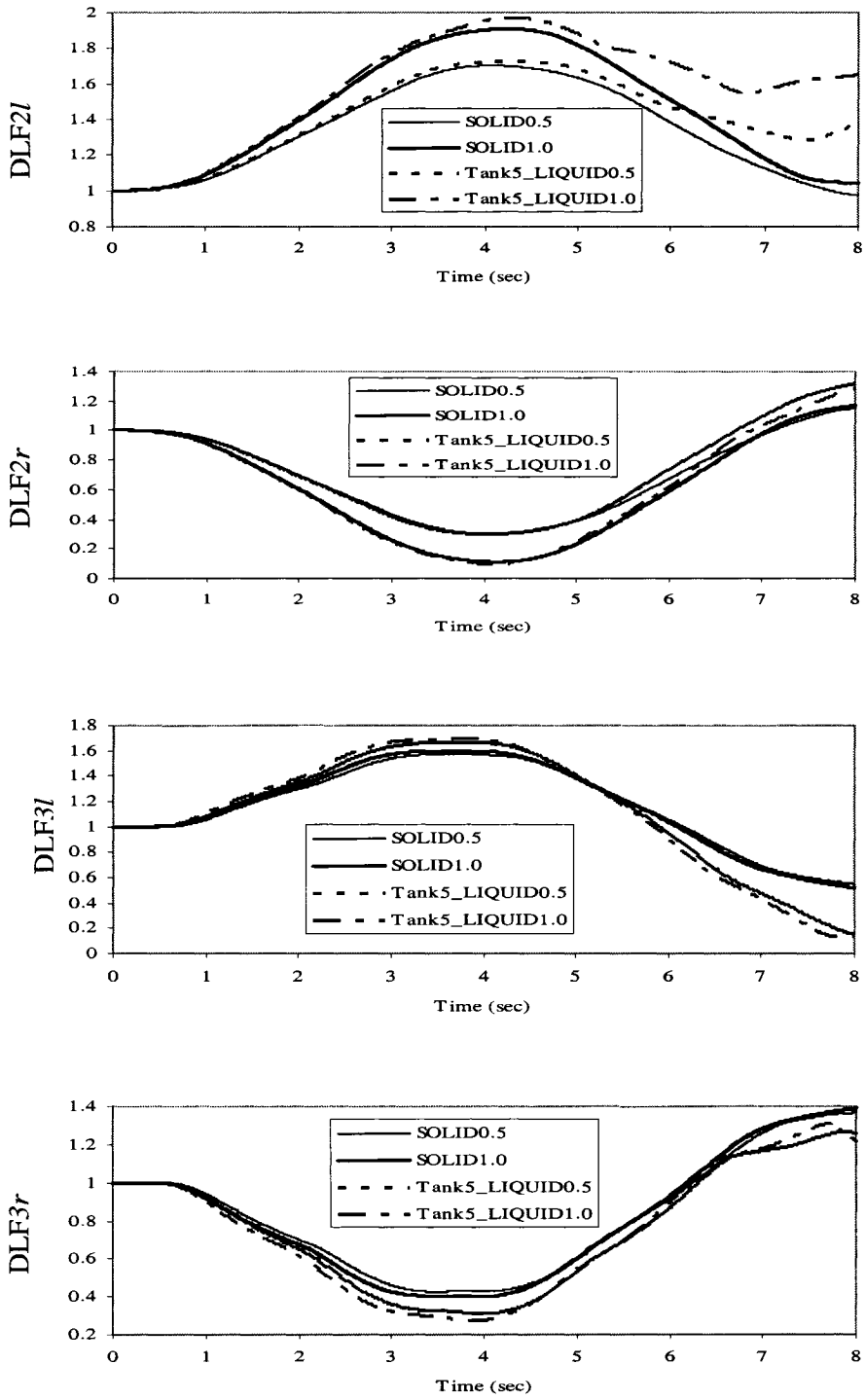

Figure 5.3: DLF responses under steering and braking at T_b=10 psi, β=0.5.

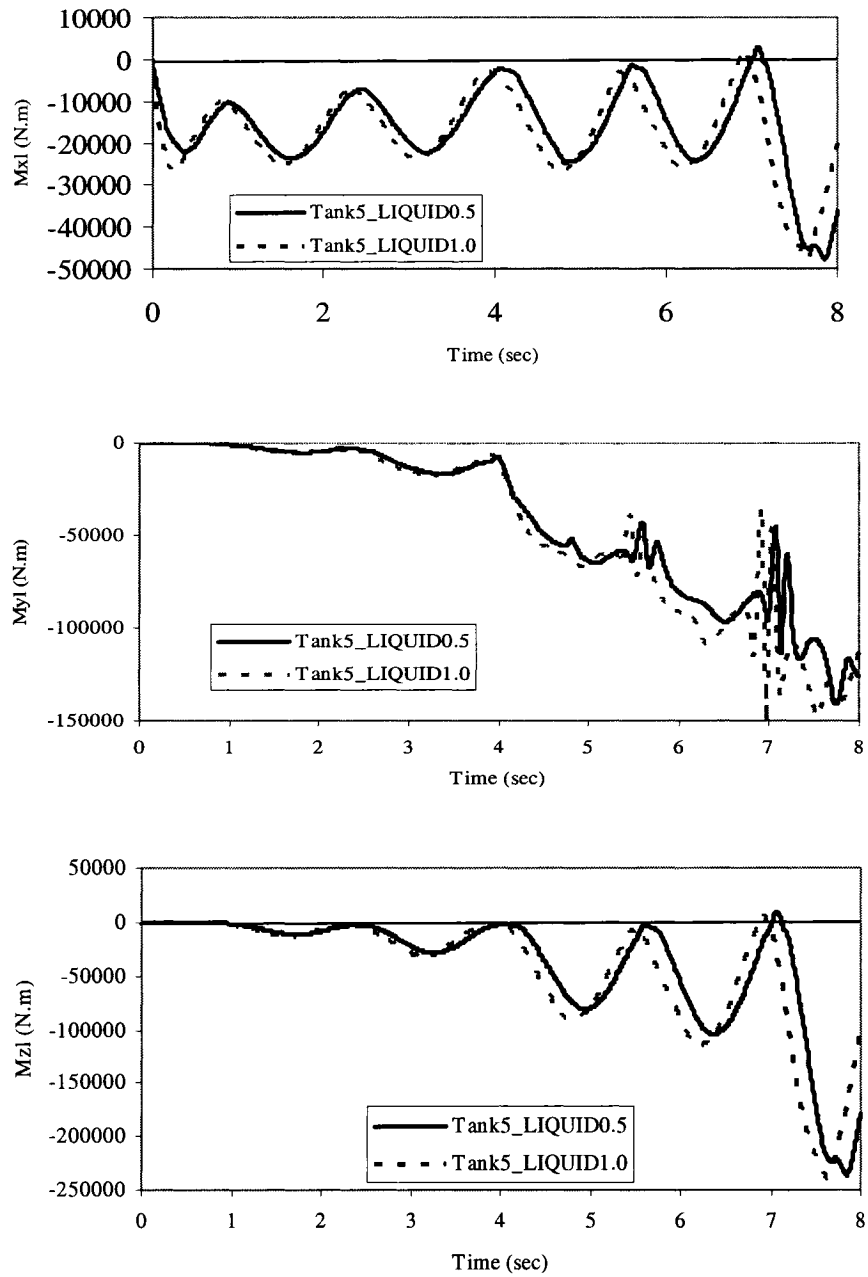

Figure 5.4: Moments variation induced by the cargo cg under steering and braking (T_b=10 psi, β=0.5).

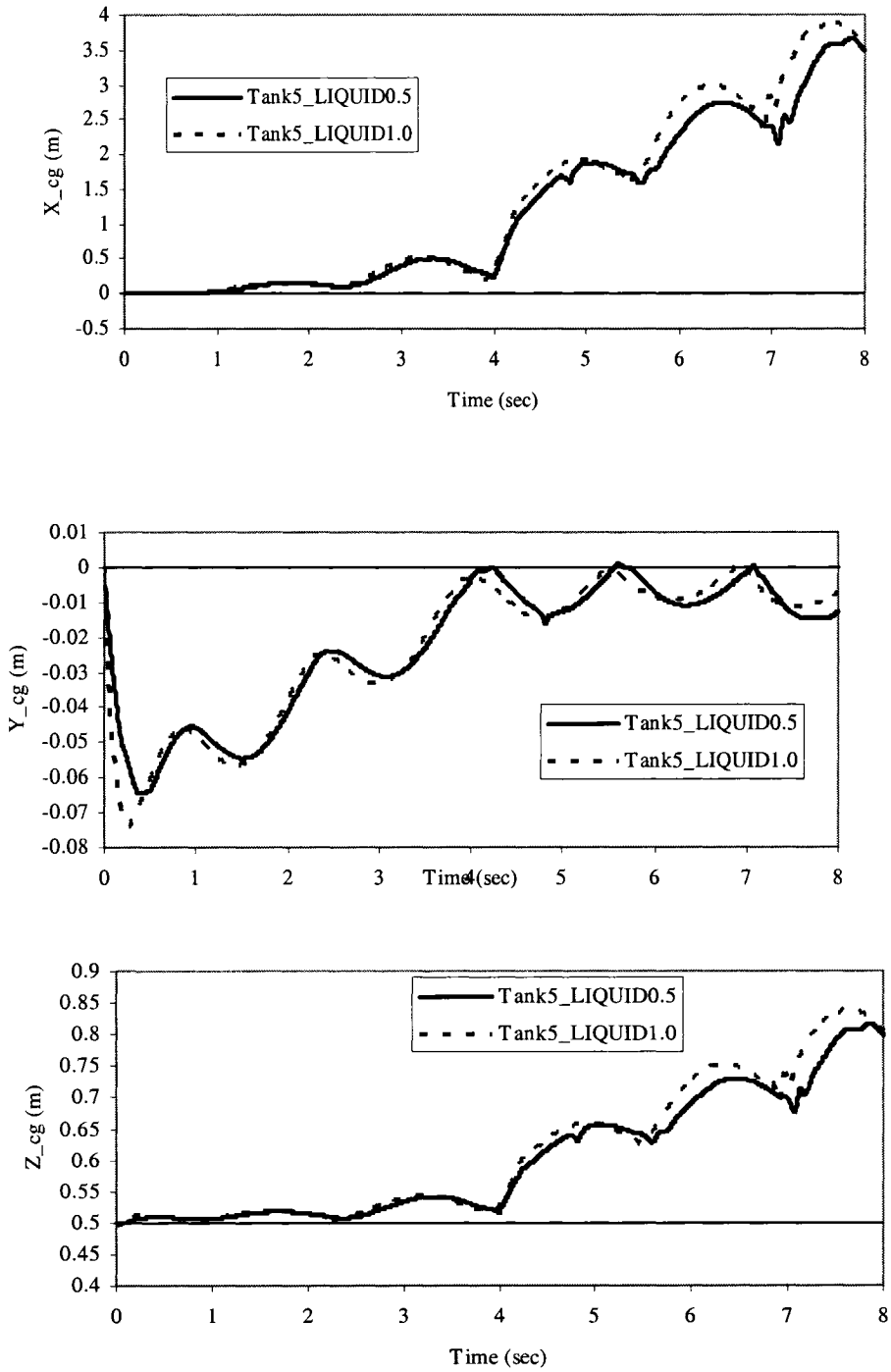

Figure 5.5: The cg motion of the liquid cargo under steering and braking, (T_b=10 psi, β=0.5)

5.3.3 The Influence of the Braking Treadle Pressure

Two different values of braking treadle pressure (10 and 30 psi), represented as LIQUID10 and LIQUID30 in the following figures) are used to analyze the directional response characteristics of the liquid cargo vehicle. At the steering angle of 0.5°, filling condition of 50%, the response characteristics of the liquid cargo contained in the tank of section T_5, are shown in Figures 5.6 to 5.9. The semitrailer loaded with solid cargo experiments larger longitudinal acceleration than the equivalent vehicle loaded with liquid cargo. This may be due to the sloshing effect of the fluid within the tank, as shown in Figure 5.9, and then the variation of the braking effects on each wheel set, only after braking during steering. However, the effect is inverse in lateral direction; the lateral acceleration of the liquid loaded semitrailer is higher than the one of the semitrailer loaded with solid cargo. The DLF for a combination is significantly increasing for a liquid tanker after braking is applied in steering, as shown in Figure 5.7, the larger braking treadle pressure yields the larger variation of the DLF response.

5.3.4 The Influence of the Cargo Fill Level

The performance evaluation is carried out on the same partly filled liquid cargo vehicle under the provision of a fill level of 50% and 70%, steering angle at 0.5° and 1.0°, and brake treadle pressure at 10 psi, respectively. The results will reveal the role of fill level in the dynamic behavior of an articulated liquid tank vehicle performing braking under steering. As shown in Figure 5.11, at 70% fill level volume, the magnitude of DLF response on the front and rear wheels of the trailer are smaller than those corresponding to 50% fill condition. This condition is mainly due to the cg shift due to sloshing, as illustrated in Figure 5.12. The longitudinal and lateral accelerations under steering

maneuver are quite similar for 0.5 and 0.7 fill level under 0.5° and 1° steer angle, However, when 10 psi braking pressure is applied, these acceleration responses are obviously strong at the condition of 0,5 fill level, as shown in Figure 5.11. Furthermore, at the 0.5 fill level condition, the cg shift in the longitudinal and vertical directions are almost double distance and double stronger than those at 70% fill level condition. The variations of moment along three axles during braking and steering, as shown in Figure 5.13, are oscillated rapidly along Y- and Z-axles. For the fill level at 0.5, these tendencies are obviously stronger than those at 70%. But the variation of moment along Z-axle at fill level 0.5, is less than at fill level 0.7. This result confirms that at 50% fill condition, a liquid tanker vehicle performance more dangerously than the same vehicles under 70% fill level conditions.

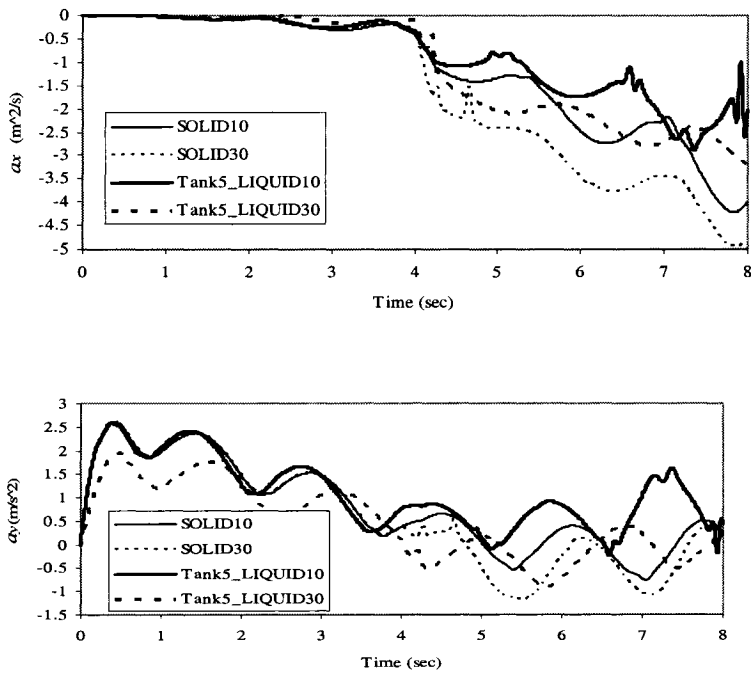

Figure 5.6 :The influence of the braking treadle pressure on the longitudinal and lateral accelerations (δ_f=0.5 degree, β=0.5)

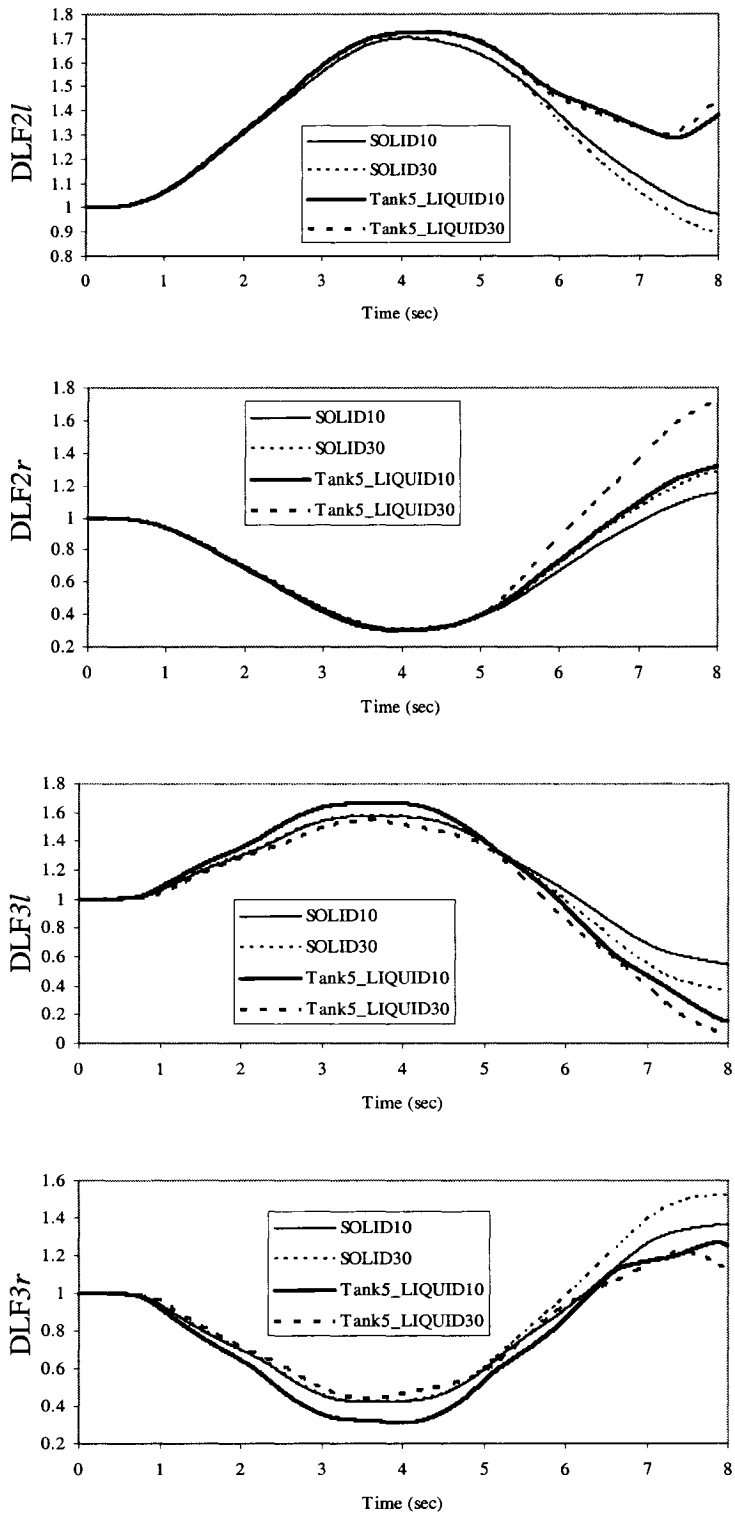

Figure 5.7: The influence of the braking treadle pressure on the DLF response (δ_f=0.5 degree, β=0.5)

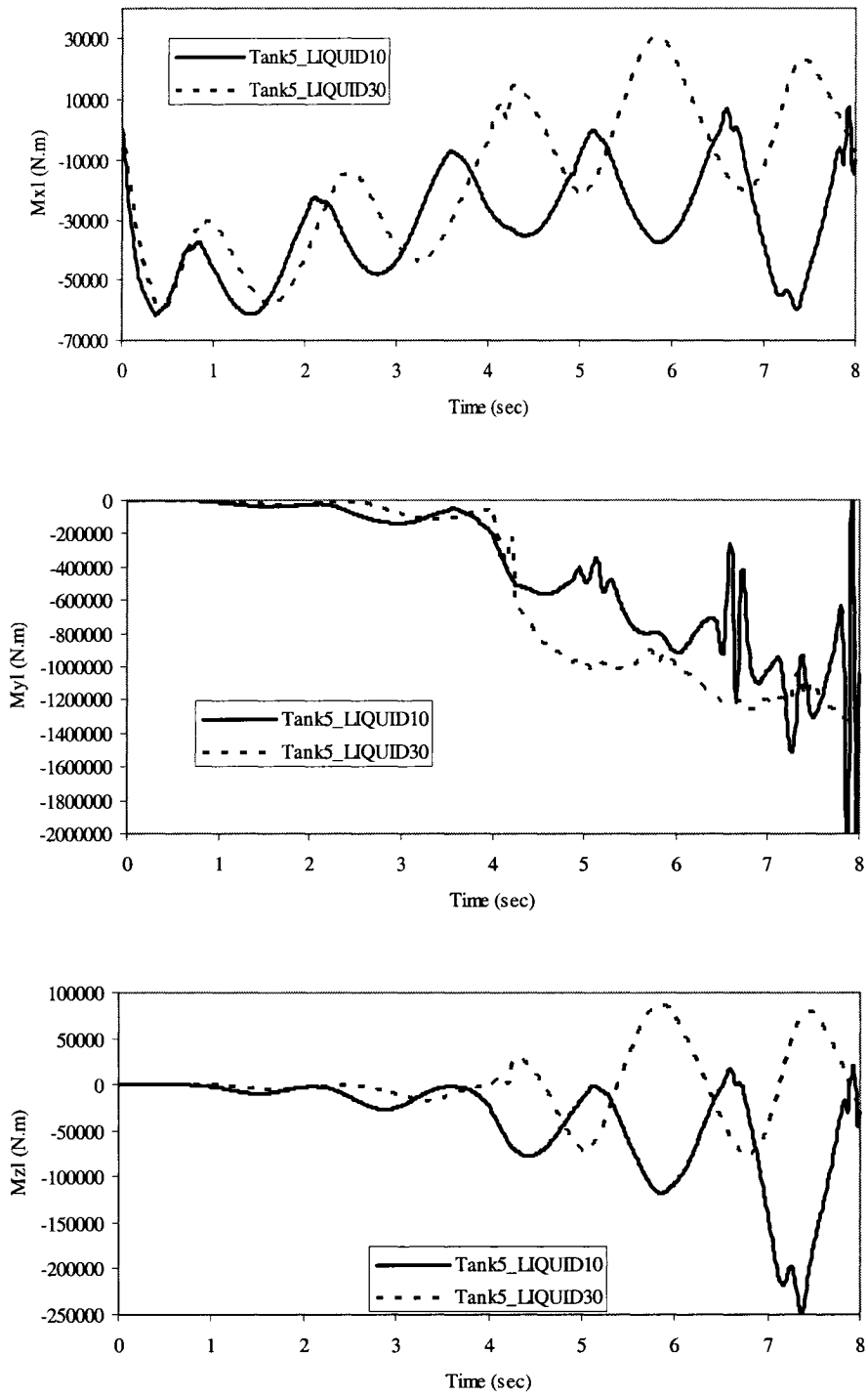

Figure 5.8: The influence of the braking treadle pressure on the moments. (δ_f = 0.5 degree, β=0.5)

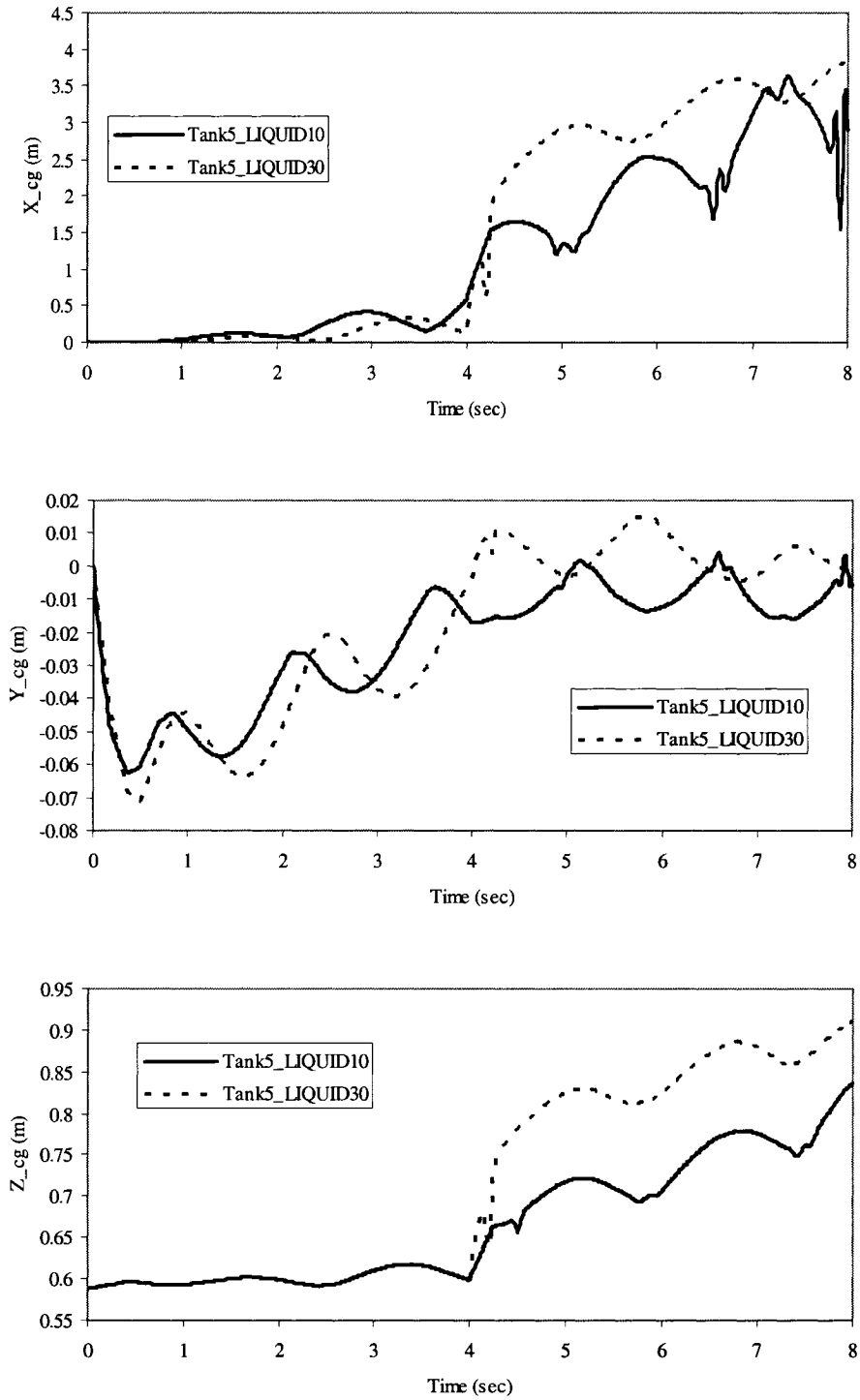

Figure 5.9 The influence of the braking treadle pressure on the shift of c. g motion (δ_f=0.5 degree, β=0.5)

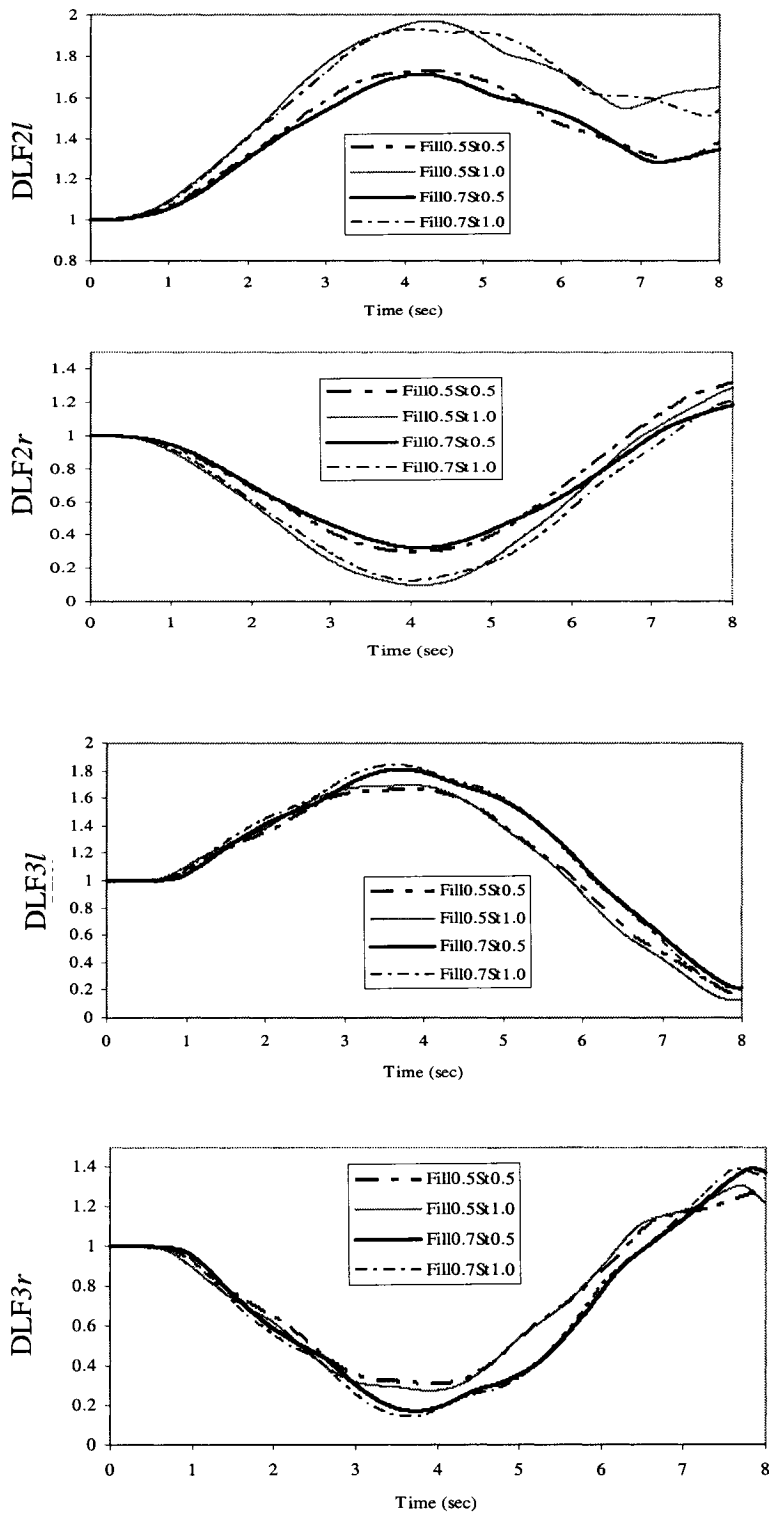

Figure 5.10: The influence of the fill level on the responses of DLF, under steering and braking.

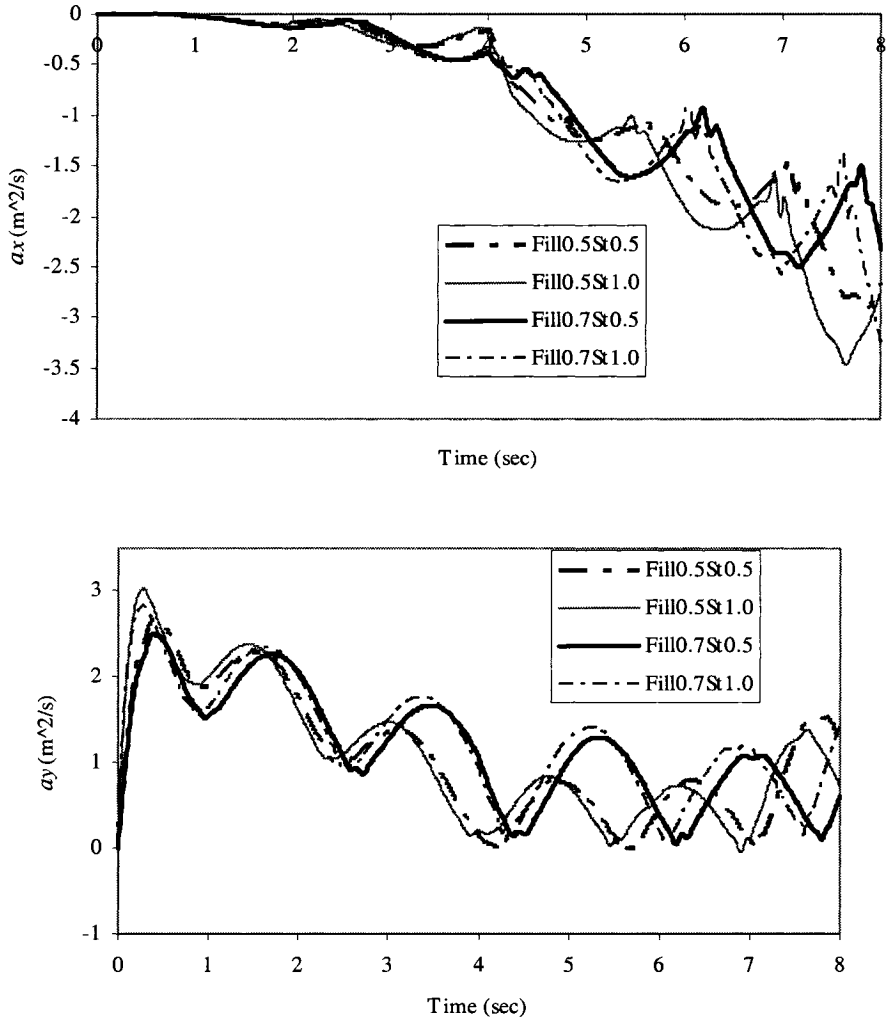

Figure 5.11 The influence of the fill level on the longitudinal and lateral accelerations response, under steering and braking.

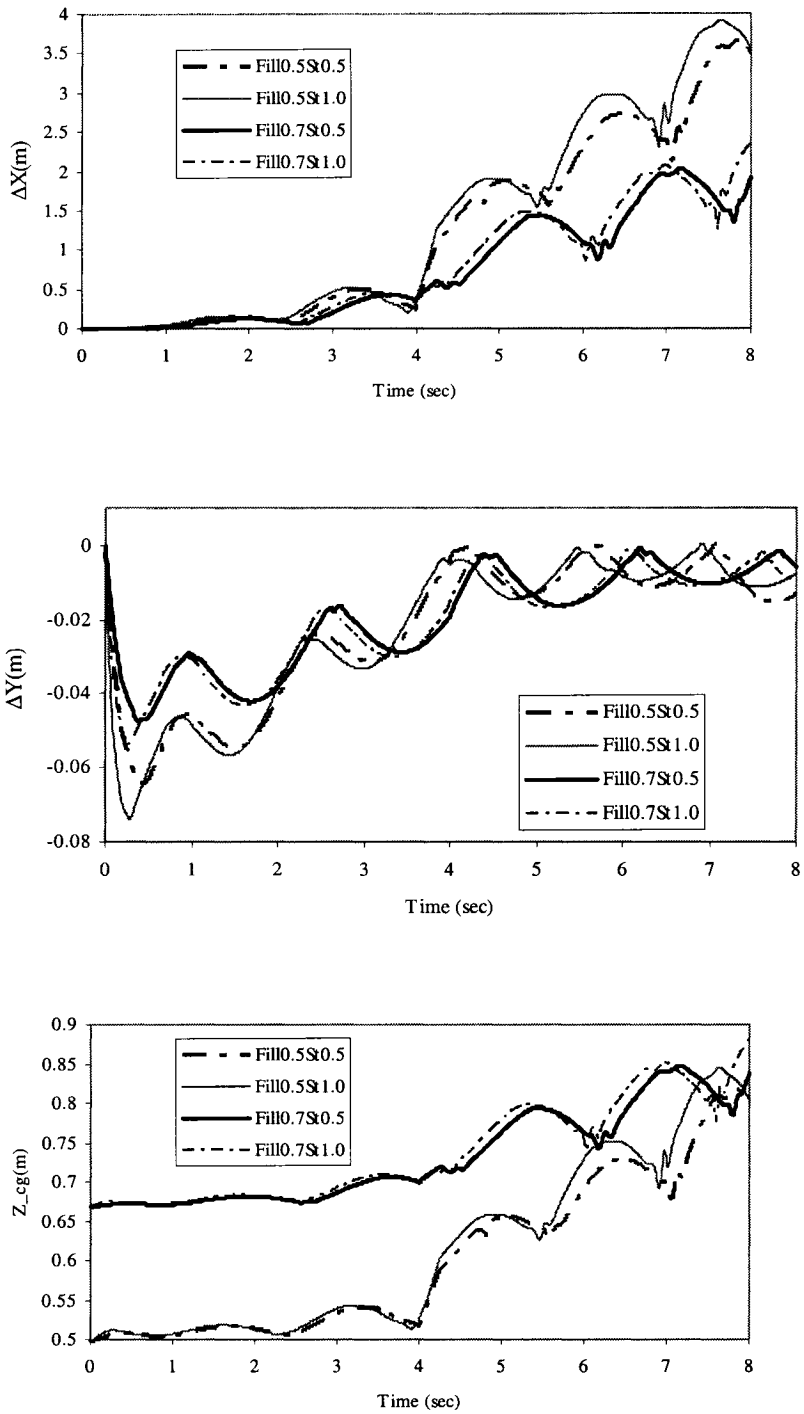

Figure 5.12: The influence of the fill level on the response of the c. g shifts (δ_f=0.5°, β=0.7), under steering and braking.

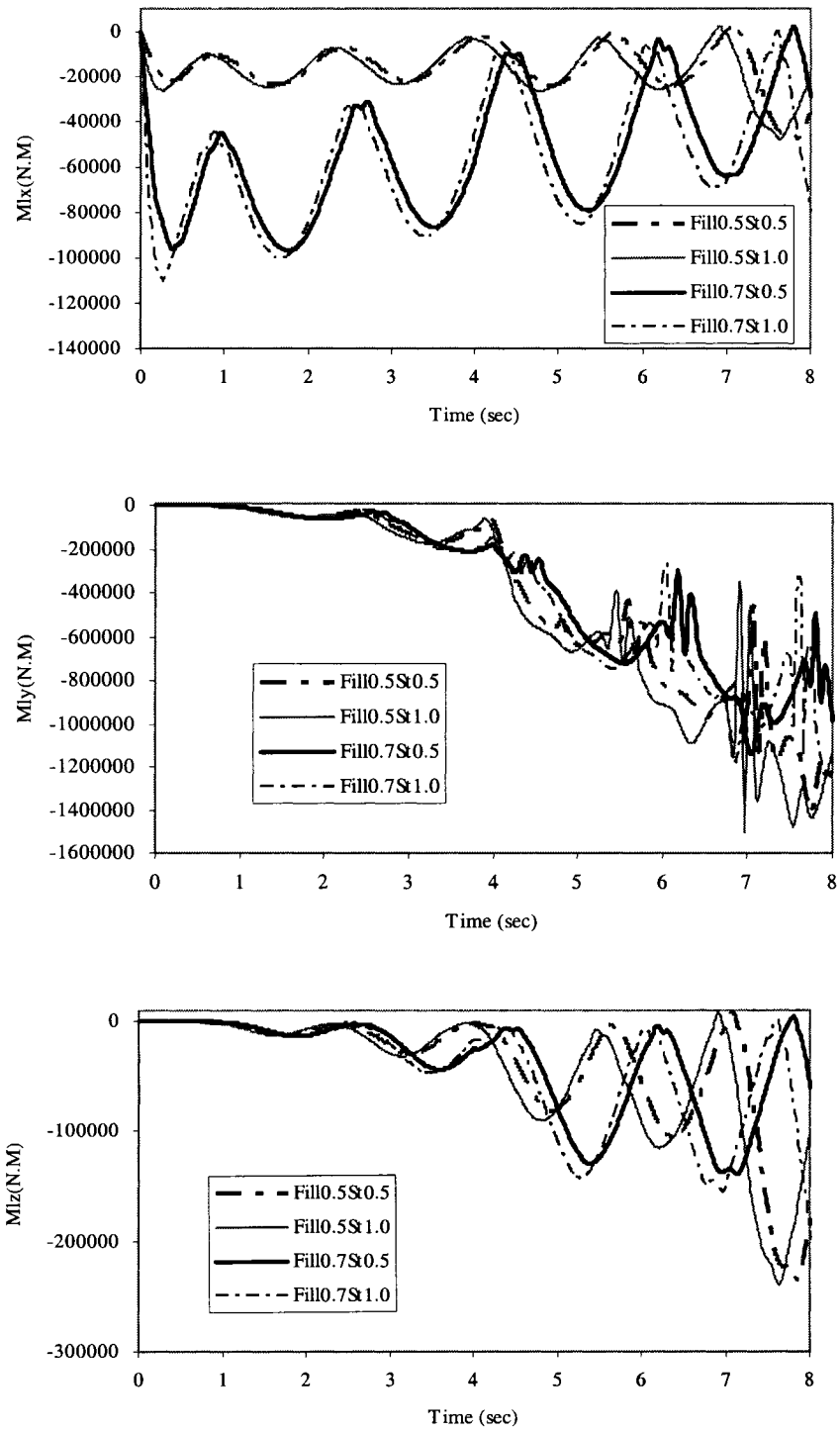

Figure 5.13: The influence of the braking treadle pressure on the variation of moments (δ_f=0.5 degree, β=0.5), under steering and braking.

5.3.5 The Influence of the Geometry of the Tank

The dynamic characteristics of the five proposed geometries tanks are evaluated under braking and steering manoeuvres. The simulation results of this evaluation are further used to compare the performance of the optimal of the 3-D designed tanks and select an optimum. The simulation conditions for these analyses are the follwoing: the vehicle is moving at the initial speed of 80 km/h, loaded at 50% fill level condition, liquid cargo specific weight: 1.3847 ton/m^3, subject to a steer input of 1.0° and the braking treadle pressures of 10 psi.

As shown in Figure 5.14, T_5 performs at a relatively lower response of the LTR under both steering and braking maneuvers. The magnitudes of the LTR for T_5 are lower than the other four types of tanks. The maximum deflection values of the trailer for T_1 to T_5 are: 0.821, 0.808, 0.813, 0.875, and 0.763 respectively. This shows that the value of LTR of T_5 is lower than T_3: approximately for 6.55%.

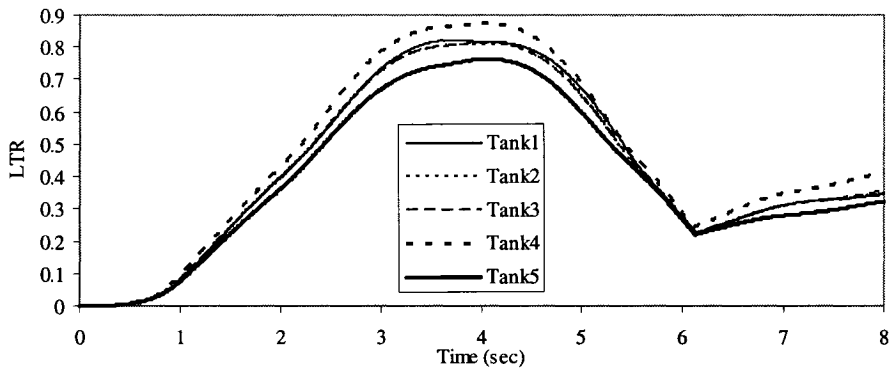

Figure 5.14: Influence of the configuration of the tank on the response of LTR (δ_f=0.5°, β=0.5), under steering and braking.

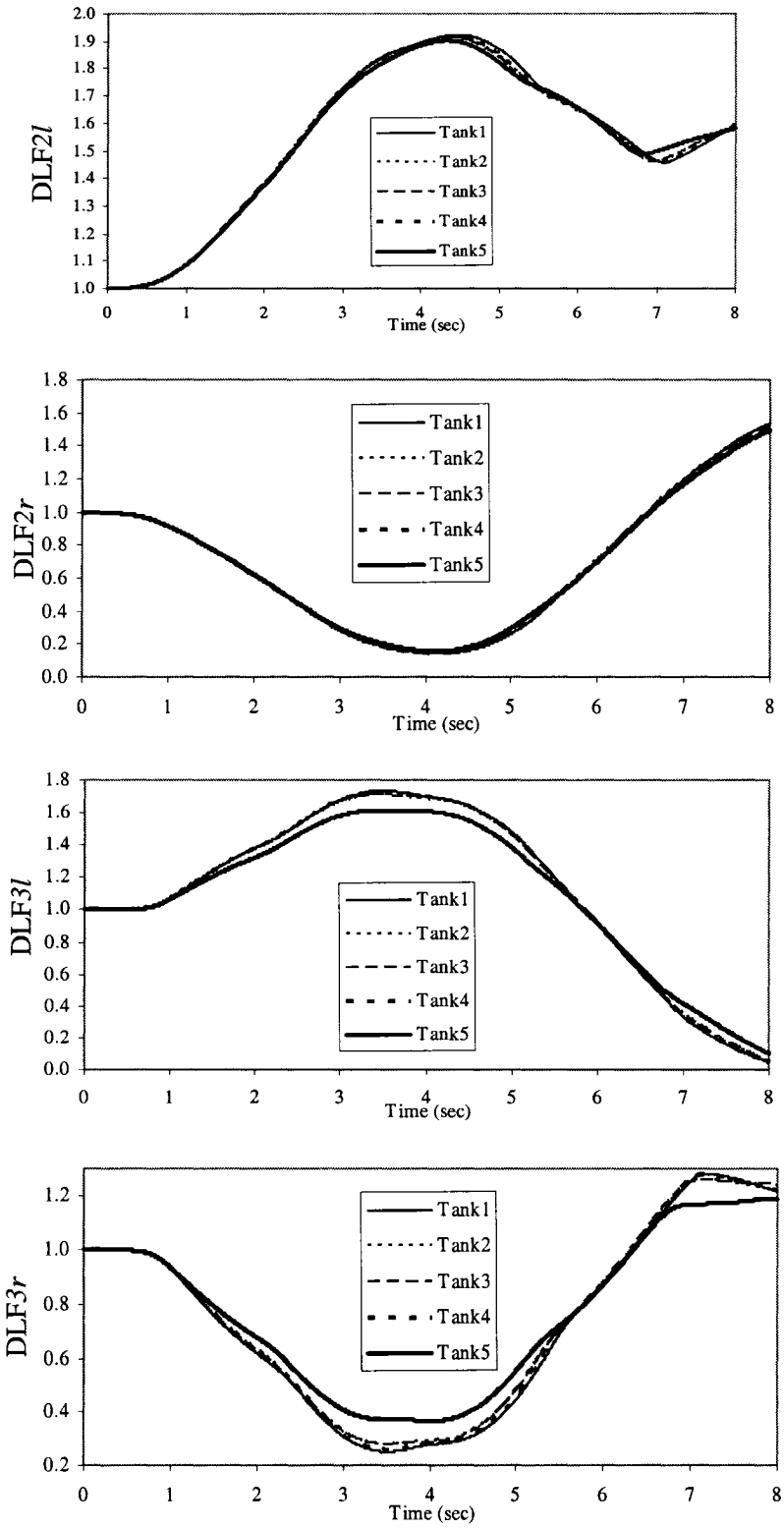

Figure 5.15: The influence of the geometry of the selected tanks on the response of the DLF (δ_f=0.5°, β=0.5)

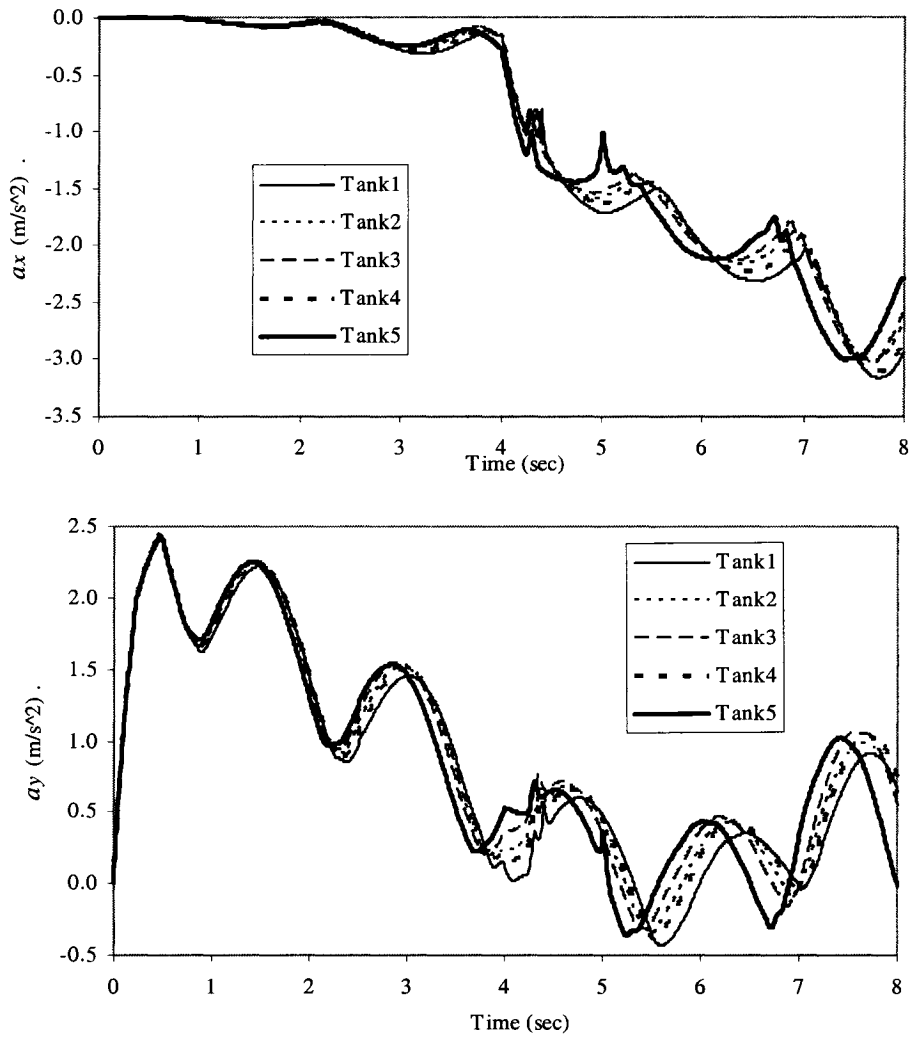

Figure 5.16: The influence of the geometry of the selected tanks on the lateral accelerations, (δ_f=0.5°, β=0.5), under steering and braking.

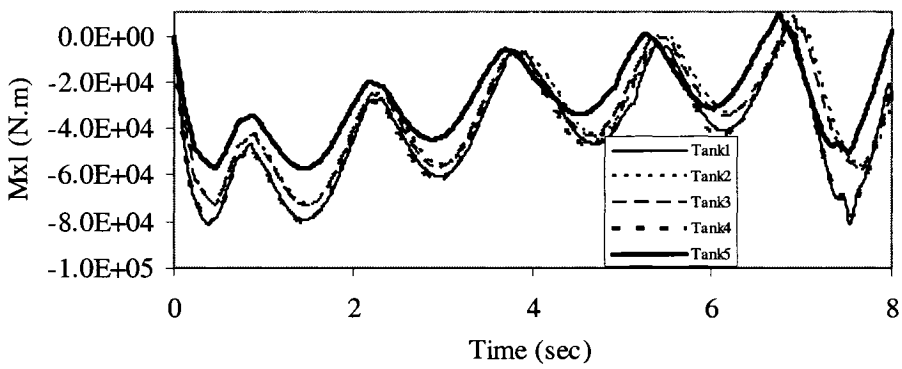

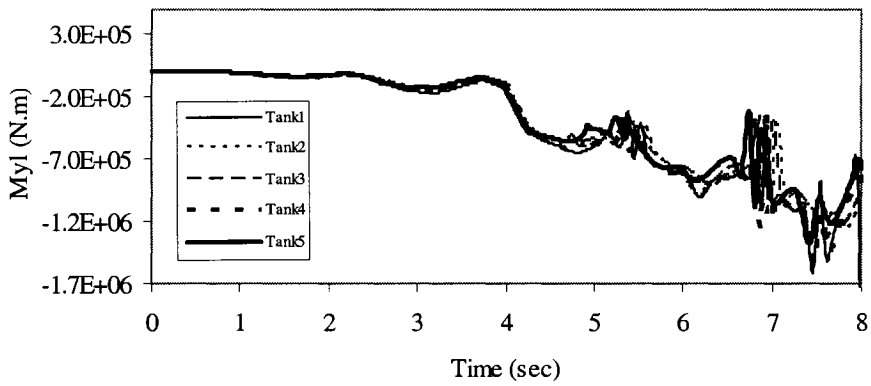

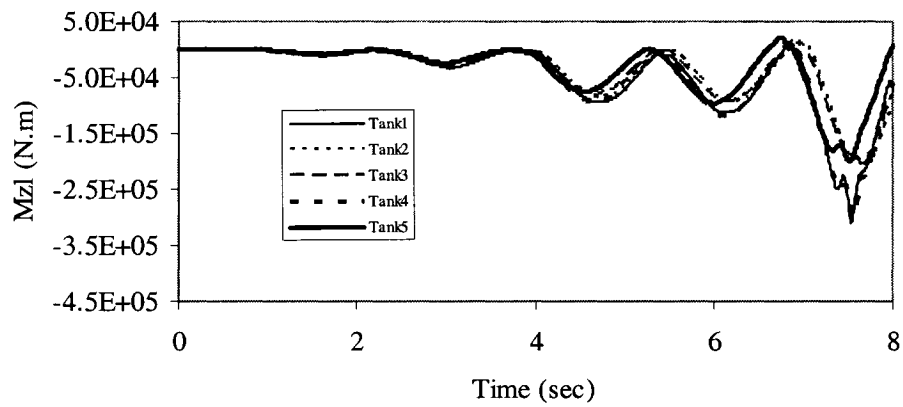

Figure 5.17: The influence of the geometry on the response of Moment (δ_f=0.5°, β=0.5)m, under steering and braking.

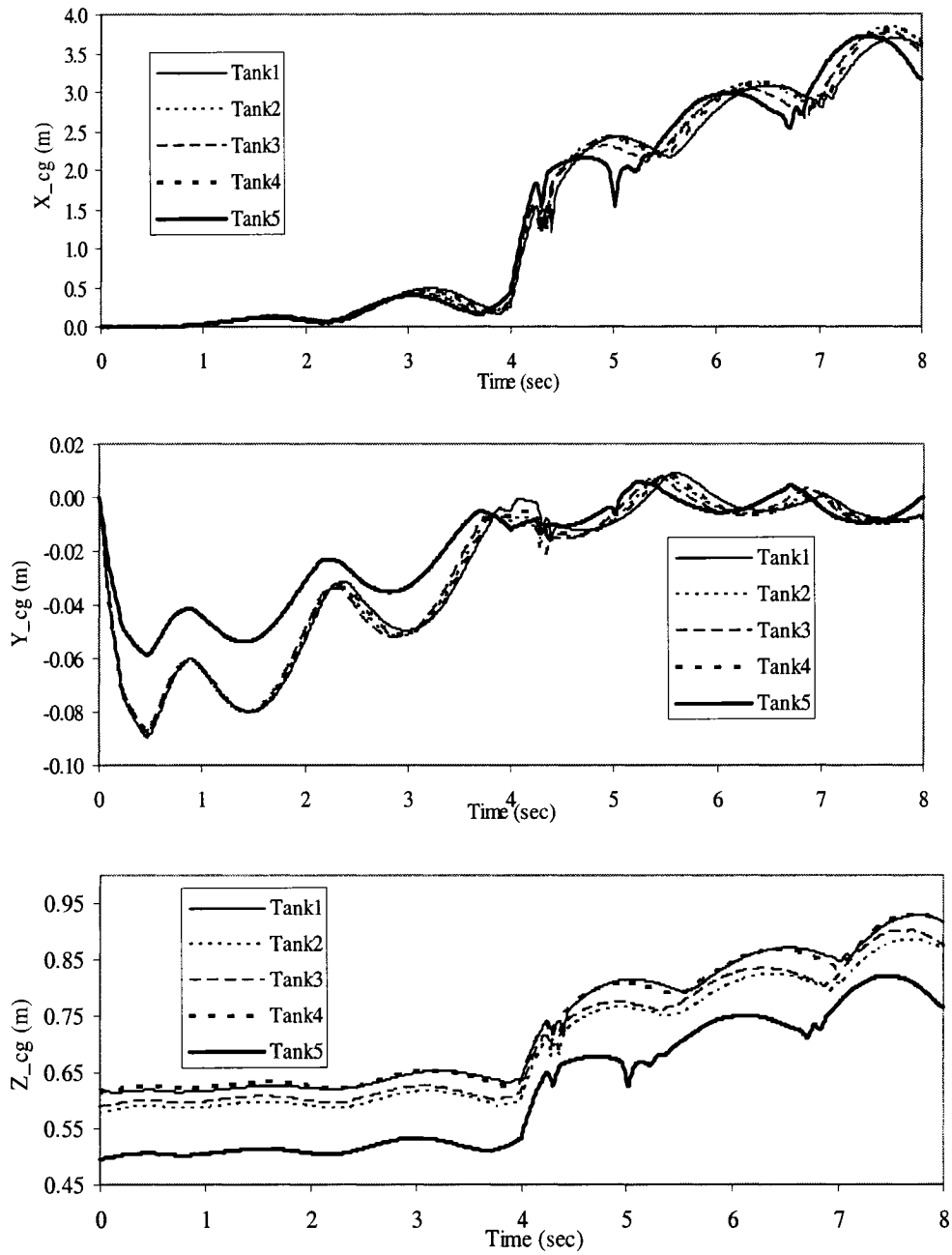

Figure 5.18 The influence of the geometry of the selected tanks on the response of c. g variation (δ_f=0.5 °, β=0.5)

As shown in Figure 5.15, T_5 demonstrates that the other benefits rather than the dynamic response of DLF are extended to this geometry. The magnitudes of the variation of the DLF during the steering and braking maneuvers are smaller than the ones for all

the other selected geometries. The peak values of the DLF of the wheel sets of the trailer are listed in table 5.6.

Table 5.6 The comparison of DLF for five different tanks

	T_1	T_2	T_3	T_4	T_5
DLF_{21}	1.923	1.913	1.912	1.916	1.902
DLF_{22}	0.144	0.147	0.145	0.145	0.155
DLF_{31}	1.734	1.710	1.709	1.727	1.615
DLF_{32}	0.251	0.277	0.278	0.259	0.367

Under braking and turning maneuver, the liquid will move forward and outward. Therefore, the DLF of the exterior tires of the trailer will increase as the transfer of the liquid load due to the centrifugal force occurs. Refer Table 5.6, the peak value of the DLF of T_5 are 10.8% higher for the interior tires and 11.2% less for the exterior tires than T_3 in the rear wheel set.

As illustrated in Figure 5.18, during the braking maneuver, the cg position of the liquid will move forward and up rapidly as shown by the combination of the regular oscillations in pitch, roll, and yaw planes. T_5 yields the lowest cg position in the vertical direction, the shortest cg shift in the lateral direction and prompt response in the cg shift in longitudinal direction under steering and braking. The lateral shift of the cg becomes narrower; which may be due to the decreasing of the forward speed of the vehicle. The identical responses are expressed on the variation of the moments in three planes, as shown in Figure 5.17.

The results of the simulation for five types of designed tanks showed that the

dynamic characteristics of the designed tanks, T_1, T_2, performed similar responses for the same operating conditions. The configuration T_5 performance better dynamic response under steering and braking maneuvers, this statement is based on the following: Minimal magnitudes of the variation in cg shift, DLF, and LTR, and faster response during operating maneuvers represent the main benefits of the optimized geometry of the liquid tank. These characteristics represent significant benefits in the safe operation of vehicles.

5.4 Conclusion

The dynamic characteristics of the liquid tank trucks are illustrated by the combination of the vehicle construction and the operating conditions. The fine tune of the construction parameters and the combination of the relevant equipment will lead to different results in the simulations. However, an optimized shape of liquid tank will reduce the side and front effect of the liquid slosh in the liquid tank, and therefore, the influence of the load on the tires. This will yield more uniform performance of the vehicle. An optimal combination for the characteristics of the partially filled liquid tank will enhance the response of the vehicle to braking and steering maneuver. The cg positions, the moment, the liquid motion along the three directions represent criteria to evaluate the performance of the liquid tank vehicle combination. The braking strength and the steering angle limits represent control parameters whom threshold indicate the performance of liquid tank vehicle.

The dynamic response comparison among the five proposed tank geometries in the dynamic simulation point towards the fact that the performance of the tank T_5 yields clearly the better dynamic characteristics under steering and braking in each of the surveyed parameters.

CHAPTER 6 CONCLUSIONS AND RECOMMMENDATIONS FOR THE FUTURE WORK

6.1 Major Contributions of the Dissertation Research

Following are perceived as the noteworthy contributions of this dissertation research:

- Identification of optimal longitudinal section of the tank to limit the fore-aft load shift of the fluid within a partly filled tank, when subjected to a longitudinal acceleration field.
- Realization of three-dimensional tank geometry through integration of the optimal longitudinal section reported in the literature.
- Formulation of a three-dimensional kineto-static liquid load shift model applicable to generic tank geometry, and analyses of load shifts and mass moments of inertia of the moving cargo, under applications of lateral and longitudinal acceleration fields.
- Development of a three-dimensional directional dynamic model of an articulated freight vehicle with partly-filled generic tank geometry for analyses of directional performance under simultaneous applications of braking and steering.
- Relative performance analyses of optimal tank geometry for different fill condition.

6.2 Major Conclusions

The major observations and conclusions drawn from the study are summarized below:

- Conventional tanks of uniform longitudinal section yield most significant fore-aft load shift under low level decelerations, when partly-filled.
- An optimal longitudinal section of nearly elliptical shape can limit the longitudinal load shift considerably under application of a longitudinal acceleration field.
- The proposed longitudinal section also limits the variations in the pitch and yaw mass moments of inertia of the moving cargo.
- The integration of an optimal lateral section to the identified longitudinal section yields significant reductions in both the lateral and longitudinal load shifts, and thereby the destabilizing forces and moments, when compared to those of a conventional circular cross – section tank.
- For 30% fill condition, and 0.6g longitudinal and 0.4g lateral acceleration excitations, the proposed optimal geometry yield 8% and 5% lower lateral and longitudinal load shifts, respectively, when compared to those of the conventional tank.
- The surface area of the proposed geometry is 8% less than that of the conventional geometry, while the volumes of both tanks are identical. This would result in lower weight, which could partly offset the high fabrication cost of the optimal geometry.
- The optimal as well as conventional tanks yield high roll mass moment of inertia of the moving cargo under a higher fill condition and high deceleration magnitude, the corresponding yaw and pitch mass moments of inertia, however, decrease with increasing deceleration level.

- The simulation results show that at 50% fill condition, the vehicle is more easier to lift off than that at 70% fill condition, based on the identical environment conditions.
- The vehicle with optimal tank design, comprising optimal longitudinal and lateral sections (configuration T_5) yields considerably lower lateral and longitudinal load transfer than the conventional cylindrical tank (configuration T_3) when subject to braking and turning inputs for 50% fill condition.
- Under 50% fill condition and subject to 0.5 degree steer input and 10 psi brake treadle pressure at an initial speed of 80 km/h, the vehicle with T_5 tank yields near 11% lower lateral load transfer and 6.5% lower longitudinal load transfer of tire forces, when compared to those of the vehicle with T_3 tank.

6.3 Recommendations for the Future Work

The present research work yields a fundamental concept in optimal design of a liquid tank to reduce the magnitudes of load shift and thereby the destabilizing forces and moments under lateral and longitudinal acceleration fields, when partly filled. While the potential performance benefits of the optimal geometry are demonstrated through development and analyses of tank vehicle model comprising a simple kineto-static model of the fluid motion and idealized inputs, considerable further efforts would be desirable to establish definite benefits of the proposed geometry. These are suggested as follow:

- The dissertation research was limited to the longitudinal optimal section only, which was coupled with the reported lateral section. A design optimization of both the section in the presence of lateral as well as longitudinal acceleration

fields would be desirable to identify a possibly more desirable geometry.

- The manufacturing challenge associated with the optimal geometry should be explored and more realistic limit constraint on the design vector may be imposed in the optimization problem.
- A study on stress analyses of the optimal geometry should be undertaken to ensure that the peak stresses are not only within the acceptable limits but are also comparable or less than those of the conventional tank.
- It would also be desirable to study the transient response of the optimal geometry in terms of load shift, transient slosh forces and moments, using dynamic fluid models.
- Experimental verifications of the results would be desirable through developments to ensure the applicability of results and conclusions for the current vehicle configurations.

REFERENCE

1. Matthew Aquaro, *Stability Analysis of Partially Filled Tanker Trucks Using a Finite Element Modeling Approach.* M.A. Sc thesis, West Virginia University, 1999.

2. Wang, Z., Rakheja, S. and Sun, C., *Influence of Partition Location on the Braking Performance of Partially-Filled Tank Truck*, SAE Paper No. 952639, 1995.

3. Strandberg, L., *Lateral Stability of Road Containers*, VTI (The Swedish National Road and Traffic Research Institute) Report No. 138A, Sweden, 1978

4. Rakheja, S., Sankar, S. and Ranganathan, R., *Influence of Tank Design Factors on the Rollover Threshold of Partially Filled Tank Vehicles*, SAE Paper No. 892480, 1989

5. Kang, X., Rakheja, S. and Stiharu, I., *Optimal Tank Geometry to Enhance Static Roll Stability of Partially-filled Tank Vehicles*, SAE Paper No. 1999-01-3730, SAE Transactions J. of Commercial Vehicles, 2000

6. Ervin, R. D., *The influence of size and weight variables on the roll stability of heavy trucks*, SAE Paper, # 831163, 1983

7. Lealie A. Laird, *Measurement of Heavy Vehicle suspension Roll-Stability Properties, and a Method to evaluate Overall stability performance.* SAE Paper # 881869, 1988.

8. Vineet Gupta, *A Submodel Component Reanalysis Technique for Liquid Tanker Body Design Using the Finite Element Method.*. M.A.Sc. Thesis, Concordia University, 1988

9. Ranganathan, R. Rakheja, S. & Sankar, S., *Kineto-static roll plane analysis of articulated tank vehicles with arbitrary tank geometry*, Int. J. of Vehicle Design, 10.1, 89-111. 1989.

10. Ranganathan, R., Rakheja, S. and Sankar, S., *Directional Response of a B-train Vehicle Combination Carrying Liquid Cargo*, J. of Dynamic Systems, Measurement and Control, Transactions of the ASME, Vol. 115, No. 1, pp. 133-139, 1993

11. Ranganathan, R., Ying, Y. and Miles J. B., *Analysis of Fluid Slosh in Partially Filled Tanks and Their Impact on the Directional Response of Tank Vehicles*, SAE Paper No. 932942, 1993

12. Rakheja, S., Sankar, S., Rangannathan, R., Billing, J.R. and Mercer, W., *Field Testing of a Tank Truck and Study of Fluid Slosh*, SAE Paper # 912679, 1991.

13. Popov, G., *Dynamics of Liquid Sloshing in Road Containers*, Ph.D. Thesis, Concordia University, 1991

14. Popov, G., Sankar, S. and Sankar, T. S. *et al.*, *Liquid Sloshing in Rectangular Road Containers, Computer and Fluids*, Vol. 21, pp. 551-569, 1992

15. Popov, G., Sankar, S. and Sankar, T. S. *et al.*, *Dynamics of Liquid Sloshing in Horizontal Cylindrical Road Containers*, Pro. Inst. of Mechanical Engineers, Vol. 207, Part C: J. of Mechanical Engineering Science, pp. 399-406, 1993

16. Popov, G., Sankar, S. and Sankar, T. S., *Dynamics of Liquid Sloshing in Baffled and Compartmented Road Containers*, J. of Fluids and Structures, Vol. 7, pp. 803-821, 1993

17. Welch, J. E., *The MAC Method: a Computing Technique for Solving Viscous, Incompressible, Transient Fluid-Flow Problems Involving Free Surfaces*, Report No. LA-3425, Los Almos Scientific Laboratory, New Mexico, 1966

18. Rakheja, S., Sankar, A. and Sankar, T.S. *On the development of an early warning safety monitor for articulated freight vehicles*, Int. J. of Vehicle Design, Vol.12, No.4 pp.420-449. 1991.

19. Rakheja, S., Rangannathan, R. Sankar,S., *Field testing and Validation of Directional Dynamics Model of a Tank Truck*, Int. J. of Vehicle Design, Vol. 13, No. 3, pp. 251-275, 1992.

20. Rakheja, S. and Rangannathan, R. *Estimation of rollover threshold of heavy vehicles carrying liquid cargo: a simplified approach* Heavy Vehicle Systems, Special Series, Int. J. of Vehicle Design, Vol.1, No. 1. pp 79-98, 1993.

21. R. Ranganathan, Y. Ying, and J.B. Miles, *Development of a Mechanical Analogy Model to Predict the Dynamic Behavior of Liquids in Partially Filled Tank Vehicles,* Heavy Vehicle Dynamics and Simulation in Braking, Steering, and Suspension Systems, SAE SP-1059, 942307

22. Ranganathan, R., Rakheja, S. and Sankar, S., *Influence of Liquid Load Shift on the Dynamic Response of Articulated Tank Vehicles*, Vehicle System Dynamics, Vol. 19, No. 4, pp. 177-200, 1990

23. El-Gindy, M. and Wong, J. Y., *A Comparison of Various Computer Simulation Models for Predicting the Directional Responses of Articulated Vehicles*, Vehicle System Dynamics, Vol. 16, No. 5-6, 1987

24. Sayers, M.W. and Riley, S.M., *Modeling Assumptions for Realistic Multibody Simulations of the Yaw and Roll Behavior of Heavy Trucks*, SAE Paper No. 9610173, 1996.

25. Kang, X., Rakheja, S. and Stiharu, I., *Tank Shape Optimization for Enhancement of Roll Stability of Partially-filled Tank Vehicles in Steady Turning*, presented at ASME IMECE-2000, Orlando, Florida, Nov. 2000

26. Kang, X., Rakheja, S. and Stiharu, I., *Directional Dynamics of a Partly-Filled Tank Vehicle under Braking and Steering*, presented at SAE 2000 Bus & Truck Meeting, Portland, Oregon, Dec. 2000

27. Kang, X., Rakheja, S. and Stiharu, I., *Cargo Load Shift and its Influence on Tank Vehicle Dynamics under Braking and Turning*, Heavy Vehicle Systems, Int. J. of Vehicle Design, 2000

28. Kang, X., Rakheja, S. and Stiharu, I., *Effects of Tank Shape on the Directional & Roll Dynamic Response of a Partly-Filled Tank Vehicle*, Vehicle System Dynamics, Int. J. of Vehicle Mechanics and Mobility, 2000

29. Kang, X., Rakheja, S. and Stiharu, I., *Dynamic Response and Stability Characteristics of Partly-filled Articulated Liquid Cargo Vehicles under Braking-in-a-turn*, submitted to Automobile Engineering, Proc. of the Institute of Mechanical Engineers, Part D, U.K.

30. Kang, X, *Optimal Tank Design and Directional Dynamic Analysis of Liquid Cargo Vehicles under Steering and Braking*, Ph.D. Thesis, Concordia University, 2001

31. Ranganathan, R., Rakheja, S. and Sankar, S., *Effects of Vehicle Configurations and Tank Design Factors on Directional Dynamics of Tank Vehicles*, Transactions of the Canadian Society of Mechanical Engineering, Vol. 17, No. 4, pp. 923-942, 1993.

32. Ranganathan, R., *Stability and Directional Response Characteristics of Heavy Vehicles Carrying Liquid Cargo*, Ph.D. Thesis, Concordia University, 1990

33. Abramson, H. N., *The Dynamic Behavior of Liquids in Moving Containers*, NASA SP-106, 1966

34. J. Y. WONG, *Theory of Ground Vehicles*, A Wiley-interscience Publication, JOHN WILEY &SONS, INC. 1993.

35. C.B. Winkler, C. Mallikarjunarao, and C.C. Macadam, *Analytical Test Plan: Part I- Description of Simulation Models for Parameter Analysis of Heavy Truck Dynamic Stability,* Report of the University of Michigan Transportation Research Institute, Apr. 1981.

36. H.T. Moncarz, J.E. Bernard, and P.S. Fancher, *A Simplified, Interactive Simulation for Predicting the Braking and Steering Response of Commercial Vehicles*, Report UMHSRI-PF-75-8, University of Michigan Highway Safety Research Institute, Aug. 1975.

37. El-Gindy, M. and Wong, J. Y., *A Comparison of Various Computer Simulation Models for Predicting the Directional Responses of Articulated Vehicles*, Technical Report of Vehicle Weights and Dimensions Study, Vol. 16. Road and Transportation Association of Canada, July 1986.

38. P.M. Leucht, *The Directional Dynamics of the commercial Tractor- Semitrailer Vehicle during Braking*, Society of Automotive Engineers, paper 700371, 1970.

39. H.T. Moncarz, J.E. Bernard, and P.S. Fancher, *A Simplified, Interactive Simulation for Predicting the Braking and Steering Response of Commercial Vehicles*, Report UMHSRI-PF-75-8, University of Michigan Highway Safety Research Institute, Aug. 1975.

40. Terry D. Day, *Differences Between EDVDS and Phase 4*, SAE 1999-01-0103, Engineering Dynamics Corp., 1999.

41. Murphy, R.W., Bernard, J.E. and Winkler, C. B., *A Computer-based Mathematical Method for Predicting the Braking Performance of Trucks and Tractor-Trailers*, University of Michigan Highway Safety Research Institute, NTIS PB 212 205, 1972.

42. Bernard, J.E. and Winkler, C. B., and Fancher P.S., *A Computer-based Mathematical Method for Predicting the Braking Performance of Trucks and Tractor-Trailers, Phase II Technical Report, Moter Truck Braking and Handling Performance Study*, University of Michigan Highway Safety Research Institute, NTIS PB 221 630, June 1973.

43. Bernard, J.E., Winkler, C.B., Fancher, P.S, MacAdam, *Predicting the Braking Performance of Trucks and Tractor-Trailers - Phase III Technical Report*, UM-HSRI-76-26-1, C.C., Post, T.M., June 1976.

44. MacAdam, C.C., Fancher, P.S., Hu, G.T., Gillespie, T.D., *A Computerized Model For Simulating the Braking and Steering Dynamics of Trucks, Tractor-Semitrailers, Doubles, and Triple Combinations, Users' Manual - Phase 4* UM-HSRI 80-58, September 1980.

45. Tong, X., Tabarrok, B. and El-Gindy, M., *Computer-Based Analysis of the Dynamics Performance of Log Hauling Trucks*, SAE Paper No. 952637, 1995

46. A. A. Seireg, Jorge Rodriguez, *Optimizing of the Shape of Mechanical Elements and Structures*, 1997

47. M. Zuczkowski, *Structural Optimization under Stability and Vibration Constraints*, Technical University of Cracow, 1989.

48. U. Kirsch, *Structural Optimization, Fundamentals and Applications*, Technion-Israel Institute of Technology, 1993.

49. Galileo Galilei Linceo, Discorsie Dirnostranioni Matematiche Intorno, a Due Nuove Scienze Attenenti Alla Mecanica et I Movimenti Locali, Leida 1638, [46].

50. Cauchy, A. L., "*Methode General pour la Resolution des Systems D'Equations Simultanees*," Comptes Rendus, Academic de Sciences, Paris, vol.25, 1847. pp 536.

51. Hadamark, J., "*Lessons on the Calculus of Variation*," Gauthier-Villards, Paris, 1910.

52. Schmit, L. A., "*Structural Synthesis by Systematic Synthesis*," Proceedings Second Conference on Electronic Computation ASCE, New York, 1960, pp 105-122.

53. Armand, J. L., "*Numerical Solutions in Optimization of Structural Elements,*" First International Conference on Computing Methods in Non-linear Mechanics, TICOM, Austin, 1974.

54. Gallagher, R., and Zienkiewicz, O.C. "*Optimum Structural Design*," John Wiley & Sons, New York, 1973.

55. Hafta, R.T. and Kamat, M. p., "*Elements of Structural Optimization,*", Martinus Nijhoff Publishers, Boston, 1985.

56. Kirk,D, E., "*Optimal Control Theory*," Prentice-Hall, Englewood Cliffs, N.J. , 1970.

57. Leitmann, G. (editor), "*Optimization Techniques with Applications to Aerospace Systems,*" Academic press, New York, 1962.

58. Esping,, B. J. D., *A CAD Approach to the Minimum Weight Design Problem*, International Journal of Numerical Methods in Engineering, vol. 21, pp 1049-1066, 1985.

59. Braibant, V., and Fleury, C., " *Shape Optimal Design: An Approach Matching CAD and Optimization Concepts*, " In "*Optimization in Computer- Aided Design*", edited by J.S. Gero, Elsevier Science Publishers, IFIP 1985.

60. Wang, S., Sun, Y., and Gallagher, R. H., "*Sensitivity Analysis in Shape Optimization of Continuum Structures*", Computers and Structures, vol. 20, no. 5, pp 855-867, 1985.

61. Ding, H., and Gallagher, R.H., *Approximate Force Method Reanalysis Techniques for Structural Optimization*, International Journal of Numerical Methods in Engineering, vol. 21, pp 1253-1267, 1985.

62. Hirotaka Nakayama, *Simulation-Based Optimization Using Computational Intelligence*, Optimization and Engineering, 3, 201-214, 2002.

63. Richard L. Fox, *Optimization Methods for Engineering Design*, Case Western Reserve University, 1970.

64. Schittkowski, K., "*NLQPL: A FORTRAN-Subroutine Solving Constrained Nonlinear Programming Problems*," Annals of Operations Research, Vol. 5, pp 485-500, 1985.

65. Biggs, M.C., "*Constrained Minimization Using Recursive Quadratic Programming*," Towards Global Optimization (L.C.W. Dixon and G.P. Szergo, eds.), North-Holland, pp 341-349, 1975.

66. Han, S.P., "*A Globally Convergent Method for Nonlinear Programming*," J. Optimization Theory and Applications, Vol. 22, p. 297, 1977.

67. Powell, M.J.D., "*The Convergence of Variable Metric Methods for Nonlinearly Constrained Optimization Calculations*," Nonlinear Programming 3, (O.L. Mangasarian, R.R. Meyer and S.M. Robinson, eds.), Academic Press, 1978.

68. Powell, M.J.D., "*A Fast Algorithm for Nonlinearly Constrained Optimization Calculations*," Numerical Analysis, G.A.Watson ed., Lecture Notes in Mathematics, Springer Verlag, Vol. 630, 1978.

69. Bauer, H.F., *Dynamic Behavior of an Elastic Separating Wall in Vehicle Containers: Part I*, Int. J. of Vehicle Design, Vol. 12, No. 1, 1981.

70. Rakheja, S., Sankar, S. and Ranganathan, R., *Roll Plane Analysis of Articulated Tank Vehicles during Steady Turning,* Vehicle System Dynamics, Vol.17, pp.18-104, 1988.

71. Broge, J. L., *Heavy Duty Truck Safety Systems,* Automotive Engineering International, pp 101-105, May 2000.

72. Blower, D., Perris, L., *Trucks Involved in Fatal Accidents, Codebook 1996,* Technical report UMTRI-98-14, University of Michigan Transportation Research Institute, Ann Arbor, MI, USA, 1998.

73. Blower, D., Perris, L., *Trucks Involved in Fatal Accidents, Codebook 1997,* Technical report UMTRI-98-18, University of Michigan Transportation Research Institute, Ann Arbor, MI, USA, 1999.

74. Harrs. R. J. W., *Cost of Roll Over Accidents*, Personal Communication, 1995.

75. Kusters, L. J. J., *Increasing Roll Over Safety of Commercial Vehicles by Application of Electronic systems*, Smart Vehicels, pp. 362-377, Swets & Zeitlinger, Lisse, The Netherlans, 1995.

76. Abramson, H. N., *The Dynamic Behavior of Liquids in Moving Containers*, NASA SP-106, 1966

77. Roberts, J. R., Basurto, E. R and Chen, P. Y., *Slosh Design Handbook I*, NASA Technical Reports, NASA-CR-406, May 1966

78. Preliminary Standard *B620-1987* Highway Tanks and Portable Tanks for the Transportation of Dangerous Goods. Transport Canada, 1987.

79. Kusters, L.J.J., *Increasing Roll Over Safety of Commercial Vehicles by Application of Electronic Systems*, Smart Vehicles, pp. 362-377, Swets & Zeitlinger, Lisse, The Netherlans, 1995.

80. Chieh Chen and Masayoshi Tomizuka, *Lateral control of commercial Heavy Vehicles*, Vehicle System Dynamics, 33(2000), pp. 391-420.

81. Rakheja, S., Sankar, S. and Ranganathan, R., *Influence of Tank Design Factors on the* Rollover *Threshold of Partially Filled Tank Vehicles*, SAE Paper No. 892480, 1989.

82. Ranganathan, R., Rakheja, S. and Sankar, S., *Effects of Vehicle Configurations and Tank Design Factors on Directional Dynamics of Tank Vehicles*, Transactions of the Canadian Society of Mechanical Engineering, Vol. 17, No. 4, pp. 923-942, 1993.

83. The Canadian Standards Association CAN/CSA-B621-98 (Highway Tanks, Portable Tanks, Cargo compartments, and Containers for the Transportation of Dangerous Goods)

84. Roy, D. N., *Applied Fluid Mechanics*, Ellis Horword Limited, England, 1988.

85. Streeter, V. L. and Benjamin, W. E., *Fluid Mechanics*, McGraw-Hill Book Co., Sixth Edition, 1975.

86. Rakheja, S. and Wang, Z., *Analysis of Braking Process of a Partially-Filled Tractor Tank Semitrailer,* Advances in Transportation Systems, CSME Forum SCGM, pp. 326-333, 1996

87. Blower, D., Pettis, L., *Trucks Involved in Fatal Accidents, Codebook*, 1996, Technical Report UMTRI-98-14, University of Michigan Transportation Research Institute, Ann Arbor, MI, USA, 1998.

88. Natural Resources Canada, *Energy Efficiency Trends in Canada* 1991-1998, October 2000.

89. Shadle, S. G., Emery L. H. and Brewer, H. K., *Vehicle Braking, Stability and Control*, SAE Paper No. 830562, 1983

90. Radlinski, R. W., *Braking Performance of Heavy U. S. Vehicles*, SAE Paper No. 870492, 1987

91. Tong, X., Tabarrok, B. and El-Gindy, M., *Computer-Based Analysis of the Dynamics Performance of Log Hauling Trucks*, SAE Paper No. 952637, 1995

92. John c. Dixon, *Tires, Suspension and Handling, Second Edition*, SAE Inc, Warrendale, Pa. 1996.

93. Giancarlo Genta, *Motor Vehicle Dynamics, Modeling and Simulation*, World Scientific Publishing Co. Pte. Ltd. 1997

94. Sankar, S., Guntur, R. and Sankar, T. S, *Effect of Wheel Slip on the Stability and Stopping Ability of a Road Vehicle*, Int. J. of Vehicle Design, Vol. 3, No. 1, pp. 77-89, 1982

95. I. M. Lbrahim, M. A. EI-Nashar and Y, K, Younes, *Ride Behavior of Trucks Transporting Liquids*, Paper of Int. J. of Vehicle Design, Vol.5, No. 3 1998.

96. Yang, Y. S., *Direction Response Characteristics of Liquid Tank Vehicles Subjected to Dynamic Liquid Load Shift,* M.S. Thesis, University of Missouri, Columbia, Dec, 1992.

97. T. D. Gillespie, C. C. MacAdam, *Constant Velocity Yaw/Roll Program User's Manual*, UMTRI, Oct 1982.

98. *Manual on design and application of leaf springs-ASE J788a*, SAE Information Report, 4th Edition, SAE Spring committee (SAE), 1982.

99. Bernard, J. E., Winkler, C. B. and Fancher, P. S., *A Computer-Based Mathematical Method for Predicting the Directional Response of Trucks and Tractor-Trailers, Phase II Technical Report*, Motor Truck Braking and Handling Performance Study, Highway Safety Research Institute, The University of Michigan, Ann Arbor, PB-221-630, June 1973

100. MacAdam, C. C., Fancher, P. S. and Hu, G. T. *et al.*, *A Computerized Model for Simulating the Braking and Steering Dynamics of Trucks, Tractor-Semitrailers, Doubles, and Triples Combinations*, User's Manual, Phase 4, MVMA Project 1197, UM-HSRI-80-58, Sept. 1980

101. Geory Rill, *Vehicle Dynamics*, Fachhochschule Regensburg, University of Applied Sciences, Nov. 2002.

102. Bernard, J. E., Winkler, C. B. and Fancher, P. S., *A Computer-Based Mathematical Method for Predicting the Directional Response of Trucks and Tractor-Trailers, Phase II Technical Report*, Motor Truck Braking and Handling Performance Study, Highway Safety Research Institute, The University of Michigan, Ann Arbor, PB-221-630, June 1973

103. Baraket, Z.; Fancher, P., *Increased Capacity Automobile Transporter Feasibility Study and Road-Handling Analysis,* UMTRI, 2000

104. Terry D. Day, *Differences between EDVDS and Phase 4*, SAE Paper: 1999-01-0103, 1999.

105. Limpert, R. and Warner, C. Y., *Proportional Braking of Solid-Frame Vehicles*, SAE Paper No. 710047, 1971

106. Dorion, S. L. and Pickard, J. G., *Feasibility of Anti-Jackknifing Systems for Tractor Semitrailers*, SAE Paper No. 891631, 1989

107. Stribersky, A. and Fancher, P. S., *The Nonlinear Behavior of Heavy-Duty Truck Combinations with Respect to Straight-line Stability*, J. of Dynamic Systems, Measurement, and Control, Transactions of ASME, Vol. 111, pp. 577-582, 1989

108. Liu, P. J., Analysis, *Detection and Early Warning Control of Dynamic Rollover of Heavy Freight Vehicles*, Ph.D. Thesis, Concave, Concordia University, Jan. 1999.